University of Nevada, Reno

Real-Time Monitoring of FM1-43-Labeled Plasma Membrane in Adrenal Chromaffin Cells Exposed to 5 ns Electric Pulses Reveals Differential Membrane Potential Changes and Ca^{2+}-dependent Exocytosis in the Absence of Phospholipid Scrambling

A thesis submitted in partial fulfillment of the

requirements for the degree of Master of Science in

Electrical and Biomedical Engineering

By

Rita Aoun

Dr. Josette El Zaklit / Thesis Advisor

Dr. Gale L. Craviso / Thesis Co-Advisor

August, 2020

THE GRADUATE SCHOOL

We recommend that the thesis
prepared under our supervision by

RITA AOUN

Entitled

Real-Time Monitoring of FM1-43-Labeled Plasma Membrane in Adrenal Chromaffin Cells Exposed to 5 ns Electric Pulses Reveals Differential Membrane Potential Changes and Ca^{2+}-dependent Exocytosis in the Absence of Phospholipid Scrambling

be accepted in partial fulfillment of the
requirements for the degree of

MASTER OF SCIENCE

Josette El Zaklit, Ph.D., Advisor

Gale L. Craviso, Ph.D., Co-Advisor

Bahram Parvin, Ph.D., Committee Member

Normand Leblanc, Ph.D., Graduate School Representative

David W. Zeh, Ph.D., Dean, Graduate School

August, 2020

ABSTRACT

In response to depolarizing stimuli, neurons and neuroendocrine cells secrete neurotransmitters and other bioactive molecules via Ca^{2+}-dependent fusion of secretory vesicles and granules with the plasma membrane, a process called exocytosis. When exocytosis occurs, the surface area of the plasma membrane increases due to fusion of the secretory vesicles and granules, which can be monitored electro-physiologically in real-time by cell membrane capacitance measurements. A complementary fluorescence imaging approach for monitoring in real-time secretory vesicle and granule fusion due to exocytosis is use of the fluorescent membrane marker FM1-43. When FM1-43 is present in the bathing solution, exocytosis is observed as an increase in cell surface fluorescence. However, FM1-43 fluorescence is also known to be sensitive to other changes in the labeled membrane induced by depolarizing stimuli, such as the transmembrane potential (TMP).

Our group has long been interested in examining the potential for **n**anosecond duration **e**lectric **p**ulses (NEPs) to serve as a novel bioelectric stimulus of neurosecretion using adrenal chromaffin cells as our cell model. We have shown that exposing chromaffin cells to 5 ns electric pulses at an electric (E)-field intensity of 5 MV/m causes catecholamine release in a manner that relies on Ca^{2+} influx via voltage-gated Ca^{2+} channels (VGCCs) and that occurs via Ca^{2+}-dependent exocytosis. To further investigate this novel secretory stimulus, we recently monitored NEP-evoked exocytosis in real-time using total internal reflection fluorescence microscopy (TIRFM) in which secretory

granules were labeled with the fluorescent dye acridine orange. We found that for a train of 10 pulses delivered at 1 Hz, exocytotic events occurred with a delay of several seconds as the pulse train was being delivered, contrasting with nicotinic receptor stimulation that caused exocytosis within milliseconds.

The goal of the present study was to use a complementary approach to monitor NEP-evoked exocytosis in real-time using cell membrane staining with FM1-43. Initial experiments were carried out to evaluate the feasibility of using FM1-43 to monitor exocytosis using high [K^+] as the depolarizing stimulus. Perfusing the cells with a balanced salt solution (BSS) containing 3 μM FM1-43 caused the dye to incorporate quickly into the plasma membrane, as detected by an increase in membrane fluorescence. After the fluorescence reached a plateau (~ 5 minutes), the perfusion of the cells with 56 mM [K^+] BSS first caused a decrease in cell-surface fluorescence when the stimulus reached the cells, followed by an increase in fluorescence that was homogeneous across the surface of the cell membrane. The initial fluorescence dip was attributed to cell depolarization due to the ability of the dye to detect TMP changes, whereas the subsequent increase in fluorescence reflected exocytosis. This latter increase was Ca^{2+}-dependent since exposing cells to high [K^+] in the absence of external Ca^{2+} did not result in an increase in membrane fluorescence, indicating a lack of exocytosis.

Application of ten 5 ns, 19.8 MV/m pulses to FM1-43 labeled cells delivered at 1 Hz also resulted in an overall increase in whole cell membrane fluorescence that was dependent on extracellular Ca^{2+}. That is, application of the pulses in Ca^{2+}-free medium did not cause an increase in fluorescence, indicating that the rise in membrane fluorescence was due to NEP-evoked exocytosis. However, unlike the initial homogenous decrease in cell membrane fluorescence evoked by high [K^+] due to membrane depolarization, there were differential changes in FM1-43 fluorescence on the poles of the cells during the application of the electric stimulus. We observed an increase in fluorescence at the anode facing pole of the cell, while the cathode facing pole exhibited a decrease in fluorescence. These differential effects, which lasted only for the duration of the applied stimulus, were caused by NEP-induced depolarization at the cathode facing pole that induces a decrease in FM1-43 fluorescence, and hyperpolarization of the anode facing pole of the cell that induces an increase in FM1-43 fluorescence. In support of this conclusion, changing the polarity of the delivered pulses reversed the differential effects between the poles of the cells. Interestingly, the equators of the cells also exhibited a decrease in fluorescence, indicating that these regions of the cell membrane were depolarized during the stimulus. Because of these differential TMP changes that occurred during the pulse train, we could not obtain evidence of a delay in the onset of exocytosis as observed previously in the TIRFM experiments in which cells were similarly exposed to a train of ten, 5 ns pulses at 1 Hz.

To assess whether the NEP stimulus train caused phosphatidylserine (PS) externalization that contributed to the increase in FM1-43 fluorescence, exposed cells were probed with the specific PS marker Lactadherin-FITC. We found that a single train of 10 NEPs did not induce PS externalization even two minutes after stimulation. However, after a second train of NEPs, PS was identified at the anode facing pole of the cell one minute after the end of the stimulus. These results suggest that PS scrambling did not contribute to the increase in fluorescence at the anode facing pole of the cell observed during a single pulse train, or at any other part of the cell two minutes post-stimulation. After the end of the pulse train, all the membrane parts of the stimulated cell, exhibited an increase in fluorescence that was observed only in the presence of extracellular Ca^{2+}. In contrast, in the absence of Ca^{2+}, all fluorescence curves returned to baseline. This indicates that the NEP-induced increase in membrane fluorescence is mostly driven by the Ca^{2+}-dependent exocytosis.

In summary, these results imply multiple understandings into the basic use of NEPs as a biomedical application to trigger neurosecretion. The increase in FM1-43 fluorescence occurring on all parts of the membrane of the cells between the electrodes confirms the exocytotic activity due to the influx of Ca^{2+} induced by the electric stimulation. The differential polarization of the stimulated cell is important to consider during the exogenous application of NEPs for biological tissues/organs. Hyperpolarization of the anode facing poles and depolarization of the cathodic poles of the cells during the application of the NEPs can vary the excitation state of the targeted cells. A novel finding in the use of 5 ns pulses reported in this study is that using a train of 10 pulses, no PS was externalized at the anode facing pole or other parts of the cells for two minutes post-stimulation. This suggested that the exposure of ten 5 ns pulses did not induce symptoms of apoptosis in the stimulated chromaffin cells. Finally, monitoring exocytosis using FM1-43 did not rule out a delay between the initiation of NEPs and the beginning of the exocytotic response. Thus, direct measurement of the NEP-induced exocytosis is needed in the future to re-investigate the nature of this delay.

DEDICATION

To my mother and father for their endless love and devotion, to my sisters and brother for their support and inspiration, and to my husband for his encouragement and motivation. I dedicate this work to my family who had faith in me every step in my journey.

ACKNOWLEDGEMENTS

"A psalm of praise. Of David. I will exalt You, my God the King; I will praise Your name for ever and ever." Psalm 145:1. I always lean on You and You never let me fall.

This fruitful work has only been possible because of the support from my thesis advisor Dr. Josette El Zaklit, thank you for believing in me. I thank both my advisor and my co-advisor Dr. Gale Craviso, for their boundless effort and academic mentoring. You have always guided me and kept me on track through my program.

I profoundly thank Dr. Normand Leblanc for being my mentor. You have been greatly helpful and always provided exquisite recommendations for my work.

I thank Dr. Bahram Parvin for being a part of my committee. Your questions and ideas are always inspiring.

I acknowledge all the people in our research group, who have helped me, each in their own way. I thank Dr. Lisha Yang for her great advices and for being always my lab tutor. I thank Dr. Yang and my colleagues Ruby Sukhraj, Sophia Pierce and Anitha Balaji for helping in the cell preparations. I thank Dr. Jihwan Yoon and my colleague Vasilii Mansurov for all their contributions in the coding of the LabVIEW and MATLAB programs to help us control the electrical setup and analyze the data. I thank all the undergraduate students for their volunteering in our labs. Thank you all for your devotion and for being the "Piston qui fait marcher la machine" of this research group.

This work was supported by NIH grant P20 GM103650, AFOSR MURI grant FA9550-15-1-0517, and in part by AFOSR grant FA9550-14-1-0018.

CONTENTS

LIST OF TABLES

LIST OF FIGURES

LIST OF ABBREVIATIONS

DBS	Deep brain stimulation
tDCS	Transcranial direct current stimulation
E-field	Electric field
NEP(s)	Nanosecond electric pulse(s)
NEpi	Norepinephrine
Epi	Epinephrine
ACh	Acetylcholine
nAChR	Nicotinic acetylcholine receptor
VGCC(s)	Voltage-gated Ca^{2+} channel(s)
$[Ca^{2+}]_i$	Intracellular calcium levels
TIRFM	Total internal reflection fluorescence microscopy
C_m	Membrane capacitance
DMPP	1,1-dimethyl-4-phenylpiperazinium
AO	Acridine orange dye
TMP	Transmembrane potential
CCD	Charge-coupled device
PS	Phosphatidylserine
FITC	Fluorescein isothiocyanate
HBSS	Hank’s balanced salt solution
BSA	Bovine serum albumin
BSS	Balanced salt solution

EGTA	Ethylene glycol-bis(β-aminoethyl ether)-N,N,N’,N’-tetraacetic acid
LAS X	Leica Application Suite X
ROI(s)	Region of interest(s)
SE	Standard error
$V_{max\ input}$	Input Voltage amplitude
$FWHM_{input}$	Input full width at half maximum
V_{max}	Measured voltage amplitude
FWHM	Measured full width at half maximum
TPS	Transient Plasma Systems
FFT	Fast Fourier Transform
f	Frequency

Chapter 1. INTRODUCTION

1.1 Nanosecond duration electric pulses serve as a potential novel stimulus for neurosecretion

Electrical stimulation of the brain is used as a treatment strategy for various neurological diseases and disorders. For example, deep brain stimulation (DBS) is employed to treat several neurological diseases such as dystonia, Parkinson's disease and obsessive-compulsive disorder [***1, 2***]. DBS is achieved by surgically implanting electrodes deep inside the brain where microsecond duration electric pulses are delivered to targeted areas. Non-invasive techniques such as transcranial direct current stimulation (tDCS) hold promise for modulating cortical excitability, resulting in an anti-depressive effect [***3***]. In tDCS, electrodes are placed on the head without the need for invasive surgery. Yet, due to the large electrode size, tDCS can stimulate adjacent regions of the targets [***4***], which makes it less focused/specific than DBS. Electrical stimulation of the brain has been effectively employed to improve the symptoms in several neurological disorders, however the existing applications for electrical stimulation cannot be non-invasive and highly confined to small regions of the brain, at the same time.

Our research group is investigating the potential of a new type of bioelectrical stimulus, high electric (E)-field intensity (> 1 MV/m), ultrashort nanosecond electric pulses (NEPs) (< 10 ns), to be used as a non-invasive and targeted technique for neuromodulation. Due to their high frequency content and ultrashort duration, NEPs offer the opportunity to transfer the electrical energy to a small, focused area deep into biological tissues. Thus, it is theoretically possible to use wideband antennas to launch and focus ultrashort electric pulses to tissue, thereby providing targeted and non-invasive electrostimulation.

A comprehensive understanding of how nanosecond pulses interact with biological cells is essential for developing therapeutic applications based on this novel stimulus. For this reason, our group has been exploring the effects of NEPs on neuroendocrine adrenal chromaffin cells, a well-characterized model of neural type/neurosecretory cells.

1.2 Adrenal chromaffin cells, a model of neurosecretion

1.2.1 Biology of chromaffin cells

Adrenal chromaffin cells are neuroendocrine cells that are found in the medulla of adrenal glands, which are located on the top of the kidneys as shown in **Error! Reference source not found.** based on the schematic from [***5***]. These specialized cells produce, store and secrete into the blood stream a complex mixture of compounds, which include the catecholamines norepinephrine (NEpi) and epinephrine (Epi), together with neuropeptides and other molecules [***6***].

Chromaffin cells are derived from the neural crest and share many similarities with sympathetic neurons. Mainly, they receive inputs from nerves originating in the spinal cord, decode the signal, then generate an output by releasing catecholamines and other molecules via the same Ca^{2+}-dependent process of exocytosis that occurs at nerve terminals [***7***].

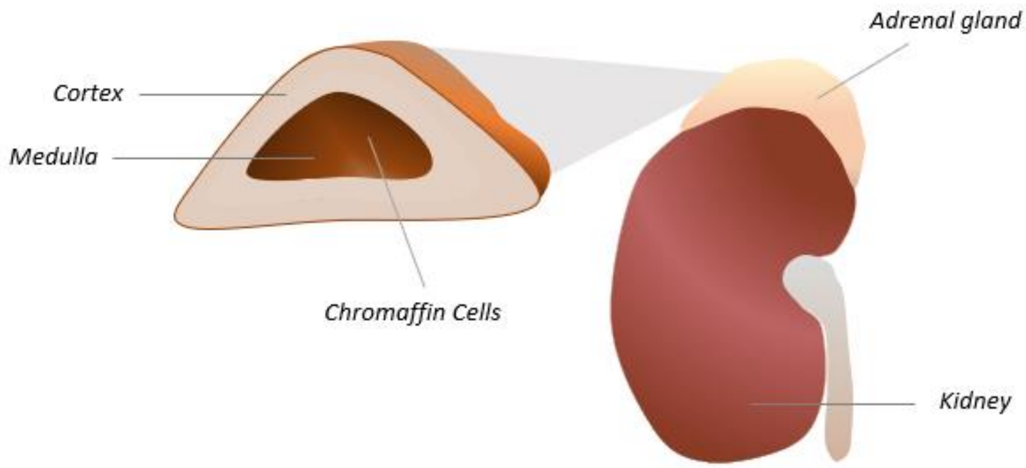

Figure 1.1 Diagram of the adrenal gland showing the localization of chromaffin cells in the adrenal medulla. The cortex surrounds the medulla that is composed of chromaffin cells which are responsible for catecholamine secretion into the blood vessels.

Chromaffin cells, isolated from bovine adrenal glands, are well-characterized, have a simple circular morphology (15 to 20 µm in diameter), and are easy to maintain in culture. A single chromaffin cell contains a large number of cellular organelles that contain the catecholamines and other compounds, the secretory granules, which occupy about 30% of the volume of the cell. Plattner et al. 1997, reported using electron microscopy that chromaffin cells present an abundant and homogeneous distribution of secretory granules in the dense core, as shown in Figure 1.2 [***8***]. Upon stimulation, these secretory granules fuse with the cell membrane and secrete their contents into the blood stream. For these reasons, isolated chromaffin cells are the ideal model to use to characterize mechanisms underlying stimulus-secretion coupling [***9, 10***].

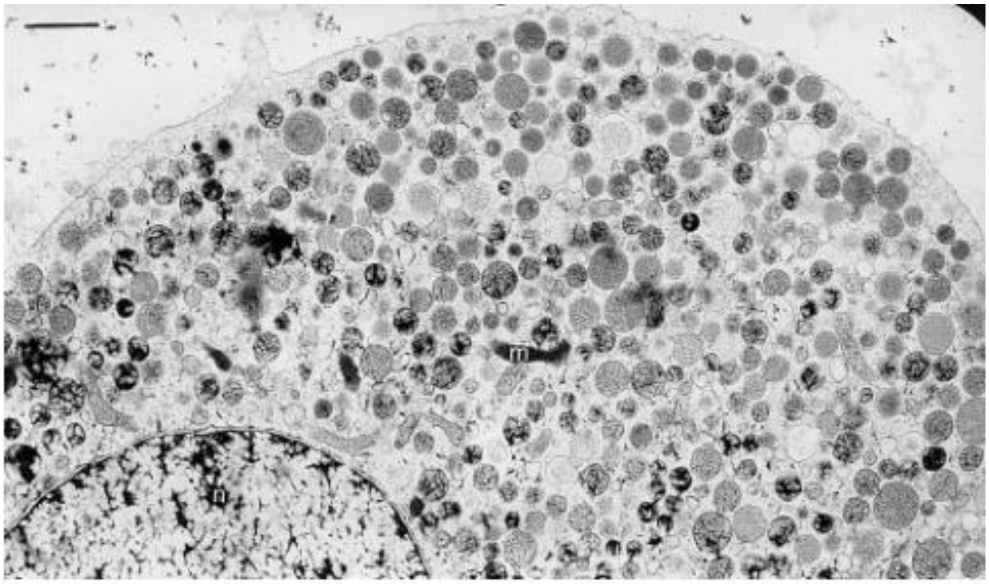

Figure 1.2 Electron micrograph of a single chromaffin cell showing the abundant and homogeneous distribution of the secretory granules in the dense core. Reprinted with permission from ©1997 Plattner et al [***8***]. Originally published in *The Journal of cell biology*, 10.1083/jcb.139.7.1709. The scale bar represents 1 μm.

1.2.2 Physiological stimulus for evoking catecholamine release

Chromaffin cells are innervated by the splanchnic nerve originating in the spinal cord. The sympathetic nerves tonically release acetylcholine (ACh) that binds to nicotinic acetylcholine receptors (nAChR) on the membrane of chromaffin cells. These receptors are ligand-gated, non-selective cation channels permeable to Na^+ and Ca^{2+}. Upon activation, nAChRs allow Na^+ to enter the cell causing membrane depolarization, voltage-gated Ca^{2+} channels (VGCCs) activation, Ca^{2+} influx, and the exocytotic release of catecholamines (Figure 1.3). During stress, ACh release increases causing a surge of catecholamines into the blood that triggers the "fight-or-flight" response [***11***].

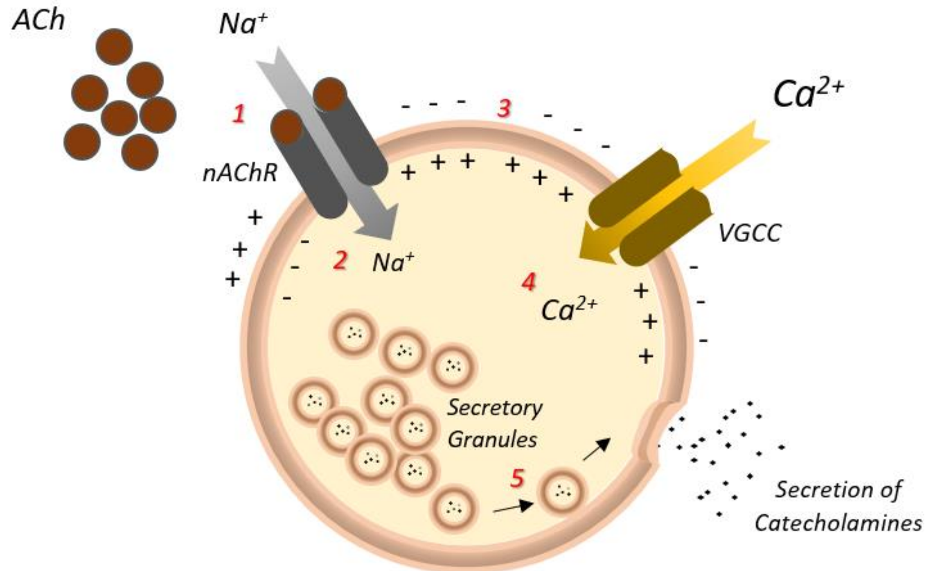

Figure 1.3 Schematic of Ca^{2+}-mediated exocytosis in chromaffin cells *in vivo* showing: 1) ACh binding to the nAChR, 2) Na^{+} influx into the cytoplasm, 3) membrane depolarization 4) Ca^{2+} influx through VGCCs, 5) Ca^{2+}-dependent granule fusion causing exocytosis and secretion of catecholamines.

1.3 Real-time monitoring of exocytosis

Exocytosis is the Ca^{2+}-dependent process by which the content of a secretory granule is released to the outside of the cell through fusion of the granule membrane with the cell membrane [***12, 13***]. Because Ca^{2+} influx through VGCCs is the trigger for exocytosis, monitoring changes in intracellular calcium levels ($[Ca^{2+}]_i$) in real-time has been used as an indirect way to monitor exocytosis in cells exposed to a stimulus.

A technique that was developed to directly measure catecholamine release in real-time is single cell amperometry [***14***]. A carbon fiber microelectrode is positioned near the cell membrane and held at a positive potential which causes the oxidation of the released Epi and NEpi as shown in Figure 1.4. The electrons produced by the oxidation of catecholamines are then translated into amperometric (electrochemical) spikes that give information about the kinetics and the quantity of catecholamines released [***15***].

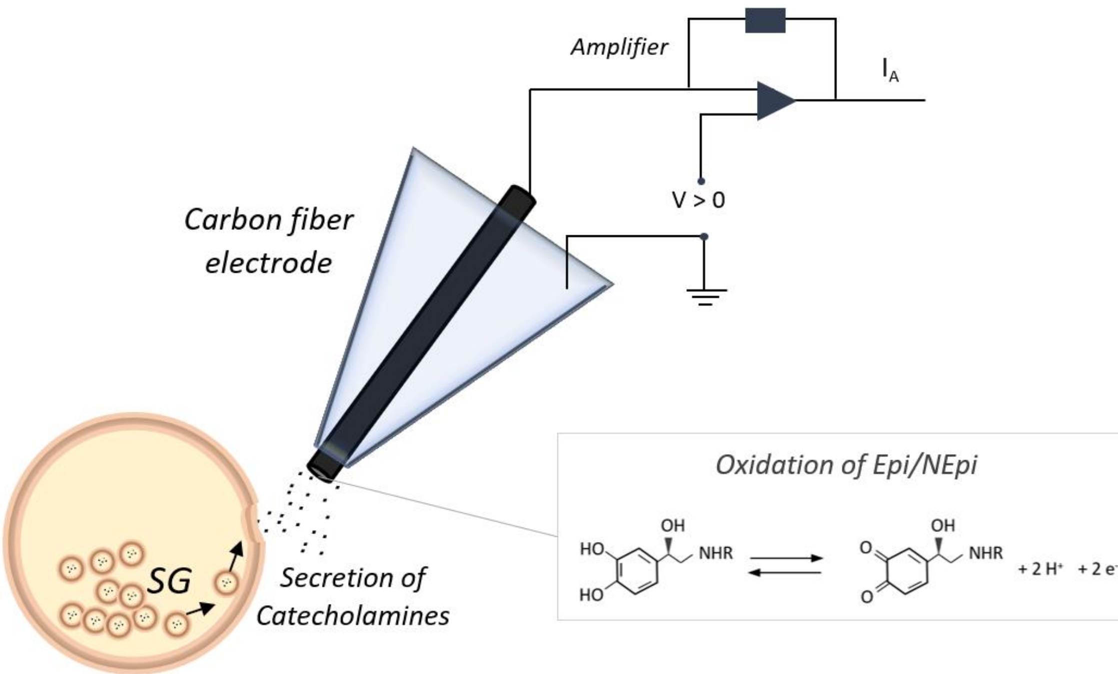

Figure 1.4 Schematic showing the measurement of catecholamine release using carbon-fiber amperometry. (A) shows the carbon fiber electrode placed in close proximity of a cell and held at a positive potential. During exocytosis, the secretory granules (SG) fuse with the plasma membrane and release their content. Exocytotic secretion is observed as a series of current spikes due to the detection of the electrons produced during the oxidation of Epi (R = methyl group) and NEpi (R = H) as shown in (B).

While the amperometry technique provides a direct quantitative approach to measure catecholamines release, total internal reflection fluorescence microscopy (TIRFM) is an optical technique that monitors in real-time exocytosis by visualizing the release of fluorescently labeled secretory granule contents [***16***]. In TIRFM, an incident laser beam arrives at the glass/oil interface at an angle higher than the critical one. At the glass interface, the light will totally reflect and return to the objective, which creates an evanescent wave that fades in the medium, as shown in the schematic in Figure 1.5.

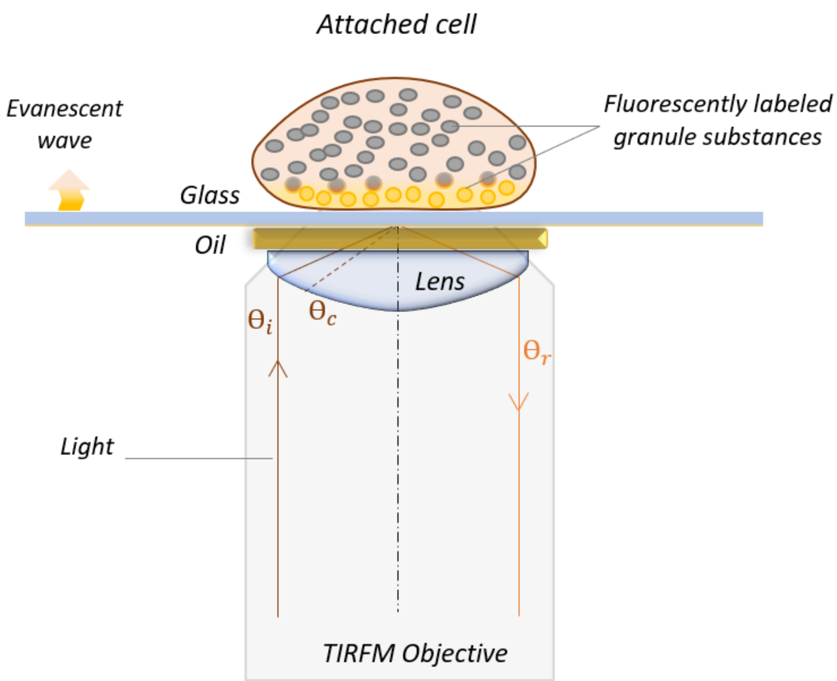

Figure 1.5 Schematic illustrating TIRFM. At an incident angle (θ_i) higher than the critical angle (θ_c), the light totally reflects along an equal angle (θ_r) and returns into the TIRFM objective. The light creates an evanescent wave at the glass/oil interface that illuminates a cell to a penetration depth of 100 to 200 nm.

Unlike wide field fluorescence, the evanescent wave in TIRFM only excites fluorescent molecules in secretory granules within a penetration depth of 100 to 200 nm from the glass. Thus, TIRFM allows the visualization of granule fusion events during exocytosis that occur at the cell membrane at the part of the cell attached to the glass.

Two other techniques have been developed in which the increase in cell membrane area due to the fusion of secretory granules is monitored in real-time as a representation of exocytotic activity. One is an electrophysiological technique that measures cell membrane capacitance (C_m) provided by the whole cell patch technique in voltage clamp mode (Figure 1.6). In response to a stimulus, C_m recordings show an increase in surface area as a function of time that is proportional to the fusion of secretory granules with the plasma membrane during exocytosis [***17***]. Such measurements have been employed separately or in combination with amperometric studies [***14***].

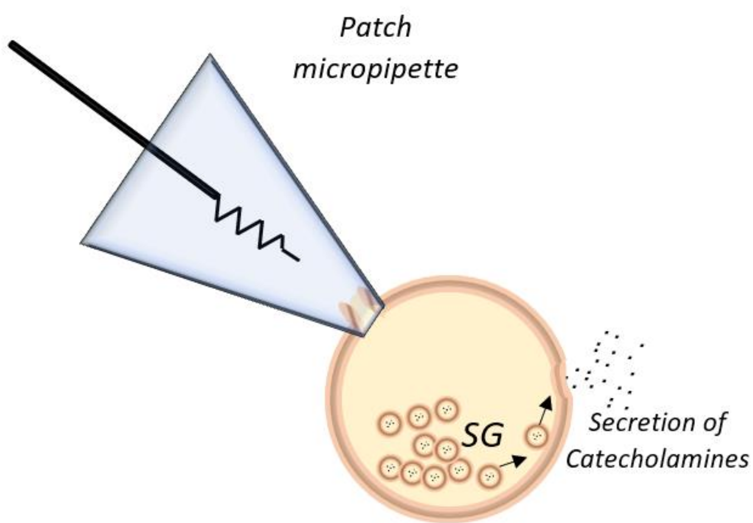

Figure 1.6 Schematic for whole-cell patch clamp for capacitance measurements. The graphic shows a single chromaffin cell during exocytosis where the secretory granules (SG) fuse with the lipid membrane and release catecholamines. The measurements detected by the electrode in the micropipette are amplified.

The second technique is a fluorescence imaging approach that uses the fluorescent styryl dye FM1-43 to monitor exocytosis in nerve terminals [***18***] and in chromaffin cells

[***19***]. FM1-43 reversibly labels the lipid membrane and cannot cross it due to its hydrophilic head group. During exocytosis, FM1-43 yields a fluorescent signal that increases proportionally to fusion of the secretory vesicles/granules with the plasma membrane. In this project, we used FM1-43 to examine in real-time the exocytotic activity of chromaffin cells in response to a depolarizing stimulus (high [K^+]) or to the application of NEPs. Section 1.5 of this chapter discusses in detail the use of FM1-43 as an indicator of exocytosis in adrenal chromaffin cells.

1.4 Effects of 5 ns electric pulses on bovine adrenal chromaffin cells

1.4.1 5 ns pulses induce Ca^{2+} entry into cells that in turn triggers catecholamine release

For over a decade, our group has been investigating the effect of 5 ns, 5-6 MV/m pulses on adrenal chromaffin cells. Craviso et al. 2009 showed that a single 5 ns, 5 MV/m pulse causes entry of Ca^{2+} into the cells through different types of VGCCs, triggering exocytosis and secretion of catecholamines [***20***]. For the latter determination, chromaffin cells were placed in electroporation cuvettes where they were exposed to a 5 ns, 5 MV/m pulse. Immediately after the E-field exposure, the cuvettes were cooled on ice to stop secretion, and the cells pelleted in the cuvettes by centrifugation. Aliquots of the supernatant fraction were analyzed for the amount of released Epi and NEpi by high performance liquid chromatography coupled with electrochemical detection as described in [***21***]. Similarly to the catecholamine release evoked by the nicotinic receptor agonist 1,1-dimethyl-4-phenylpiperazinium (DMPP), a single NEP induced catecholamine release that was dependent to the influx of Ca^{2+} via VGCCs [***20***].

On a subsequent study, Craviso et al. 2010 reported that NEP effects on the intracellular $[Ca^{2+}]_i$ were dependent on extracellular Na^+. That is Na^+ entry into the cells was required to activate multiple types of VGCCs (L-, N-, and P\Q-type), responsible for the Ca^{2+} entry. Based on the results and the lack of involvement of voltage-gated Na^+ channels [***22***], it was hypothesized that the pathway for Na^+ influx might be either membrane permeabilization that may involve lipid nanopores formed in the cell membrane [***22, 23***] or non-selective protein ion channels [***22***].

1.4.2 TIRFM imaging of chromaffin cells stimulated by 5 ns pulses show a delay in exocytosis

In Craviso et al. 2009, catecholamine release was quantified minutes after NEP application [***20***]. However, in a more recent study (unpublished data), exocytosis was monitored in real-time by imaging cells in which secretory granules were labeled with the fluorescent dye acridine orange (AO) using TIRFM. The time course of the changes in $[Ca^{2+}]_i$ as well as exocytotic events were investigated after the application of two different types of stimuli: a train of ten, brief applications of the nicotinic receptor agonist DMPP and a train of ten, 5 ns, 5 MV/m pulses. Both stimuli were delivered at 1 Hz. Although both stimuli caused an instantaneous rise in $[Ca^{2+}]_i$, exocytosis occurred with a delay of several seconds after initiation of the NEP train, contrasting with DMPP stimulation that caused exocytosis to occur as soon as the train of DMPP applications started. Thus, relative to receptor agonist stimulation, NEPs may be causing effects on the plasma membrane that affect the time course of exocytosis.

Interestingly, a recent study by Henkel et al. 2019 used FM1-43 to monitor the exocytotic activity of neonatal hippocampal neurons in response to electrical stimulation (1 ms bipolar rectangular current pulses of 50 mA at 30 Hz for 20 s delivered with two platinum wires 1 cm apart) [***24***]. Although a different electrical exposure system was used, their findings were similar to what we recently found with TIRFM. By measuring FM1-43 release from pre-labeled synapses as a measure of exocytosis, the researchers reported a delay in exocytotic activity in a sub-population of the synapses. That is, despite an immediate influx of Ca^{2+}, some synapses were completely inactive for a few seconds after the electric stimulation. Both the mean delay time and the percentage of the delayed synapses were higher when the frequency of the stimulation was decreased from 30 Hz to 10 Hz. Further investigation suggested that the mechanism for the delay was due to “kiss and run” exocytosis. As shown in Figure 1.7, during the “kiss and run” mode, synaptic vesicles transiently fuse with the membrane in the shape of an omega structure (Ω), forming narrow pores instead of full fusion and complete loss of the shape in case of the “full collapse” exocytosis. During the “kiss and run” mode, FM1-43 molecules (size ~ 1.5 nm) could not escape the synaptic vesicles because of the small sizes of the fusion pores. This demonstrated that the observed delay was associated with fusion pore expansion kinetics [***24***].

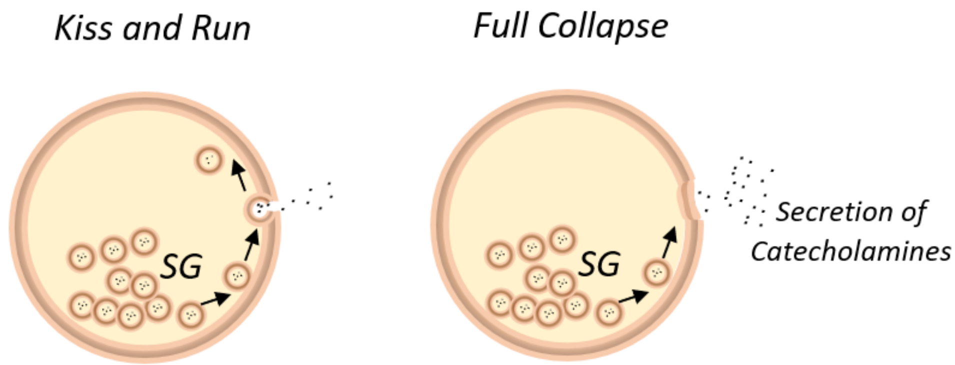

Figure 1.7 Schematic showing the difference between the "kiss and run" (left) and "full collapse" (right) modes of exocytosis. In the "kiss and run" mode, the secretory granules (SG) transiently fuse with the plasmalemma in an Ω shape unlike the "full collapse" exocytosis where the granules fully fuse with the membrane and completely lose their shape.

Given that TIRFM monitoring of exocytosis evoked by NEP stimulation of chromaffin cells indicated that exocytosis occurred with a delay of several seconds, the goal of the present study was to further investigate the kinetics of exocytosis in cells stimulated a similar train of ten NEPs applied at different frequencies. Because TIRFM visualizes the secretory activity only at a small patch of the cell membrane, we used a complementary approach to monitor exocytosis in response to the application of NEPs, using the fluorescent styryl dye, FM1-43, which is considered an effective approach to study cumulative exocytotic events occurring over the surface of the cell [***19, 25***]. Examining the time course of exocytotic activity using FM1-43 would allow us to investigate any possible delay of exocytosis following the application of NEPs.

1.5 The use of FM1-43 as a complementary approach to study exocytotic events

1.5.1 FM1-43, a lipid membrane marker

The chemical structure of FM1-43 (N-(3-Triethylammoniumpropyl)-4-(4-(dibutyl-amino) styryl) pyridinium dibromide) is depicted in Figure 1.87. FM1-43 is an amphiphilic molecule composed of two parts linked with a double-bond bridge: A) a di-cationic hydrophilic head that makes the dye non-permeant across the lipid membrane because it contains a permanent positive charge due to the presence of ammonium (valence +2), and B) a hydrophobic tail consisting of four carbon atoms that incorporates within lipid structures with a reversible and fast association (in the order of milliseconds).

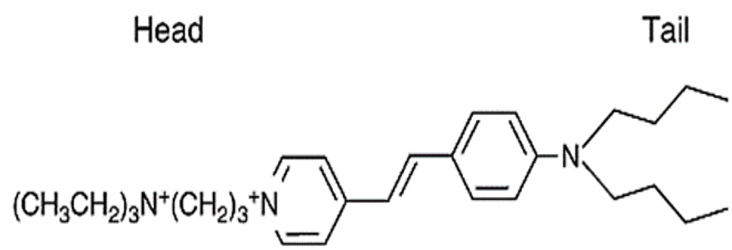

Figure 1.8 Chemical structure of FM1-43. Unlike the hydrophilic head with two ammonium cations, the hydrophobic tail with long carbon chains can bind with lipid structures in a reversible association [***26***].

The staining process of this FM dye lies on the fact that once its lipophilic tail partitions into the lipid membrane, the quantum yield of the fluorophore increases by 350 times [***27***]. Kay et al. 1999 indicated that once bound to the hydrophobic environment, the chemical structure of the fluorophore becomes spatially stable. This transformation drastically increases the radiative transitions resulting in the significant emission of light [***28***].

FM styryl dyes are soluble in aqueous medium and non-toxic to biological cells. Free FM1-43 molecules are non-fluorescent in the external aqueous solution surrounding the cells. The dye molecules become fluorescent only when their tails partition into the outer leaflet of the lipid membranes. Their association and dissociation from lipid membranes are insensitive to pH [***29***].

1.5.2 **FM1-43, a useful tool to monitor exocytosis**

Upon stimulation, secretory granules fuse with the plasma membrane of chromaffin cells resulting in exocytosis. Figure 1.9 shows that the pore forming during the fusion of secretory granules allows free FM1-43 molecules in the extracellular solution surrounding the cells to bind to the added lipid membrane and fluoresce. Thus, the fluorescence signal of the labeled cell increases proportionally to the increase in membrane surface due to exocytosis. The total fluorescent signal is then the combination of the baseline labeling level with the added membrane due to exocytosis.

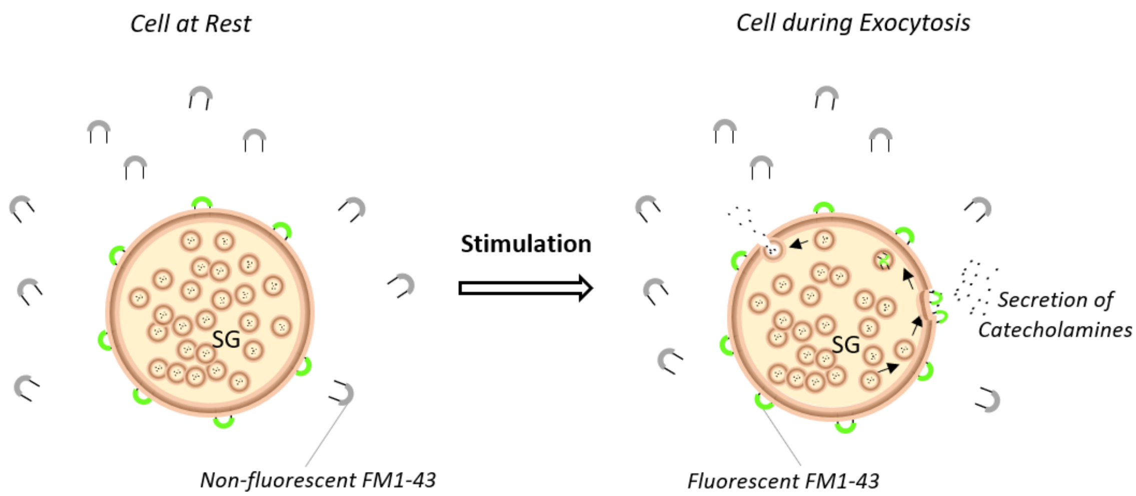

Figure 1.9 Mechanism of action of FM1-43. During exocytosis, the free FM1-43 molecules in the bathing solution are able to incorporate into lipid structure added to the membrane by the fused secretory granules (SG). This results in an increase in fluorescence relative to the basal labeling of the lipid membrane.

The properties of FM1-43 dye make it an ideal probe for visualizing lipid membranes and their exocytotic activity in excitable chromaffin cells [***26***] and has been used by many groups for this purpose as well as to study endocytosis. For example, by simultaneously using the patch clamp technique to monitor C_m and FM1-43 to label the membrane, Smith and Betz, 1996 studied the ability of FM1-43 to monitor exocytosis independently from endocytosis in bovine chromaffin cells [***19***] in response to a depolarizing pulse (from -90 mV to 0 mV for 1 second) or a stronger stimulus like 50 mM Ca^{2+} in the patch pipette. They demonstrated that both cell capacitance and FM1-43 fluorescence increased at the same rate and magnitude in response to the stimuli. Only when endocytosis started, the changes in capacitance leveled off while FM1-43 fluorescence kept on increasing, a process associated with the internalization of FM1-43 molecules in the endosomes. Thus, limitation of using this dye is that the increase in cell fluorescence, after stimulation can reflect both exocytosis and endocytosis.

Studies like in Perez et al., 2007 and Rosa et al., 2011 also employed FM1-43 in mouse chromaffin cells as a marker of exocytosis. After labeling of chromaffin cell membranes with FM1-43, they found that a high [K^+] depolarizing stimulation caused an increase in cell fluorescence that reflected the increase in cell surface due to the fusion of secretory granules with the plasma membrane during exocytosis [***30, 31***]. The level of fluorescence increased after the first stimulation and reached a higher plateau reflecting a measurement for exocytosis. The labeled membrane was only destained after washing or stimulating the cells with a dye-free solution.

1.5.3 FM1-43, an indicator of membrane potential change

In addition to its ability to monitor exocytosis, FM1-43 has been reported to be sensitive to transmembrane potential changes (TMP), which means that changes in FM1-43 fluorescence occur upon a change in TMP. A detailed study of several voltage sensitive dyes, including FM1-43, investigated the changes in the emission spectra of voltage sensitive dyes during action potentials in the mammalian neurohypophysis [***32***]. The difference between the fluorescence during an action potential and the one at rest was measured using a standard fiber-optically connected charge-coupled device (CCD) array detector. The study showed that during the application of a depolarizing stimulus, the TMP change during the action potential manifested a decrease in the amplitude of fluorescence of the FM1-43 dye, caused by a shift in the emission spectrum relative to its spectrum at the resting state.

Using confocal microscopy, Smith and Betz, 1996 reported a decrease in fluorescence of FM1-43 labeled mouse chromaffin cell membrane in response to an electrical stimulus (a pulse of 1 s duration from – 90 mV to 0 mV). This decrease reflected the sensitivity of the dye to detect membrane potential changes that occurred during the stimulus, which was around 3.4% per 100 mV [***19***]. Similarly, Neves et al, 1999 showed that a rapid change in FM1-43 fluorescence was sensitive to the membrane potential in bipolar neurons from goldfish retina (reported as 7.8% per 100 mV). They found that in response to a hyperpolarizing stimulus (5 s duration square pulse from – 50 mV to – 85 mV), a higher level of fluorescence of the FM1-43 labeled neurons was detected right at the rising edge of the stimulus, which persisted during the 5 s hyperpolarization. The original level of fluorescence was retrieved when neurons were depolarized at the falling edge of that stimulus [***33***]. Taken as a whole, these results demonstrate that a depolarizing stimulus causes a decrease in FM1-43 fluorescence whereas a hyperpolarizing stimulus causes an enhanced FM1-43 fluorescence.

1.5.4 FM1-43, a marker for phosphatidylserine externalization

The lipid membrane in healthy cells is known to have an asymmetric distribution of phospholipids, such that phosphatidylserine (PS) usually resides on the inner leaflet of the plasmalemma in normal cells. However, PS is externalized on the surface of apoptotic cells [***34***] as well as non-apoptotic cells as reported during the activation of platelets [***35***].

Moreover, in neuroendocrine chromaffin cells, PS redistribution has been reported to accompany Ca^{2+}-dependent exocytosis [***36, 37***]. PS translocation occurs at the vicinity of the secretory granule fusion sites due to the activity of the phospholipid scramblase-1 [***37***].

Usually, PS externalization is monitored using the specific PS marker Annexin-V in a Ca^{2+}-dependent manner [***38***]. Interestingly, the lipid membrane marker FM1-43 was also reported to be sensitive to PS scrambling independently of Ca^{2+} in Jurkat human leukaemic T-cells [***39***].

Because of its ability to detect PS externalization, FM1-43 was used in studies investigating the effects of E-field exposure on the plasma membrane. Vernier et al. 2006, used Annexin-V in parallel with FM1-43 to demonstrate the PS externalization occurring in RPMI 8226 human multiple myeloma cells exposed to multiple 4 ns, 8 MV/m pulses [***40***]. In a subsequent study using FM1-43, the researchers showed that thirty 4 ns, 8 MV/m pulses lead to the translocation of PS from the inner leaflet to the outer leaflet of the lipid bilayer in Jurkat T lymphoblasts [***41***]. PS translocation is hypothesized to be possibly happening via a lateral diffusion in the forming nanopores due to the E-field exposure [***40, 41***]. Furthermore, PS externalization was occurring preferably on the anode facing part of the cells which was interpreted by a possible attraction of the negatively charged PS by the anode (positive electrode). Such perturbations to the membrane, are conditioned by the intensity, number and duration of the delivered pulses in a cell-type selective manner [***42***].

In summary, there is a possibility that PS scrambling occurs during or after the application of NEPs, which can be symptomatic of apoptosis, an undesired effect of E-field exposure of biological cells that our research group has not yet investigated in chromaffin cells exposed to NEPs of ultrashort duration (5 ns). Additionally, since the externalization of PS to the outer leaflet of the membrane can be detected using the styryl dye FM1-43, this project will investigate whether this membrane disturbance occurs in response to the NEPs exposure using the specific PS fluorescent marker, lactadherin-FITC (i.e. fluorescein isothiocyanate).

1.6 Objectives of the project

The main objective of this project is to investigate exocytosis in adrenal chromaffin cells stimulated with 5 ns electric pulses. The experimental approach is to monitor the exocytotic responses in real-time using the fluorescent styryl dye FM1-43. The main question being addressed is whether a delay in exocytosis, like the one observed in the TIRFM experiments, would similarly be observed using this complementary approach. This is important because it may reveal novel effects of the application of NEPs that will be helpful in the future, especially in the design for biomedical devices to deliver NEPs as a modality for evoking neurosecretion.

After testing the parameters of the delivered pulses using our new bipolar pulse generator, a thorough analysis was performed to determine the E-field amplitude needed to stimulate a rise in $[Ca^{2+}]i$ in chromaffin cells labeled with the Ca^{2+} indicator Calcium Green-1. Next, the conditions for labeling the cells with FM1-43 were optimized, followed by experiments in which we investigated the effects of a depolarizing stimulus, 56 mM $[K^+]$, on FM1-43 fluorescence as a control. We then assessed the changes in FM1-43 fluorescence induced by applying one or more NEPs and explored the dependence of the responses to various pulse parameters such as the voltage amplitude and the frequency of the applied pulses.

Chapter 1 in this work provides an Introduction about the project and what is known about NEP stimulation of catecholamines secretion in isolated adrenal chromaffin cells. Chapter 2 is a detailed description of the Methods used. The Results of the experiments are presented in Chapter 3. Chapter 4 comprises the Discussion and Chapter 5 presents the Conclusions and Future Work.

Chapter 2. MATERIALS AND METHODS

In this project, wide field epifluorescence microscopy was used to monitor NEP-induced $[Ca^{2+}]_i$ rise and FM1-43 fluorescence changes. This chapter provides details on how chromaffin cells were prepared for experimentation, how the conditions for labeling the cell membranes with the FM1-43 dye were optimized, as well as a description of how the experiments were conducted, and the data analyzed. A detailed description of the NEP exposure system used to deliver pulses to the cells is also described.

2.1 Adrenal chromaffin cell isolation

Bovine chromaffin cells were isolated from the medulla of adrenal glands using the method described in Waymire et al., 1983 [***43***] and modified as in Hassan et al., 2002 [***44***]. Fresh adrenal glands were obtained from a local slaughterhouse (Wolfpack Meats, Reno, NV). Figure 2.1 shows a schematic that summarizes the chronological order of the steps taken to achieve the isolation of chromaffin cells from the bovine adrenal glands. Briefly, after trimming the fat off the adrenal glands, the outer cortex was removed by dissection. A plastic perfusion catheter was inserted into the main adreno-lumbar vein as shown in Figure 2.2, then secured in place using a surgical suture. To flush out red blood cells, the medulla was first perfused with a Ca^{2+}/Mg^{2+}-free Hank's balanced salt solution (HBSS) consisting of 137 mM NaCl, 5.37 mM KCl, 0.44 mM KH_2PO_4, 0.54 mM Na_2HPO_4, 4.17 mM $NaHCO_3$, 5.55 mM D-Glucose, 5 mM HEPES, 0.001% phenol red and 0.02% bovine serum albumin (BSA), pH 7.2, at room temperature for 5 minutes.

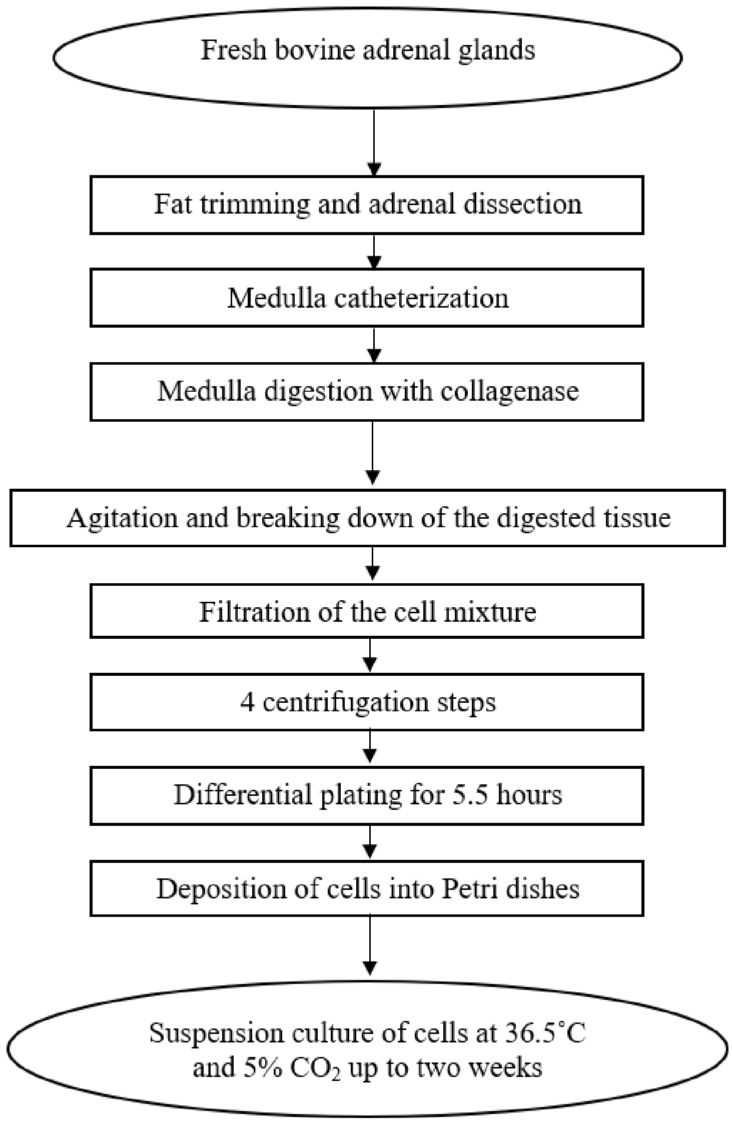

Figure 2.1 Diagram summarizing the steps taken to prepare chromaffin cells from fresh bovine adrenal glands. At the end of the preparation, chromaffin cells are maintained in culture at 36.5°C under a humidified atmosphere of 5% CO_2 up to two weeks, where they form small aggregates.

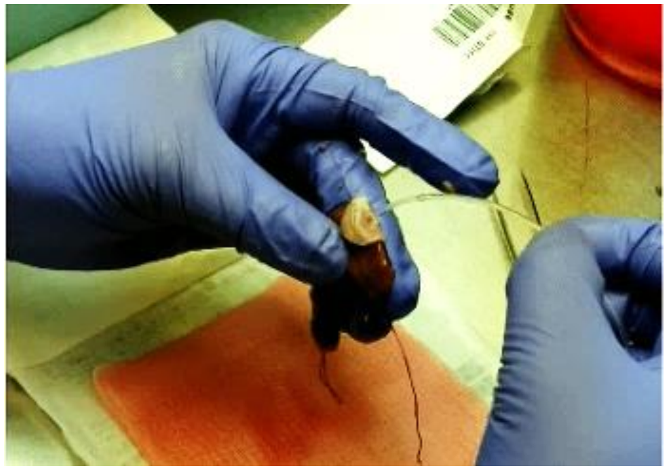

Figure 2.2 Catheterizing an adrenal medulla for perfusion. A small diameter plastic tubing was inserted into the adreno-lumbar vein of the dissected medulla then secured with a surgical suture to prepare the medulla for perfusion.

Next, the medulla was digested by perfusing HBSS containing collagenase B (0.05%) and 50 μM $CaCl_2$ for 30 to 45 minutes at 27-30 °C. The swollen medulla was then transferred into a glass beaker containing HBSS lacking collagenase. The digested tissue was then gently agitated against the walls of the beaker to break it down. The resulting cell suspension was filtered through a nylon mesh to remove tissue debris. The cell solution was then subjected to four centrifugation steps to separate chromaffin cells from any remaining red blood cells and debris. After the final centrifugation step, the cells were diluted in Ham's F-12 medium containing 10% bovine calf serum, 100 U/ml penicillin, 100 μg/ml streptomycin, 0.25 μg/ml fungizone, and 6 μg/ml cytosine arabinoside. After dilution, cells were placed into vented tissue culture flasks at an estimated concentration of 4×10^5 cells/ml and incubated at 36.5 °C under a humidified atmosphere of 5% CO_2 for 5.5 hours. This step allowed non-chromaffin cells to adhere to the bottom of the flasks whereas chromaffin cells stayed in suspension. At the end of the differential plating step, the cells were collected from each flask, distributed into 60 mm Petri dishes at a density of 1×10^5 cells/ml and maintained in suspension culture in the supplemented Hams' F12 medium at 36.5°C under a humidified atmosphere of 5% CO_2. Cells were used up until 2 weeks in culture.

2.2 Chromaffin cells dissociation and preparation for experiments

Chromaffin cells form large aggregates when in suspension culture. Thus, for all experiments, cell aggregates were dissociated into single cells with the protease dispase as previously described in Craviso, 2004 [***45***]. Briefly, protease dispase II (~ 18 U/ml) was added to the dish of cells, which were then incubated with the enzyme for at least 6 hours and no longer than 15 hours. The cells were then transferred into a conical tube and centrifuged at 30 x g for 10 minutes at room temperature. After centrifugation, the cell pellet was resuspended in Ca^{2+}/Mg^{2+}-free HBSS of the following composition: 145 mM NaCl, 5 mM KCl, 1.2 mM Na_2HPO_4, 10 mM D-Glucose, 15 mM HEPES, pH 7.4. The cells were incubated at 37 °C and the incubation was interrupted every 10 minutes to gently triturate the cells to facilitate dissociation. In short, the process of trituration and incubation was repeated 2 to 3 times until the dissociation was complete.

At the end, cell aggregates were fully dissociated into single cells or small clusters of 2 to 3 cells, and cells were plated onto fibronectin-coated glass-bottom dishes. Dishes of attached cells were kept in the incubator at 37 °C under a humidified atmosphere of 5% CO_2 and cells were used from 1 to 2 days after attachment.

2.3 Intracellular Ca^{2+} imaging

2.3.1 Preparing the cells for imaging

For Ca^{2+} imaging experiments, attached single cells were washed with balanced salt solution (BSS) of the following composition: 145 mM NaCl, 5 mM KCl, 1.2 mM NaH_2PO_4, 2 mM $CaCl_2$, 1.3 mM $MgCl_2$, 10 mM glucose, 15 mM HEPES with a pH of 7.4. Then cells were incubated with 1 µM of the cell permeant Ca^{2+}-sensitive fluorescent indicator Calcium Green-1, AM ($\lambda_{exc.}$ = 506 nm, $\lambda_{em.}$ = 531 nm) in BSS with 0.1% BSA for 45 minutes at 37 °C. At the end of the incubation, cells were washed twice with dye-free BSS lacking BSA. For experiments carried out under Ca^{2+}-free conditions, the BSS lacked Ca^{2+} and contained 1 mM ethylene glycol-bis(β-aminoethyl ether)-N,N,N',N'-tetraacetic acid (EGTA).

2.3.2 Imaging setup and analysis

The dish containing the Calcium Green-1-loaded cells was placed on the stage of an inverted DMi8 epifluorescence microscope (Leica Microsystems, Inc.) equipped with an electron multiplying CCD iXon Ultra 897 (Andor) camera. A Leica Application Suite X (LAS X) software was used to automatically control all the imaging parameters. All the experiments were performed at ambient room temperature using a 63 X dry objective.

The fluorophore was excited with a blue light ($\lambda_{exc.}$= 488 nm) illuminated by a Lambda DG4 Plus light source (Sutter Instruments) and the emitted light was detected with a FITC filter block (green emission). Ca^{2+} imaging sequences were captured at a frame rate of ~7 frames/s (150 ms exposure time). Acquired sequences of the cells before, during and after stimulus application were analyzed using LAS X software. The region of interest (ROI) included the entire cell. In all plots, cell-free background fluorescence intensity was subtracted from the fluorescence intensity of the cells ($F = F_{cell} - F_{background}$). The fluorescence intensity F was then normalized to the intensity value measured when the stimulus was applied (F_0) using a custom Excel file resulting in a normalized fluorescence of F/F_0.

2.4 Cell membrane labeling using the fluorescent styryl dye FM1-43

2.4.1 Optimizing the labeling protocol

To achieve the final labeling protocol, the first parameter that was optimized was the concentration of the dye used in the labeling solution. Concentrations reported in the literature for labeling bovine and mouse chromaffin cells ranged from 1 to 5 µM were previously reported [***19***, ***23, 27, 46***]. The first strategy that we used for labeling the cells was based on the protocol described in Perez et al. 2007 where mice chromaffin cells were preincubated for 15 minutes with 5 µM FM1-43 in a physiological salt solution (containing in mM: 145 NaCl, 5.6 KCl, 1.2 $MgCl_2$, 10 HEPES, 2 $CaCl_2$, and 10 dextrose) at room temperature. Cells were then washed for 30 minutes with dye-free bathing solution and incubated again in the presence of FM1-43 for another 15 minutes [***27***]. As the researchers indicated, the main objective of that long procedure was to eliminate the non-specific labeling and ensure that all cells reach a plateau at the end of the second incubation. Therefore, our first protocol (protocol #1) consisted of a simple incubation of the cells with FM1-43 in BSS to check for the quality of labeling of the cells. Cells were incubated for 10 minutes, which was the time needed to reach the plateau in cell fluorescence, as determined from imaging the cells using the microscope. We tried several FM1-43 concentrations ranging from 1 to 5 µM in BSS to examine the level of fluorescence and the appearance of the labeled cells. No non-specific staining was detected, however protocol #1 resulted in a low level of fluorescence at the end of the incubation period even when the concentration of the dye was increased up to 5 µM. In all cases, there was no significant enhancement in the contrast between the stained membrane and the background, which was the reason why we needed to try a labeling method other than cell incubation.

The second strategy that we used (protocol #2) consisted of cell perfusion with the labeling solution (i.e. BSS + FM1-43). To prepare the cells for perfusion, the dish containing attached cells was washed with BSS, then a plastic insert was fixed with grease to the bottom of the dish to create a perfusion chamber. The dish was next placed on the stage of an inverted Leica DMi8 microscope as shown in Figure 2.3. The inlet of the chamber was connected to a six-channel valve control perfusion system (Warner Instruments) shown in Figure 2.44, whilst the outlet tube was connected to a vacuum system to continuously carry the waste out of the chamber. All solutions were perfused at a flow rate of 0.9 ml/minute to 1.2 ml/minute.

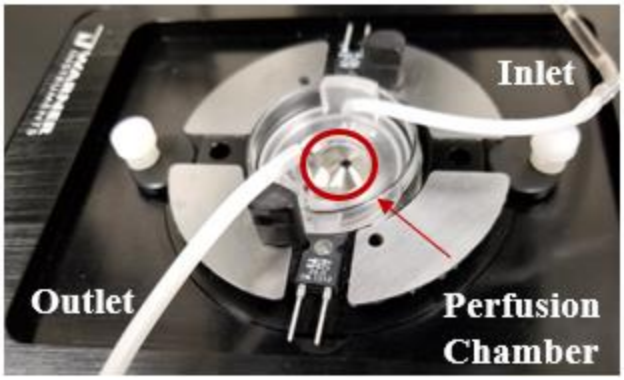

Figure 2.3 A 35 mm glass bottom dish occupied with the plastic insert and placed on the stage of the microscope.

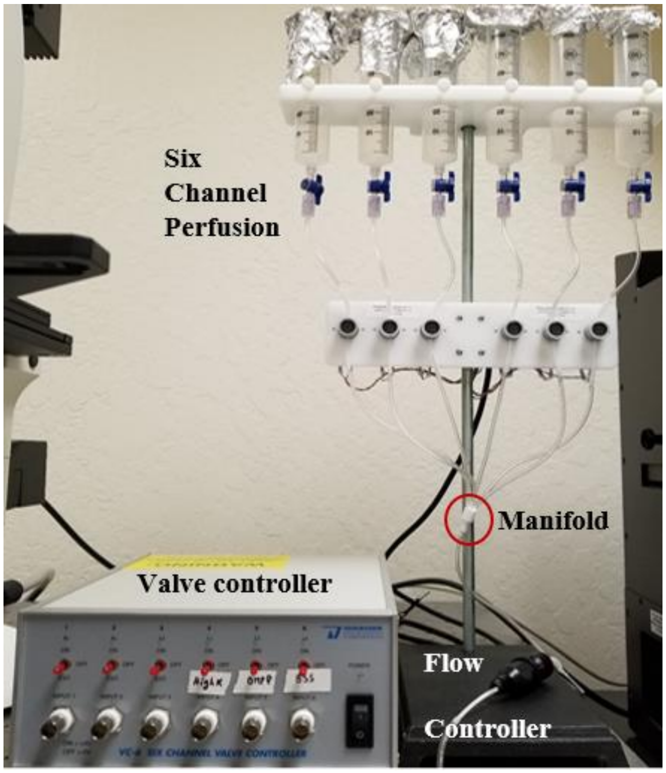

Figure 2.4 Photograph of the six channel perfusion system. The flow controller is connected to the inlet of the perfusion chamber with Tygon tubing.

Hence, to label cells with FM1-43 using the perfusion attached cells were first perfused with a dye-free BSS for 2 minutes, then with a BSS containing FM1-43 for 5 minutes, which was the time needed for the fluorescence on the membrane to reach a plateau. A diagram for labeling the cells with the dye is shown in Figure 2.5. The imaging sequence began when the perfusion of the labeling solution started, which required around 30 s to reach the dish.

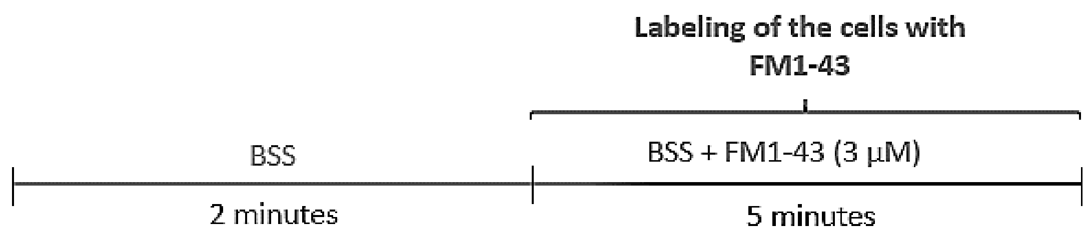

Figure 2.5 Schematic showing protocol # 2 used for monitoring the labeling of chromaffin cells with FM1-43 using a concentration of 3 µM.

Two concentrations of FM1-43 were used in this protocol, 3 and 5 µM. The appearance of the cells and the level of fluorescence was examined at the end of the cell labeling period (at ~ 5 min). Both concentrations resulted in a labeling with a high contrast between the stained membrane and the background. The final levels of fluorescence (F_{max}) achieved with different concentrations of the FM1-43 dye using incubation (protocol #1) and perfusion (protocol #2) were measured at the end of the labeling protocol then normalized to the initial fluorescence to obtain F_{max}/F_0. Figure 2.6 shows the fluorescence intensity versus FM1-43 concentration used to label the cells for each protocol.

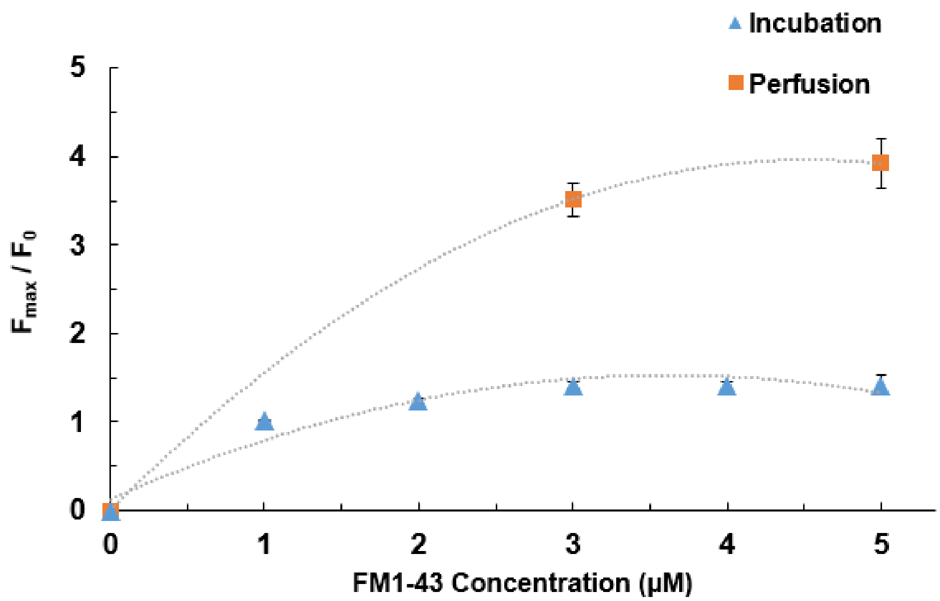

Figure 2.6 Comparison between the incubation (blue circles) and the perfusion (orange squares) protocols. Each point represents the fluorescence level measured at the end of each protocol and normalized to the initial fluorescence level F_0 at a single concentration of the FM1-43 dye.

Because protocol #2 using a 3 µM concentration of FM1-43 resulted in the most effective, shortest labeling time to achieve a high imaging contrast with low background to membrane signal to background ratio, this protocol was the one used in all FM1-43 experiments described in the Results section. Figure 2.7 displays an example of a single chromaffin cell labeled with 3 µM of FM1-43 using protocol #2.

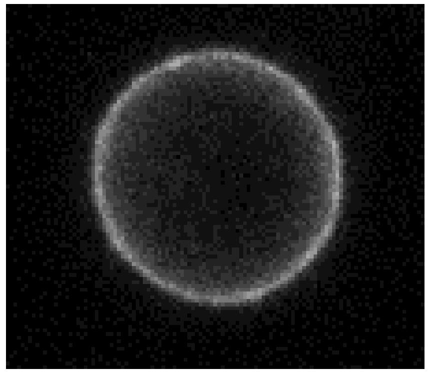

Figure 2.7 Example of a chromaffin cell labeled with 3 µM of FM1-43 for five minutes using the perfusion protocol. This fluorescence image was taken at the end of the labeling protocol shown in Figure 2.5.

2.4.2 **Imaging Setup**

As in Ca^{2+} imaging experiments, the microscope was equipped with an electron multiplying CCD iXon Ultra 897 (Andor) camera and LAS X software that automatically controls all the imaging parameters. FM1-43 experiments were performed using a 100 X oil objective. FM1-43 was excited with a blue light, $\lambda_{exc.}$ = 488 nm, and the emitted light was detected with the optical filter FITC designed for an emission wavelength of 530 nm, which covers the wavelengths at which FM1-43 molecules emit the light ($\lambda_{em.}$ = 580 nm, Figure 2.8). All FM1-43 sequences were captured at a frame rate of ~ 3 frames/s (300 ms exposure time). Cells were always monitored for at least 30 s before applying the depolarizing stimulus and for 15 s before applying the electrical stimulus. Imaging sequences had a total duration of at least 240 s in case of the depolarizing stimulus applied to cells via perfusion, and for 135 s in case of the electrical stimulation using NEPs.

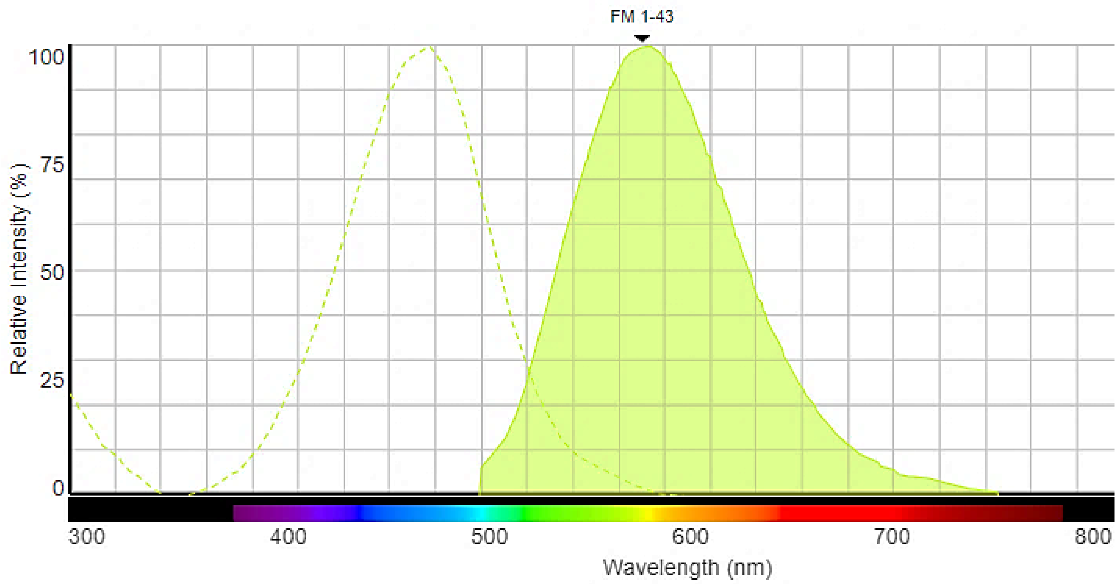

Figure 2.8 FM1-43 dye spectra. The broken line represents the excitation spectrum and the solid line refers to the emission spectrum of the dye. The peak emission intensity is around the wavelength of 580 nm [*47*].

2.4.3 **Image analysis**

All acquired image sequences of FM1-43-labeled cells were analyzed using LAS X software. To analyze the responses of FM1-43 labeled cells, three distinct image analysis techniques were performed to investigate the time courses of whole cell fluorescence, or fluorescence at distinctive parts of the cell membrane. Figure 2.9 shows the three different image analysis approaches used for monitoring the changes in fluorescence of stimulated cells:

A. In whole-cell fluorescence, an ROI was drawn over the entire surface of the cell.
B. Line profiles were measured by drawing rectangles of 5 µm in width and 25 µm in length passing through the cell along two orientations: 0˚ and 90˚.

This analysis was used to investigate any heterogeneous responses of the FM1-43 labeled membranes before and after cell stimulation and provided information on any dye internalization. A and B were used when a depolarizing as well as an electrical stimulus was applied to cells.

C. In the case of NEP application, four parts of the membrane were investigated relative to their position to the electrodes used to deliver the pulses. ROIs were represented as 2 μm width rectangles around the membrane of the cells and were referred to as “Cathode facing”, “Anode facing”, “Equator Left”, and “Equator Right”. These ROIs respectively reflect the fluorescence signals from the sides of the membrane facing the anode, the cathode, or away from the electrodes to the left and right.

For both A and C, the background fluorescence intensity was subtracted from the fluorescence intensity of the cells ($F = F_{cell} - F_{background}$) then normalized to the intensity value measured when the stimulus was applied (F/F_0). For the image analysis using the line profiles (in B), the fluorescence profile plots (F_{line}) were subtracted from the level of fluorescence detected outside of the cell at 0 μm, that correlates with the beginning of the drawn lines ($F_{0\,\mu m}$). The subtraction resulted in $F = F_{line} - F_{0\,\mu m}$ and was performed to set a reference for the fluorescence. A custom Excel file was used to automatically compute the final fluorescence of F and F/F_0 for all the fluorescence plots.

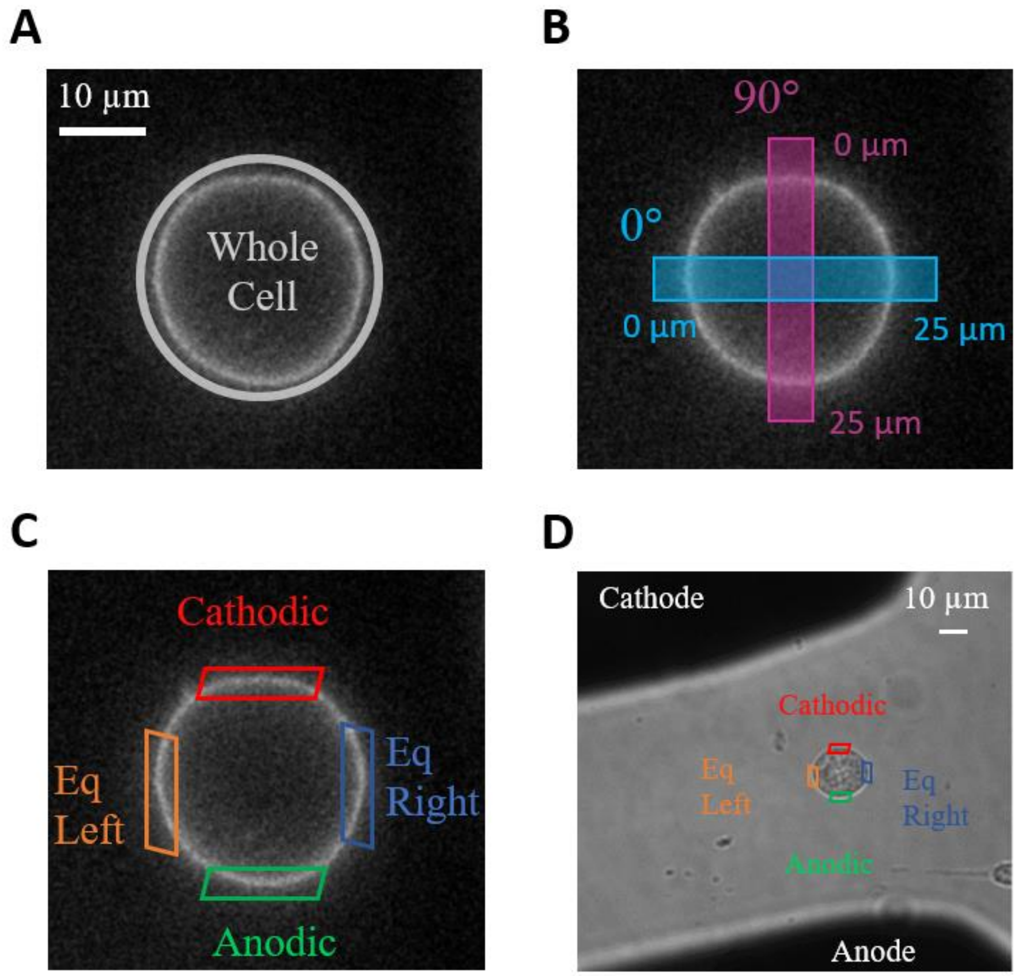

Figure 2.9 Image analysis techniques. (A) shows the whole cell fluorescence. (B) illustrates the orientations (0˚ and 90˚) at which the line profile plots were performed. (C) shows the parts of the membrane identified as "Cathodic", "Anodic", "Equator Left" and "Equator Right" relative to the electrodes as shown in the brightfield image in (D).

2.5 Depolarizing stimulus

A high [K^+] (56 mM [KCl]) solution was prepared by reducing NaCl accordingly to maintain isotonicity. At the end of the labeling protocol #2 previously described, the 56 mM K^+ BSS containing 3 µM of FM1-43 was continuously perfused to the cells to induce cell depolarization. All solutions were perfused at a rate of ~1 ml/minute. Fluorescence intensity changes were monitored before, during and after stimulus application. A time-course of the whole cell fluorescence as well as line profiles before and after stimulus application were generated.

2.6 Assessing PS externalization using Lactadherin-FITC

2.6.1 **Preparing the cells for imaging**

The fluorescent indicator lactadherin-FITC ($\lambda_{exc.}$ = 488 nm, $\lambda_{em.}$ = 530 nm) was used to measure PS externalization. Attached cells were washed with BSS then incubated in the dark with lactadherin-FITC for 10 minutes at room temperature using each of the following concentrations of the dye: 0.3, 0.87, or 2.61 µM [***48***].

At the end of the incubation period, cells were washed twice with dye-free BSS and the cells were then ready for imaging. All the experiments were done at room temperature and in the presence of extracellular Ca^{2+}.

2.6.2 **Imaging setup and analysis**

For PS imaging experiments, the dish containing lactadherin-FITC stained cells was placed on the stage of the inverted Leica DMi8 epifluorescence microscope equipped with an electron multiplying CCD iXon Ultra 897 (Andor) camera. LAS X software was used to automatically control all the imaging parameters. All PS imaging was done using a 63 X dry objective.

The fluorophore was excited with a blue light ($\lambda_{exc.}$= 488 nm) illuminated by a Lambda DG4 Plus light source (Sutter Instruments) and the emitted light was detected with a FITC filter block. All imaging sequences were captured at a frame rate of ~7 frames/s (150 ms exposure time), and acquired sequences of cells before, during and after stimulus application were analyzed using LAS X software. The ROIs were chosen around the whole cell as well as over its anode and cathode facing poles as shown respectively in (A) and (C) of Figure 2.9 to assess the time course of PS externalization due to NEP application. For these plots, cell-free background fluorescence intensity was subtracted from the fluorescence intensity of the cells ($F = F_{cell} – F_{background}$). The fluorescence intensity F was then normalized to the intensity value measured when the stimulus was applied (F_0) using a custom Excel file resulting in a normalized fluorescence of F/F_0.

2.7 Statistical analysis

All the experiments described in Chapter 3 were repeated at least twice and cells were taken from different cell preparations and on different days in culture. Data from different experiments were combined and the results were represented as the mean ± standard error (SE). An unpaired Student's *t* test was used to determine the statistical significance between two means of different groups. ANOVA test was performed to assess the variance among the means of different groups. p values ≤ 0.05 were considered statistically significant.

2.8 NEP exposure setup

This project investigated the effects of two different types of NEPs on FM1-43 fluorescence. Some experiments used multiple 30 ns pulses as the cell stimulus. Later studies examined the effects of 5 ns pulses applied at various E-field amplitudes.

2.8.1 Delivery of 30 ns electric pulses

When NEP experiments first got performed, a 10-100 ns variable amplitude (± 1-5 KV) bipolar pulse generator (FID GmbH-Germany) was the only pulse generator available in our laboratory. We used this pulse generator to deliver the 30 ns duration pulses to attached cells. All 30 ns pulses were applied at a voltage amplitude of 1,000 V.

2.8.2 Delivery of the 5 ns electric pulses

The majority of the studies carried out in this project used a 2-10 ns variable amplitude (± 1-5 KV) bipolar pulse generator (FID GmbH-Germany) was used to deliver 5 ns duration pulses to the cells. Pulses were applied via a pair of custom-made tungsten rod electrodes (127 µm diameter obtained from A-M Systems, Sequim, WA) soldered to a BNC connector. Figure 2.10 shows the electrodes used to deliver the pulses to cells. The tips of the tungsten electrodes were separated by a 100 µm gap and positioned at 40 µm above the bottom of the dish using a micromanipulator (MP 224, Sutter Instruments), with the cell placed in between the electrode tips (see Figure 2.9 D).

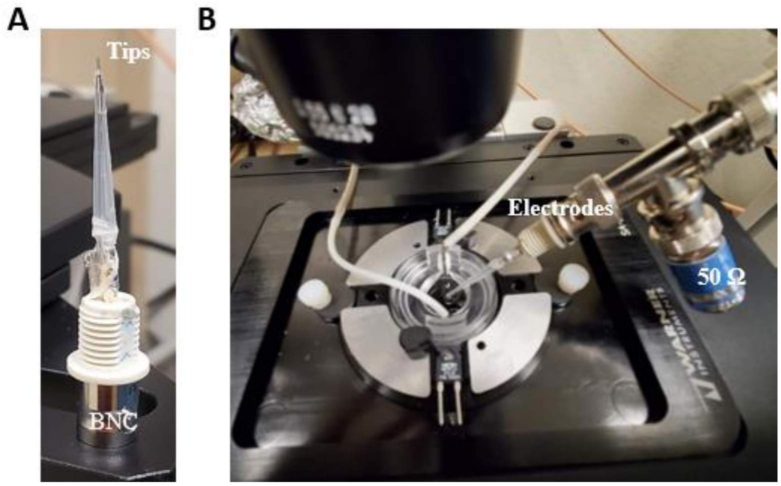

Figure 2.10 Photographs of the electrodes used to deliver NEPs to cells. (A) is a close-up of the electrodes soldered to a BNC connector. (B) shows the electrodes immersed in the glass-bottom dish. At the T-connection is connected the 50 Ω terminator.

Figure 2.11 is a schematic of the pulse generator showing all the connections made to generate, measure, and deliver NEPs to cells attached on a glass-bottom dish. Control knobs on the front panel of the pulse generator adjust the input pulse voltage amplitude ($V_{max\ input}$) and the input pulse full width at half maximum ($FWHM_{input}$) of the pulses. A high-voltage tap-off (243 HMFNFP-100, Barth electronics) was connected to the output of the pulse generator. The role of the tap-off was to attenuate, from one end, the signal going from the output of the pulse generator into the oscilloscope (TDS 3054B, 500 MHz, Tektronix) by a factor of 100. An additional -20 dB attenuator was added at the input of the oscilloscope to further attenuate the signal by a factor of 10. The oscilloscope allowed us to measure the output parameters of the delivered pulses, such as the measured voltage amplitude (V_{max}) and the measured duration at full width at half maximum (FWHM). The oscilloscope was also connected to a customized program written in LabVIEW that allowed us to capture the pulse traces applied to cells during experiments and store them on a computer. Acquisition of the traces was possible when a single exposure was applied and in the case of multiple pulses, only the first trace was stored. To deliver the high voltage pulses to the cells, the other end of the tap-off was connected to the electrodes via a T-connector associated with a 50 Ω high voltage terminator to match the impedance at the output of the pulse generator.

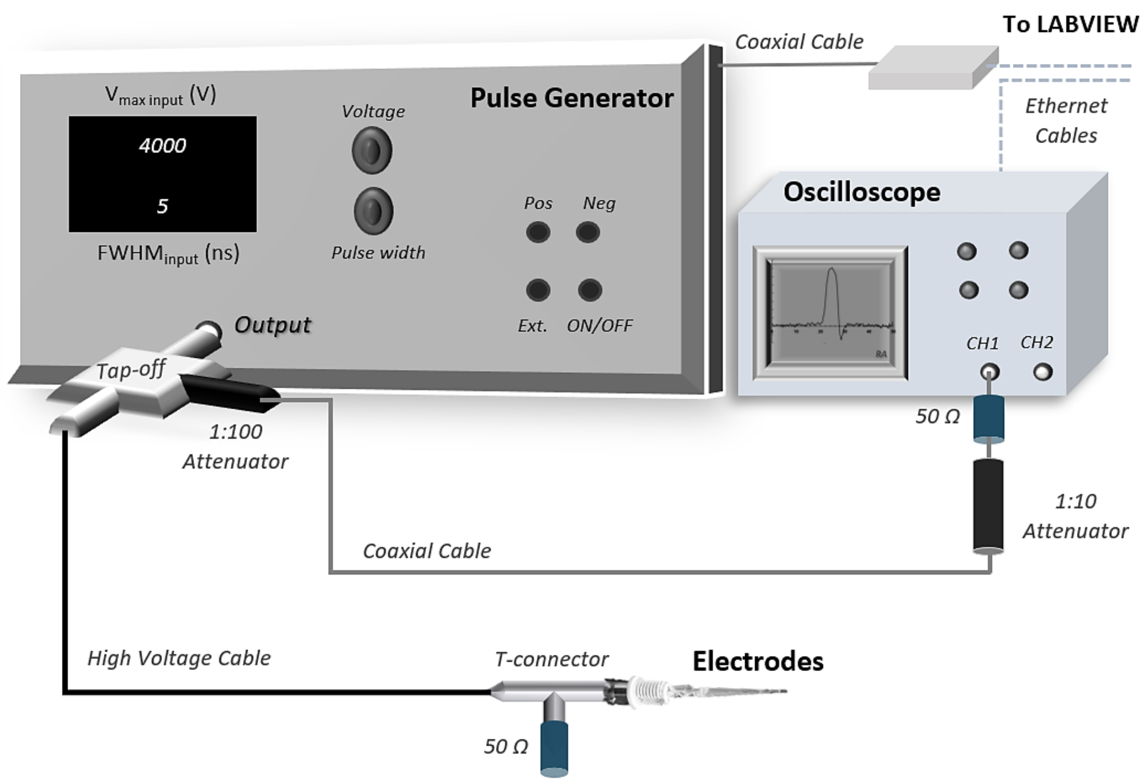

Figure 2.11 Schematic showing the NEP exposure system. The pulse generator output was connected via the tap-off to the oscilloscope, via a coaxial cable, and to the electrodes, via a high voltage cable. The cables were terminated with a 50 Ω resistor.

Because the FID 2-10 ns bipolar pulse generator was newly acquired, we first compared the 5 ns pulse traces obtained from the FID pulser to those obtained from the fixed duration (5 ns) pulse generator by Transient Plasma Systems (TPS), that was used for all the previous studies [***23, 49, 50***]. Figure 2.12 shows a comparison of the traces obtained from each pulse generator along with their Fast Fourier Transform (FFT) analysis. The pulse parameters were 3,500 V and 5 ns FWHM for both. The main difference observed between the two pulse traces is the faster rise and fall time of the pulse obtained by the FID pulser compared to the one obtained by the fixed duration TPS pulser. In addition, the more rapid fall time of the pulses obtained by the FID pulse generator resulted in a negative undershoot observed at the end of the falling phase of the pulse.

Another variable was the frequency (f) component of the pulses. FFT analysis revealed that the pulse produced by the FID generator possesses lower DC (where $f = 0$) magnitude compared to the TPS generated pulse. However, due to their fast rise and fall properties, FID pulses possessed higher frequency components ($f \geq 200$ MHz) than TPS pulses.

Regarding these differences, it is currently unknown how the negative dip in the time domain and how the difference in the frequency components in the frequency domain between the pulses would affect the cellular responses. These differences are still under investigation by our research group.

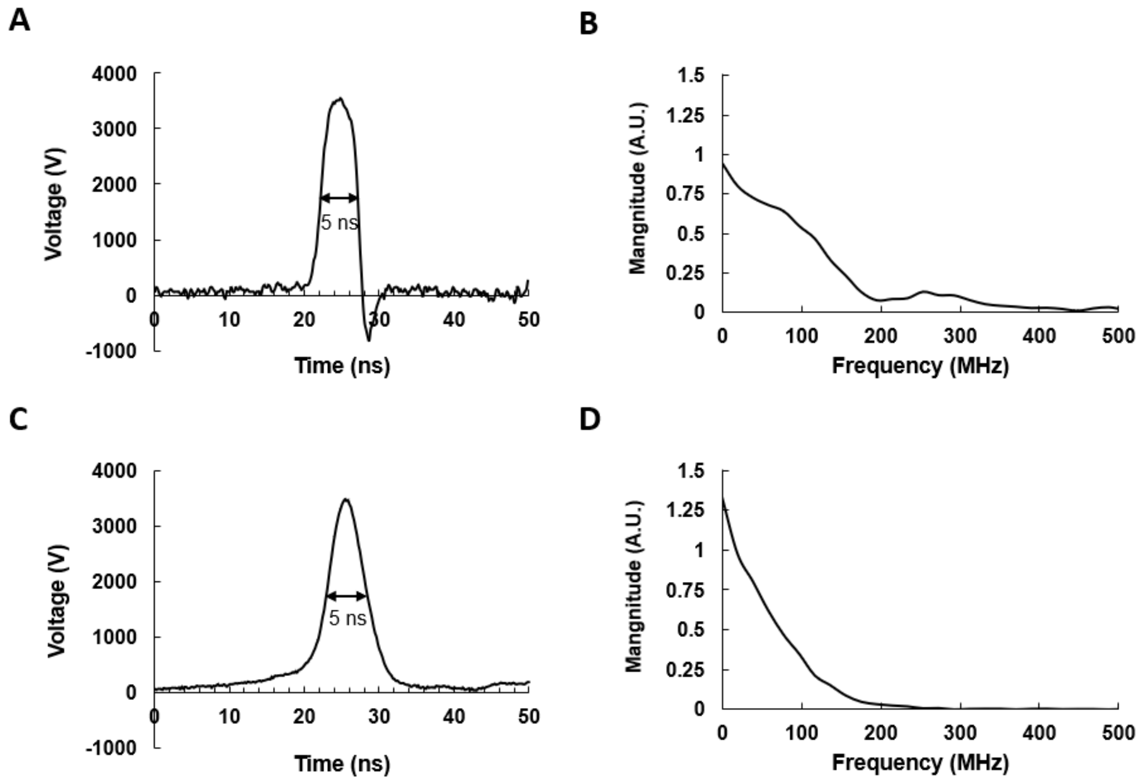

Figure 2.12 Comparison of the 5 ns pulses generated by the variable FID and the fixed duration TPS pulse generators. The graphs show representative pulse traces and their FFT analysis obtained at a voltage amplitude of 3,500 V and a measured FWHM of 5 ns. (A and B) were obtained by the new FID pulse generator and (C and D) by the fixed duration TPS pulse generator.

Figure 2.13 shows an image of an attached cell placed in between the electrode tips along with the computed E-field distribution obtained from SEMCAD X (version 14.8.5, Speag, Zürich, Switzerland). From these simulations, a scale factor (0.004954) was obtained to calculate the equivalent E-field value in MV/m that corresponds to a particular voltage value in V.

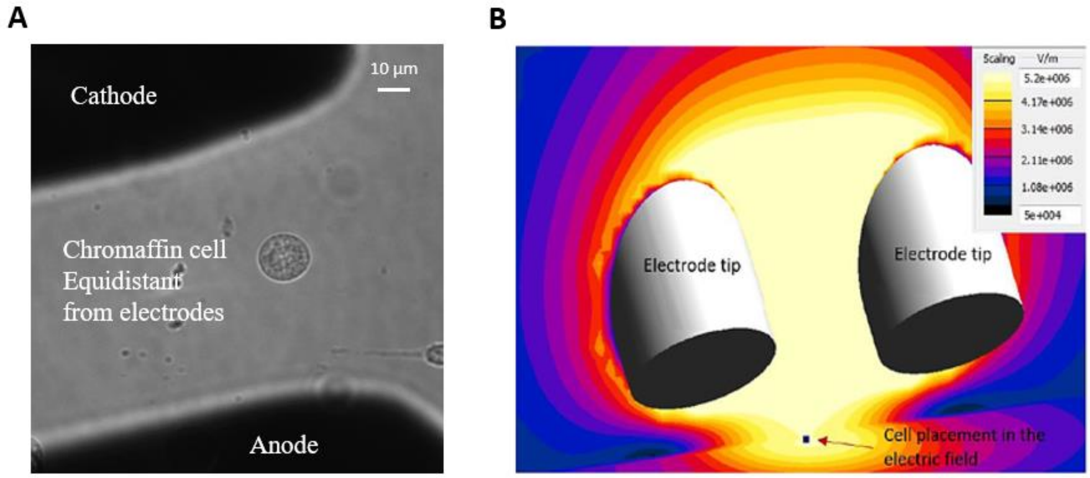

Figure 2.13 NEP exposure to a chromaffin cell. (A) Photomicrograph of a chromaffin cell located equidistantly between the tips of the electrodes, at a magnification of 63X. (B) Computed E-field distribution in the vicinity of the cell exposed to a 5 ns pulse.

2.8.3 **Testing the voltages delivered by the pulser**

Before experiments got underway, a number of tests were needed to be performed on the 2 to 10 ns pulse generator. On all cases, the pulses were measured with the electrodes totally immersed in BSS in a glass bottom dish lacking cells to mimic the experimental conditions. We recorded the pulse traces delivered using LabVIEW and compared V_{max} recorded on the oscilloscope to $V_{max\ input}$, the input voltage set on the control panel of the pulser.

Three replicates were performed for each input voltage ranging from 1,000 to 5,000 V for the 2 ns $FWHM_{input}$ (lowest achievable on the pulser). Figure 2.14-A shows the average of these measurements. We found that each measured V_{max} amplitude was lower than the value set using the pulse generator, which resulted in a deviation from the input

($\Delta V = V_{max\ input} - V_{max}$). The error was calculated as $\Delta V/V_{max\ input}$ (Figure 2.14-B). The voltage drop was not linear resulting in a variable error, i.e. it was higher at lower voltages and lower at higher voltages. Similar measurements were obtained for a 10 ns pulse duration (highest achievable on the pulser) (Figure 2.15). The deviation between V_{max} and $V_{max\ input}$ also resulted in a variable error, similar to what we obtained with the measurements done at 2 ns.

In summary, the deviation between the input and the measured voltage amplitudes was important to take into consideration when delivering pulses using the variable duration FID pulse generator. To obtain a desirable voltage output, the deviation has to be compensated for by adjusting $V_{max\ input}$.

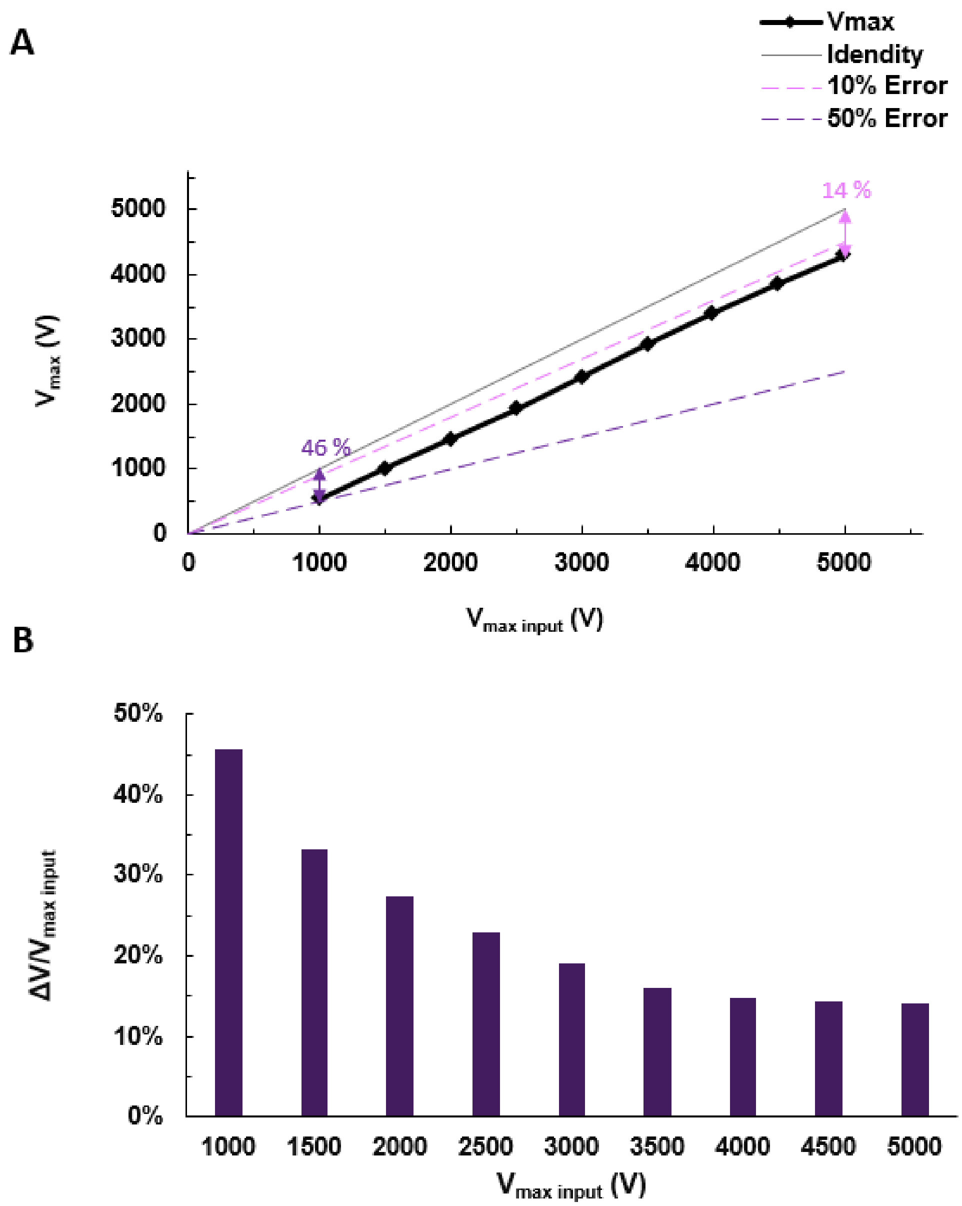

Figure 2.14 Average of three measurements of V_{max} performed at the lowest $FWHM_{input}$ (2 ns) with electrodes immersed in BSS. (A) shows the measured V_{max} (black diamonds) plotted against the input amplitudes. Error lines at 10% (pink and dashed) and 50% (purple and dashed) were used to visualize the deviation from the identity line that represents $y = x$ (grey). (B) displays the error calculated at each $V_{max\ input}$.

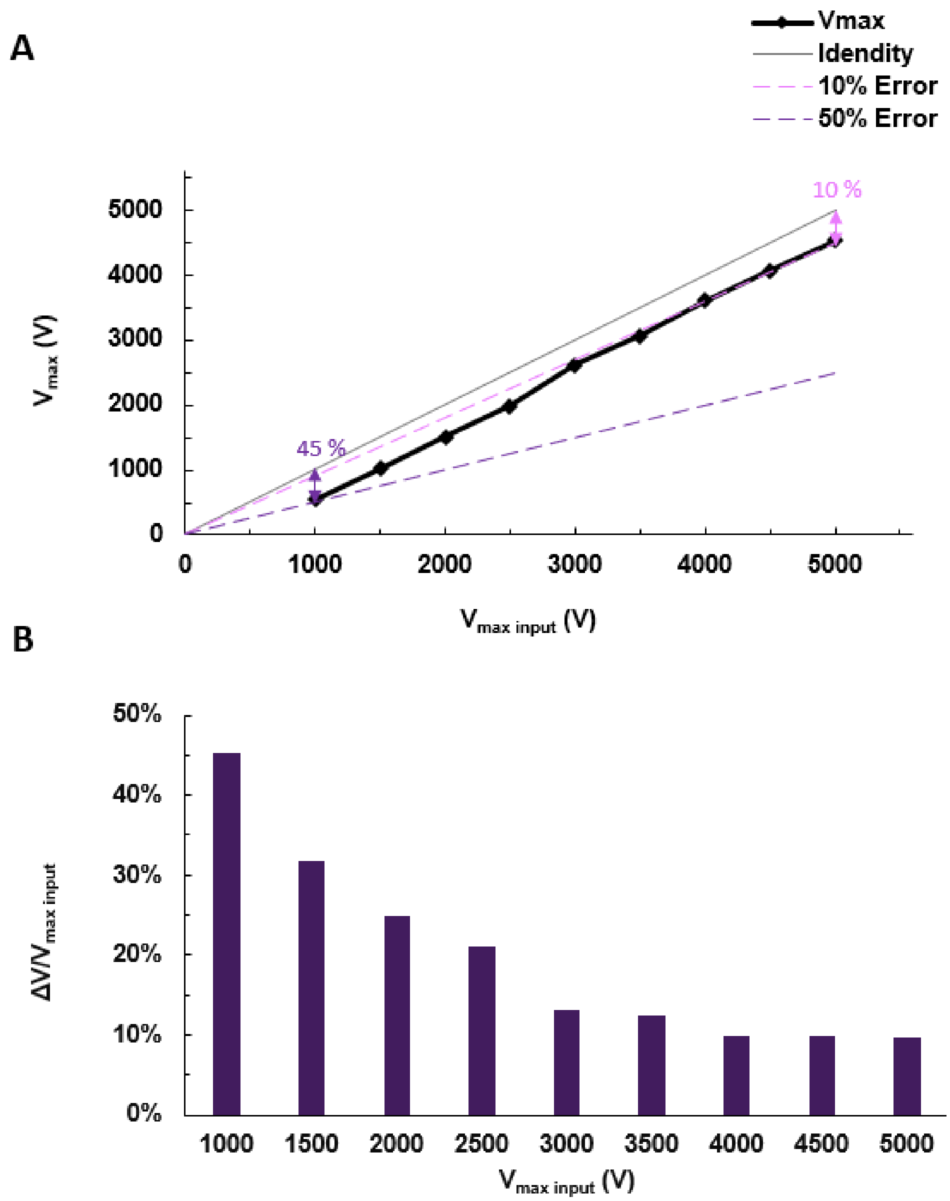

Figure 2.15 Average of three measurements of V_{max} performed at the highest $FWHM_{input}$ (10 ns) with electrodes immersed in BSS. (A) shows the measured V_{max} (black diamonds) plotted against the input amplitudes. Error lines at 10% (pink and dashed) and 50% (purple and dashed) were used to visualize the deviation from the identity line that represents *y* = *x* (grey). (B) displays the error calculated at each $V_{max\ input}$.

2.8.4 Testing the pulse width

The pulse generator is designed to deliver pulses ranging from 2 to 10 ns duration at 90% of V_{max}, which results in wider durations of FWHM. We found that the pulse shape changed when varying the pulse duration was varied. At the shortest durations, the shape of the pulse was a “bell shape”. As the duration of the pulse increased, the shape of the pulse became trapezoidal. Figure 2.16 shows examples of pulses produced at the same $V_{max\ input}$ of 4,500 V for three $FWHM_{input}$ of 2, 6, and 10 ns. Of note is that the measured FWHM at this voltage amplitude were slightly higher than the $FWHM_{input}$ and indicated 3, 7, and 11 ns durations respectively for the 2, 6, and 10 ns inputs. Thus, the relationship between FWHM and V_{max} was a critical factor to take into consideration when delivering pulses using this FID pulse generator.

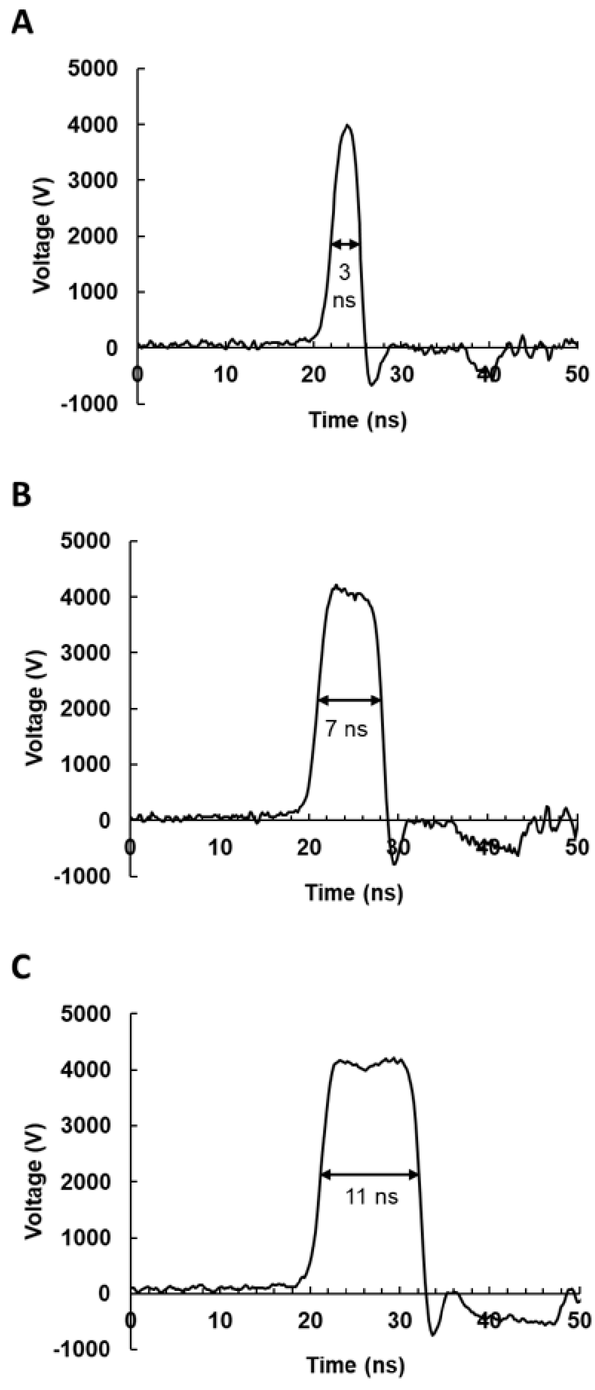

Figure 2.16 Pulse traces with $V_{max\ input}$ at 4,500 V respectively at (A) 2 ns, (B) 6 ns, and (C) 10 ns. The curves show how the width of the pulse affects the shape as well. The curves become trapezoidal as the FWHM is increased.

Another consideration was that the design of the pulser was such that the longer pulse durations were obtained for the lowest voltage amplitudes. Figure 2.17 shows the testing for the durations 2 and 10 ns, which represent the lowest and highest settings of the pulser. The data represents the average of three measurements performed with electrodes immersed in BSS under each condition. Our measurements demonstrated a deviation between the input and the measured FWHM that was more dramatic for the shortest durations compared to the longer ones. For example, for a fixed $FWHM_{input}$ of 2 ns set on the pulser, the measured pulse duration on the oscilloscope varied from 2.9 to 9.5 ns for voltage values ranging from 5,000 to 1,000 V, respectively.

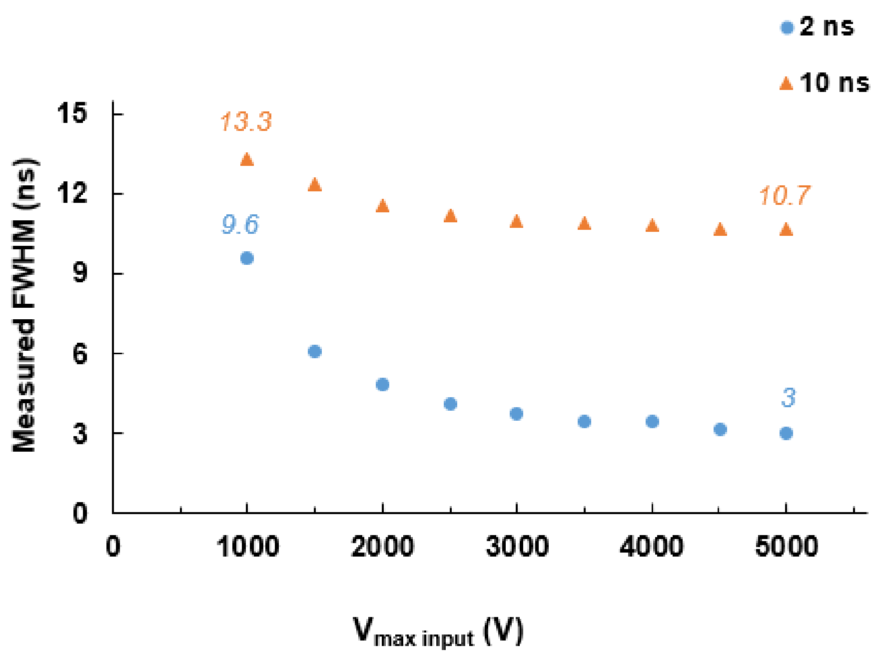

Figure 2.17 Pulse width measurements obtained by varying the $V_{max\ input}$ and fixing $FWHM_{input}$ at 2 and 10 ns. The graphs represent the average of three measurements performed with electrodes fully immersed in BSS. The numbers illustrated above each graph represent the highest and lowest possible FWHM measured respectively at the lowest and highest $V_{max\ input}$.

The FWHM got narrower as the amplitude of the voltage increased and approached the value set on the pulse generator. For example, with $FWHM_{input}$ fixed at 2 ns (blue circles), the measured pulse duration ranged from 9.5 ns at 1,000 V to 2.9 ns at 5,000 V. As a result, to reach the shortest pulse durations needed for our experiments, higher voltages had to be applied, which was not desirable in our case as we were interested in working at lower voltages to minimize adverse effects on the cells. Therefore, attenuators were needed to be placed into the circuit to reduce the maximum voltage value V_{max} of the pulses while preserving their short durations.

By performing more tests on the pulser, three attenuators (142-HMFP-3/4/8, Barth Electronics) were used. These attenuators were connected either alone or in combination at the output of the pulse generator before the tap-off, when needed. Table 2.1 and

Table **2.2** show measurements of V_{max} and FWHM with the input durations respectively set to 2 ns and 10 ns, along with the suggested attenuations: -3, -4, and -8 dB. The attenuators withstand high voltages and can be combined together, thus resulting in other attenuation ratios, such as -12 dB (obtained by adding -4 with -8 dB). This helps us to cover a wider range of voltages at which short FWHM can be achieved.

In the absence of attenuators, pulses with voltage amplitudes ranging from 543 V to 4,293 V could be delivered for pulse durations ranging from 9.54 to 2.96 ns, respectively. When the various attenuators were added either alone or in combination, the voltage values ranged from 136 V up to 3,039 V for the various pulse durations. Additionally, pulses with lower voltage amplitudes from 1,078 V up to 3,039 V can be now employed with durations as short as 2.96 ns, which was not possible without the attenuators.

Table 2.1 Voltage calculations for the suggested attenuators for a 2 ns pulse duration set on the pulse generator. The Table shows the averaged measured voltages obtained from three replicates after attenuation.

			Attenuation in dB			
FWHM$_{input}$ = 2 ns			**- 3.0**	**- 4.0**	**- 8.0**	**- 12.0**
V$_{max\ input}$ (V)	**V$_{max}$ (V)**	**FWHM (ns)**	**Attenuated V$_{max}$ (V)**			
1000	543	9.5	385	343	216	136
2000	1,450	5	1,027	915	577	364
3000	2,430	3.7	1,720	1,533	967	610
4000	3,407	3.4	2,412	2149	1,356	856
5000	4,293	3	3,039	2,709	1,709	1,078

For the 10 ns duration and in the absence of attenuators, pulses with voltage amplitudes ranging from 546 V to 4,520 V could be delivered for pulse durations ranging from 13.29 to 10.7 ns. However, when the various attenuators were added either alone or in combination, the voltage values ranged from 137 V up to 3,200 V for the various pulse durations.

Table 2.2 Voltage calculations for the suggested attenuators for a 10 ns pulse duration set on the pulse generator. The table shows the averaged measured voltages obtained from three replicates after attenuation.

			Attenuation in dB			
$FWHM_{input}$ = 10 ns			**- 3.0**	**- 4.0**	**- 8.0**	**- 12.0**
$V_{max\ input}$ (V)	**V_{max} (V)**	**FWHM (ns)**	**Attenuated V_{max} (V)**			
1000	546	13.3	387	345	218	137
2000	1,503	11.5	1,064	948	598	378
3000	2,610	10.9	1,848	1,646	1,039	655
4000	3,603	10.8	2,551	2,273	1,434	905
5000	4,520	10.7	3,200	2,852	1,799	1,135

Figure 2.18 shows an example of a -12 dB attenuation, which was the product of the combination of -4 and -8 dB. Two pulses were acquired at the same $V_{max\ input}$ at 4,500 V before and after the -12 dB attenuation. The pulse traces presented the same FWHM (3 ns) with amplitudes of V_{max} = 3,920 V without attenuation and V_{max} = 1,020 V after attenuation.

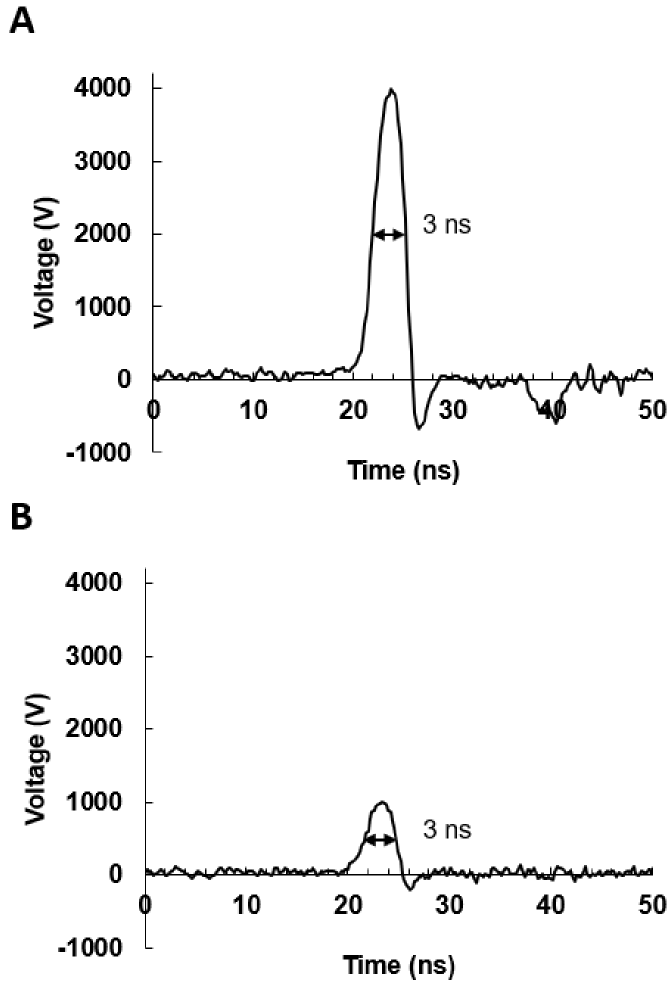

Figure 2.18 Example of attenuation at -12 dB. The graphs show two pulse traces measured at the pulse settings of 2 ns duration and a 4,500 V maximum amplitude before in (A) and after (B) the insertion of the -12 dB attenuator.

In summary, attenuators were necessary in this project for obtaining 5 ns pulse durations at low E-field amplitudes (lower than 7.4 MV/m). The attenuators would allow us to determine the lowest V_{max} that can trigger Ca^{2+} responses, referred to as threshold, as well as the threshold for triggering exocytotic responses, monitored using FM1-43, was also assessed.

Chapter 3. RESULTS

3.1 Determining the E-field threshold for evoking Ca^{2+} responses in chromaffin cells exposed to a 5 ns electric pulse

As shown in the Methods section (Figure 2.12), the pulse traces obtained from the 2-10 ns, variable amplitude (± 1-5 KV) bipolar pulse generator purchased from FID had a different shape (and frequency content) compared to the ones obtained from the fixed duration, 5 ns, TPS pulse generator used in Dr. Gale Craviso's laboratory. Therefore, the first step was to determine the threshold E-field amplitude for evoking Ca^{2+} responses in chromaffin cells exposed to a single 5 ns duration electric pulse using the FID pulser. Figure 3.1 is a bar chart that illustrates the average increase in fluorescence intensity in cells labeled with Calcium Green-1 when the cells were stimulated with a 5 ns pulse at different E-field amplitudes. By increasing the E-field amplitude of the pulses, the number of cells responding to the pulse was higher. As a result, the E-field at which 100% of the cells consistently responded to the pulse was 9.9 MV/m, which we defined as our threshold. There was a slight increase in the amplitude of the response at the highest E-fields tested that was not statistically significant ($p > 0.05$). Surprisingly, the amplitude of ~ 9.9 MV/m that was needed to induce a response in all the stimulated cells was about twice as high as the one needed (~ 4 MV/m) to stimulate 100% of cells using the TPS pulse generator. We attribute this difference to the variations observed between the pulse traces, which is currently still under investigation.

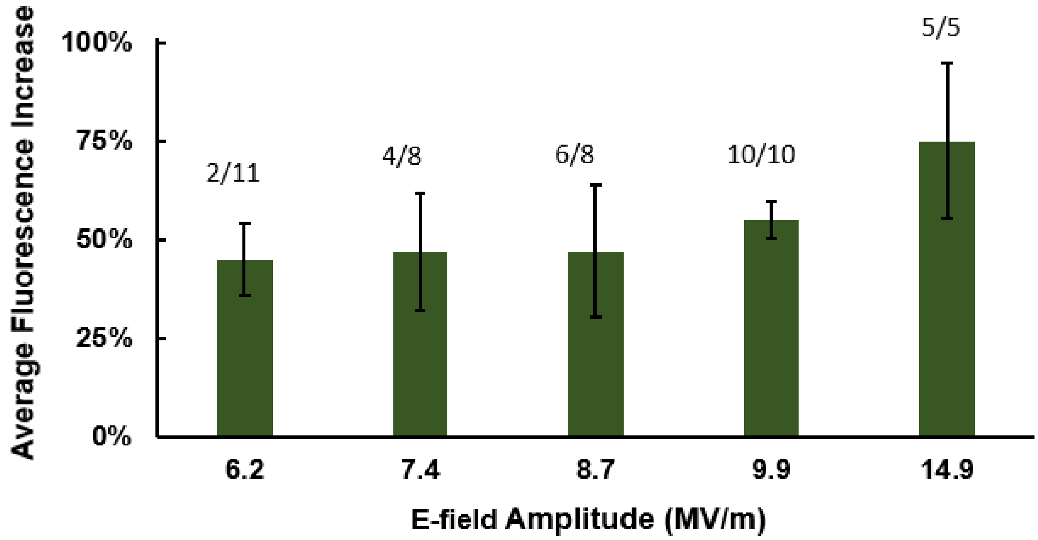

Figure 3.1 E-field threshold for evoking Ca^{2+} influx determined by fluorescence imaging of the rise in $[Ca^{2+}]_i$ in response to one 5 ns pulse. Normalized fluorescence intensity represents the mean of the peak responses of the cells ± SE. Shown above each bar is the number of cells responding to the pulse out of the total number of cells.

Typical Ca^{2+} responses of chromaffin cells exposed to a 5 ns pulse applied at 9.9 MV/m are shown in Figure 3.2. The amplitude of the Ca^{2+} responses compared well with that previously reported for cells exposed to a 5 ns, 3.4 MV/m pulse using the TPS pulse generator [***50***]. A notable difference, however, is that most cells showed fluctuations in $[Ca^{2+}]_i$ that occurred after the initial rise in Ca^{2+} triggered by the pulse. The half-width of the responses, which is the length of time for the initial rise in Ca^{2+} to decline to 50% of its maximal value, had an average of 13.6 ± 4.3 s (n = 10). This half-width was smaller than the one seen in Ca^{2+} responses evoked by the 5 ns TPS pulse generator (~ 25 s) [***50***].

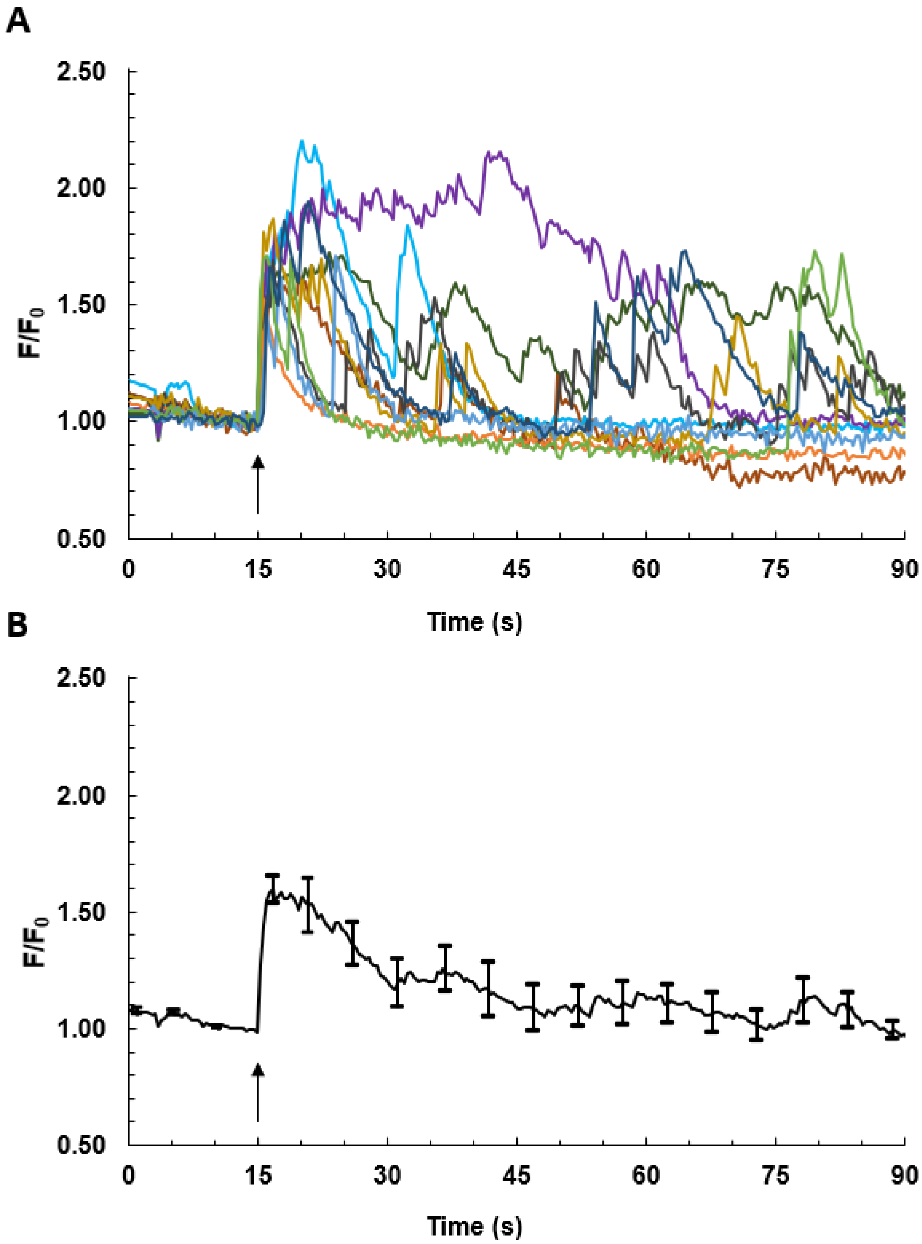

Figure 3.2 Ca^{2+} responses in chromaffin cells evoked by one 5 ns, electric pulse at 9.9 MV/m. (A) shows the individual fluorescence traces of cells (n = 10) and (B) shows the average ± SE of the representative traces with an average half-width of 13.6 s. Arrows indicate the time where the pulse was delivered to the cells.

3.2 FM1-43 labeling of the plasma membrane of adrenal chromaffin cells

As described in the Introduction, the styryl dye FM1-43 was used in this project to monitor exocytosis in neuroendocrine chromaffin cells. After identifying the threshold E-field amplitude for stimulating chromaffin cells with a single 5 ns pulse, FM1-43 was used to label the cell membrane of the cells. As described earlier, labeling the membrane of the cells was possible because the quantum yield of FM1-43 dramatically increases when it is inserted into a lipid membrane. Continuous perfusion of 3 μM FM1-43 in BSS for 5 minutes was found optimal for labeling chromaffin cell membranes (see Methods section).

Figure 3.3 shows a typical time course of labeling of the plasma membrane of chromaffin cells with FM1-43 using the 5-minute perfusion protocol. Bright field images were captured before and after labeling to ensure that cells did not undergo any morphological changes such as cell swelling. The time course shown is the average change in whole cell fluorescence ± SE obtained from cells (n = 4) on different days. Once the BSS containing the FM1-43 dye reached the dish, labeling of the membrane began, with membrane fluorescence increasing with time. A constant level of fluorescence (plateau) was reached in all the cells within 2 to 3 minutes from the beginning of labeling. The fluorescence signal at the end of the labeling period was confined to the membrane and was not internalized because FM1-43 contains a hydrophilic head that makes the dye unable to cross the lipid bilayer.

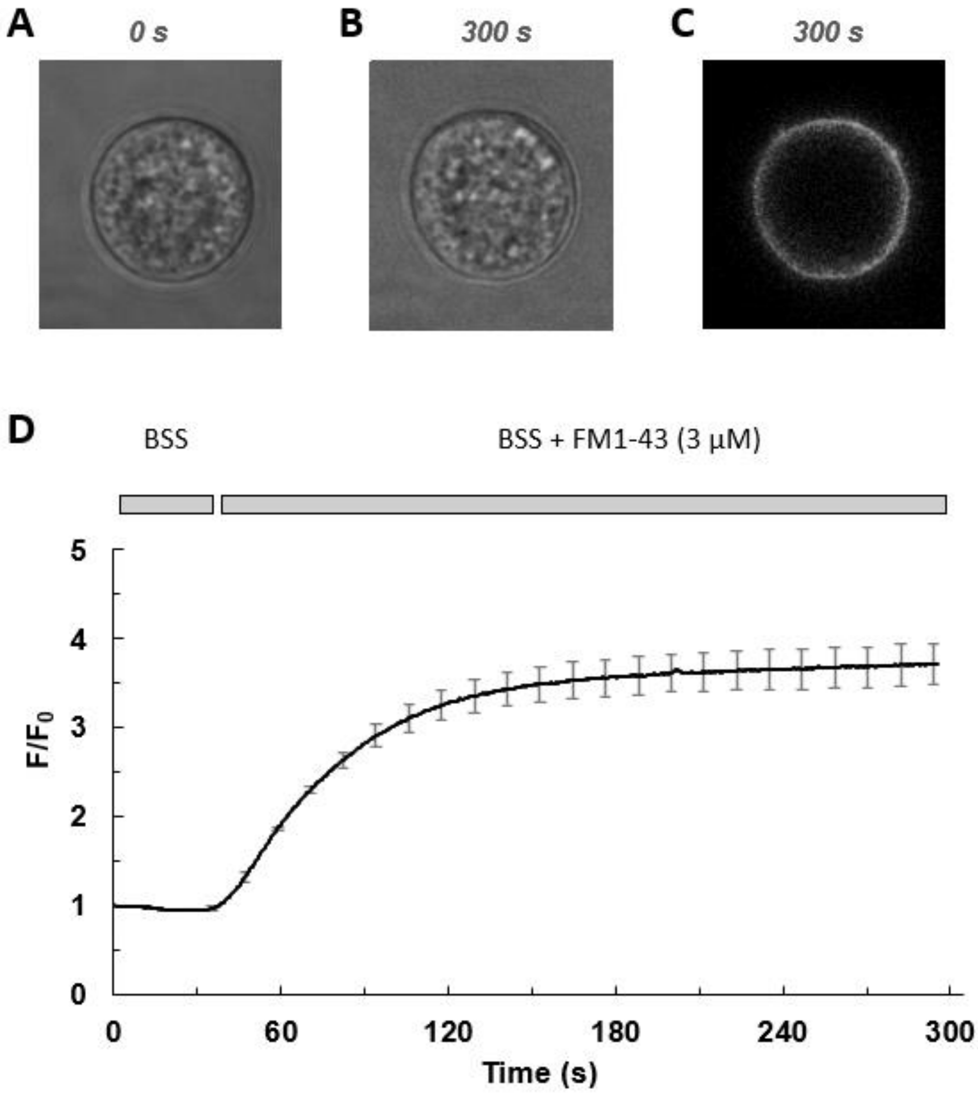

Figure 3.3 Labeling of chromaffin cells with FM1-43 using the perfusion protocol. Cells were perfused with BSS containing 3 µM FM1-43 as described in Methods. (A) and (B) are bright field images of a cell before and after labeling, respectively. (C) is a fluorescence image of the same cell captured at the end of the perfusion protocol. All images were obtained using a 100X oil objective. (D) shows a typical time course of the labeling of the plasma membrane of the cells. The graph represents the average change over time in whole cell fluorescence ± SE (n = 4) during the perfusion protocol. Here and in all subsequent graphs, the bars at the top indicate the solution that was perfused over time.

3.3 Monitoring exocytosis in FM1-43 labeled cells in response to a high [K^+] depolarizing stimulus delivered to the cells via perfusion

The use of FM1-43 dye to monitor exocytosis is explained by the ability of the dye to incorporate into the membrane of secretory granules fused with the plasmalemma during exocytosis. Thus, an increase in whole cell fluorescence is expected because of the binding of free FM1-43 molecules to the added membrane resulting from exocytosis.

3.3.1 High [K^+] stimulation caused a slow gradual increase in FM1-43 membrane fluorescence in the presence of external Ca^{2+}

We first investigated the time course and amplitude of the rise in $[Ca^{2+}]_i$ induced by the application of 56 mM [K^+] delivered to the cells by perfusion, the same way that high [K^+] would be delivered to FM1-43 labeled cells. The Ca^{2+} responses monitored in Calcium Green-1-labeled cells showed an immediate increase in $[Ca^{2+}]_i$ that returned to baseline within ~ 200 s (Figure 3.4). The return of $[Ca^{2+}]_i$ to baseline rather than being sustained could be an indication that the prolonged depolarizing stimulus could have caused the inactivation of VGCCs. This would result in an inhibition of Ca^{2+} influx even though high [K^+] was still present.

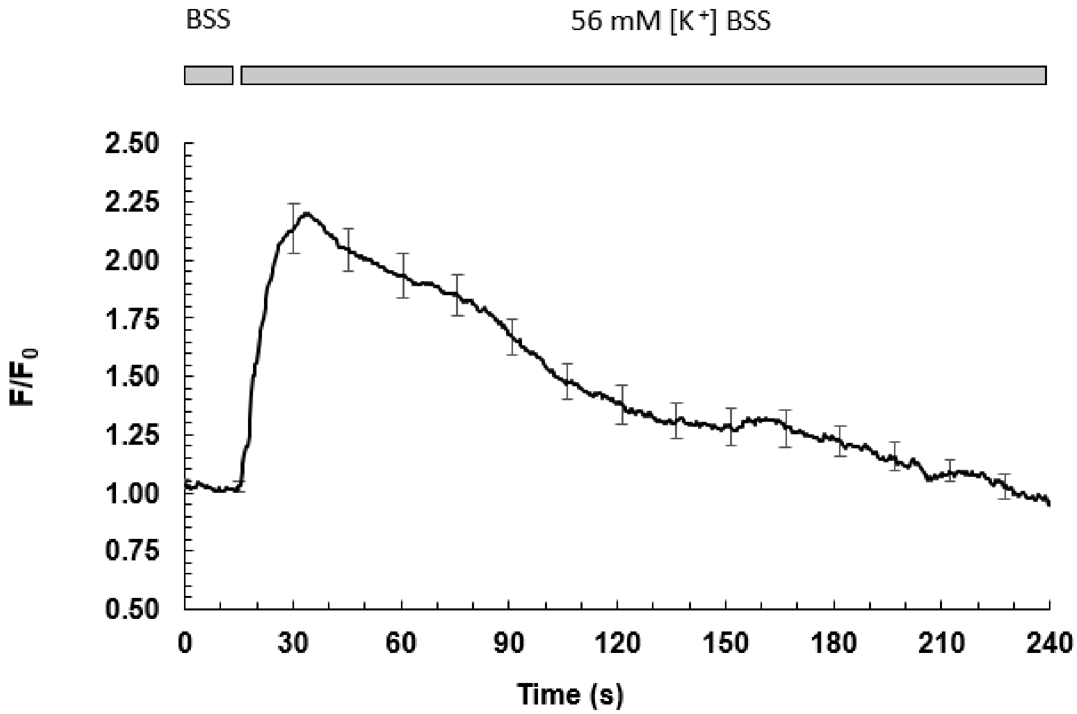

Figure 3.4 Effect of 56 mM [K^+] BSS delivered by perfusion on [Ca^{2+}]$_i$. The trace represents the averaged Ca^{2+} responses ± SE (n = 17) triggered by high [K^+] stimulation. The high [K^+] BSS was continuously perfused at a rate of ~ 1 ml/minute. The depolarizing solution reached the dish at around 15 s.

We next determined the effect of high [K^+] (56 mM KCl) BSS on FM1-43 fluorescence. After labeling the cells with FM1-43, the cells were continuously perfused with the high [K^+] BSS containing FM1-43. Figure 3.5 is a schematic diagram showing the protocol used to deliver the high [K^+] stimulus. The time course of the exocytotic response elicited by 56 mM [K^+] is shown in Figure 3.6.

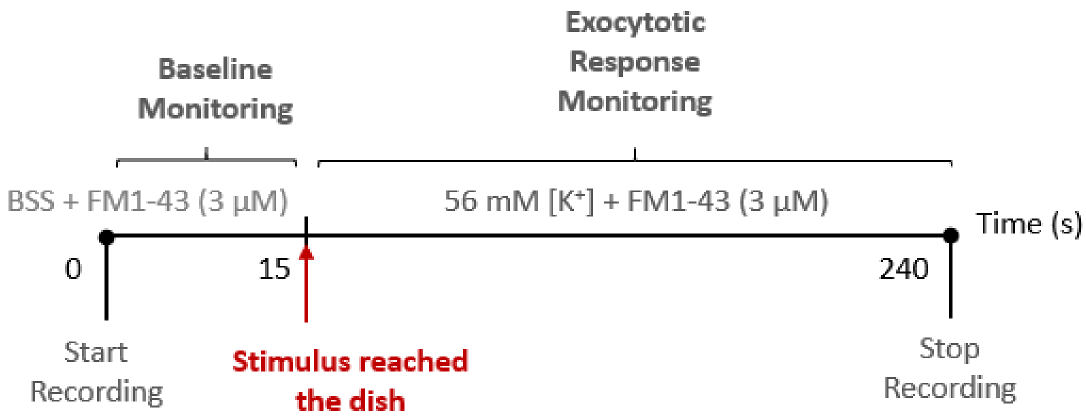

Figure 3.5 Schematic diagram showing the protocol used to monitor the exocytotic response of FM1-43 labeled cells to high [K^+] stimulation.

When the depolarizing solution reached the FM1-43-labeled cells (~ 15 s), there was a decrease in membrane fluorescence (dip) that lasted around 60 seconds, followed by a slow increase in membrane fluorescence (Figure 3.6-A). The increase in fluorescence reached ~ 35% around 4 minutes after the 56 mM [K^+] solution had reached the cells.

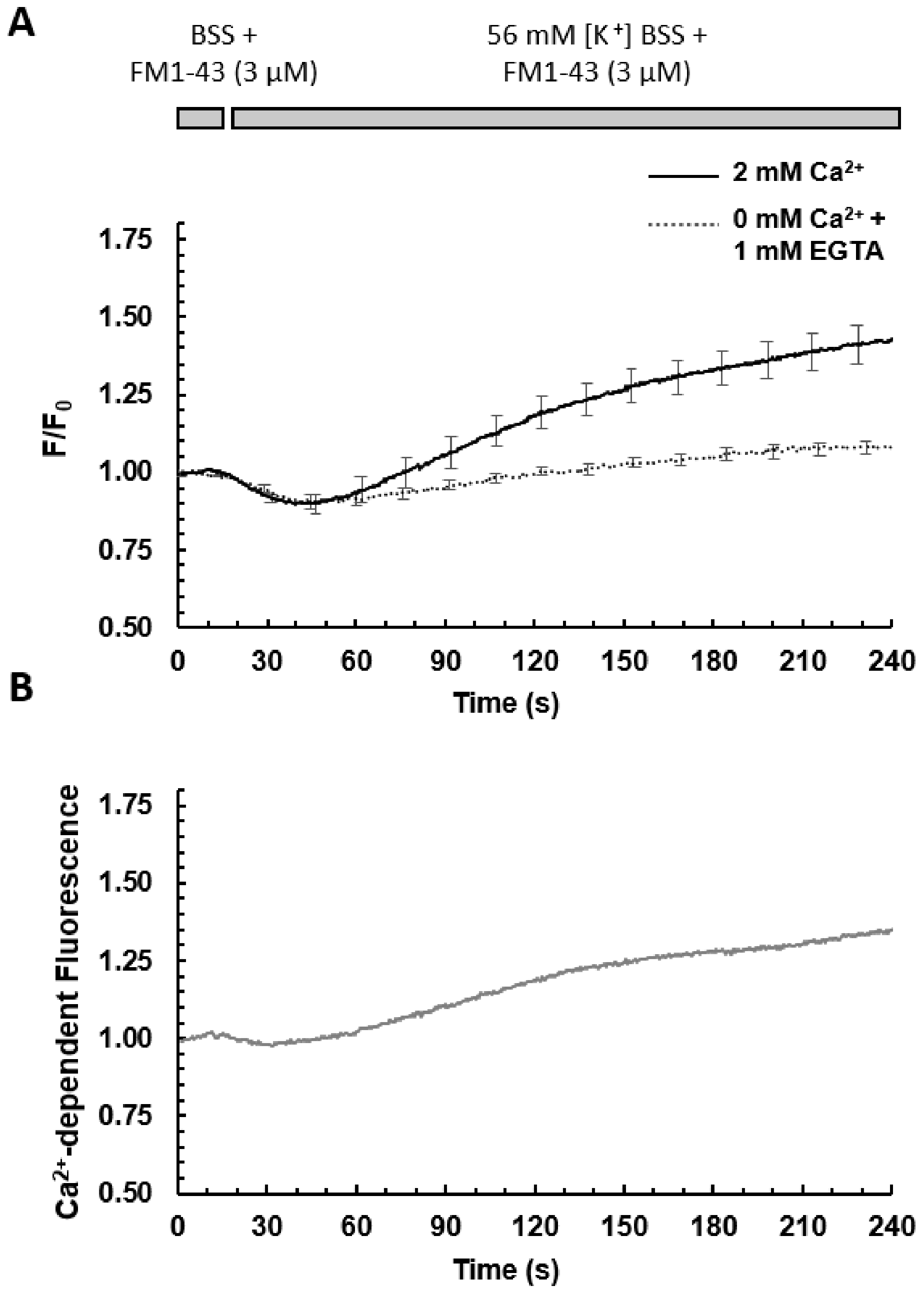

Figure 3.6 Effect of high [K^+] stimulation on FM1-43 labeled chromaffin cells. (A) shows the averaged change in whole cell fluorescence ± SE triggered by the depolarizing stimulus in the presence (n = 12) or the absence (n = 11) of external Ca^{2+}. The high [K^+] stimulus reached the cells at around 15 s. (B) represents the difference in fluorescence obtained by subtracting the responses in the absence of Ca^{2+} from those in the presence of Ca^{2+}.

To identify the mechanism responsible for the initial decrease in fluorescence, we performed experiments in the absence of external Ca^{2+} that would prevent exocytosis from contributing to the FM1-43 fluorescence changes (Figure 3.6). We found that the transient dip was still present under Ca^{2+}-free conditions, indicating that this initial effect on FM1-43 fluorescence was independent of Ca^{2+} and most likely the result of the sensitivity of FM1-43 to the changes in membrane potential [***19, 32, 33***].

Under Ca^{2+}-free conditions, the level of fluorescence returned to a level close to baseline after the dip, compared to the increasing trend observed in the presence of Ca^{2+}. Thus, by subtracting the responses measured in the absence of Ca^{2+} from the ones obtained in the presence of Ca^{2+} we could obtain the response of FM1-43 that mainly reflected exocytosis. These results are shown in Figure 3.6 B. Note that the subtraction did not totally eliminate the initial decrease in fluorescence attributed to the sensitivity of the dye to changes in membrane potential. Thus, unlike the immediate $[Ca^{2+}]_i$ rise induced by the application of 56 mM $[K^+]$, FM1-43 labeled cells exhibited a delayed increase in whole cell fluorescence. Three minutes after the start of the 56 mM $[K^+]$ perfusion, $[Ca^{2+}]_i$ was returning to baseline while FM1-43 fluorescence was still increasing toward a higher plateau.

Taken together, these results show that the change in TMP induced by the depolarizing stimulus resulted in an initial transient decrease in FM1-43 fluorescence that was independent of Ca^{2+}. The subsequent increase in fluorescence was mainly the result of Ca^{2+}-dependent exocytosis.

3.3.2 Line profile analysis of membrane fluorescence showed homogeneous fluorescence increase in FM1-43-labeled cells due to the high [K^+] stimulation

To determine whether the increase in FM1-43 membrane fluorescence exhibited the same intensity at different locations on the cells, we performed a line profile analysis. For this analysis, we generated 5 µm wide line scans across the cell, as described in the Methods section, and visualized the shift in fluorescence from membrane to cytosol before and after high [K^+] stimulation. The 0˚- and 90˚-line orientations were chosen for the line profile analysis.

Figure 3.7 shows the fluorescence images of a high [K^+]-stimulated chromaffin cell along with the line profiles measured at 0 s (Figure 3.7 A and B) and at 240 s, the end of the stimulation period (Figure 3.7 C and D). We found that before stimulus application, fluorescence intensity on the membrane was homogenous around the cell, as detected by the peaks in fluorescence at 5 and 19 µm (Figure 3.7 B), with little fluorescence observed intracellularly. After stimulation the cell was brighter (Figure 3.7 A and C) and the increase in fluorescence intensity was mainly observed on the membrane of the cell, as revealed by the higher fluorescent peaks (Figure 3.7 B and D) at 5 and 19 µm in both the 0˚ (~ 45% increase) and 90° orientations (~ 49% increase). There was also an increase in intracellular fluorescence level, which can be caused by the internalization of the dye via compensatory endocytosis [***19, 30***]. An additional explanation for this intracellular fluorescence increase is a possible blurring artifact occurring in the plane of focus due to the use of a conventional wide field fluorescence microscopy.

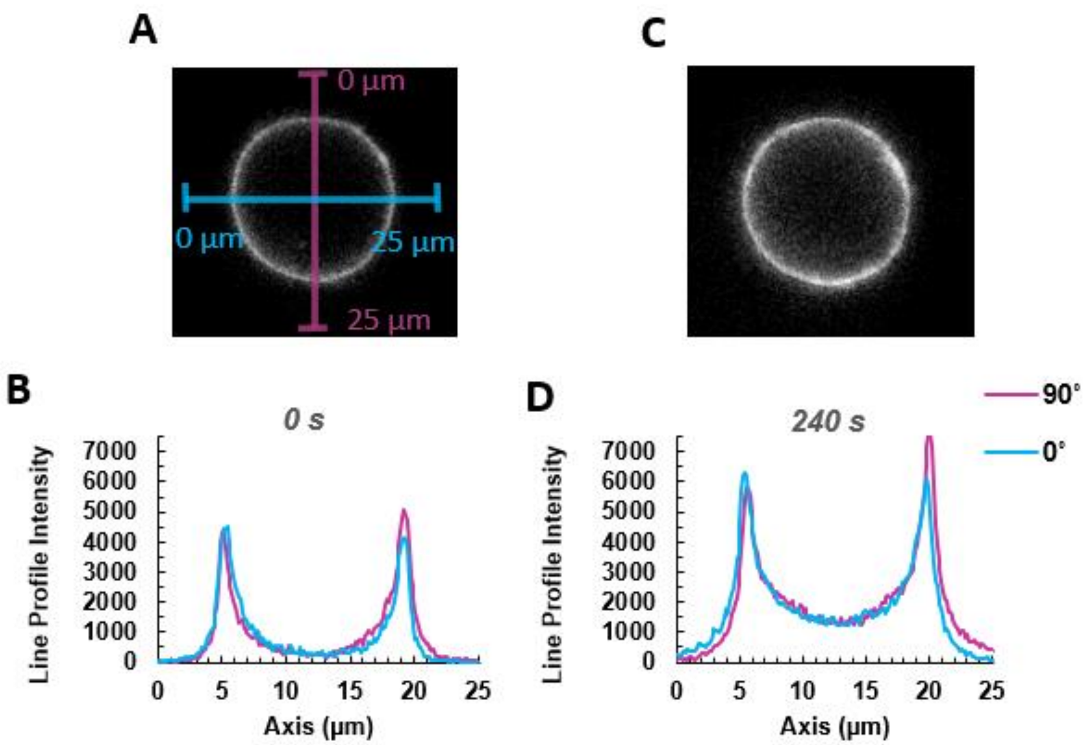

Figure 3.7 Line profile analysis of a cell stimulated with high $[K^+]$ in the presence of external Ca^{2+}. (A) and (C) are fluorescence images showing a chromaffin cell labeled with FM1-43 along with the line profiles at two specific orientations 0˚ and 90˚ (blue and magenta, respectively). (B) and (D) are the corresponding line profile analysis captured before stimulation (0 s), and at the end of the stimulation (240 s), respectively.

We also performed the line profile analysis in the absence of external Ca^{2+} and found that unlike the increase in membrane fluorescence observed in the presence of Ca^{2+}, eliminating Ca^{2+} from the external solution caused no significant increase (≤ 10% in both orientations) in membrane fluorescence as seen in Figure 3.8, indicating that the observed response was Ca^{2+}-dependent.

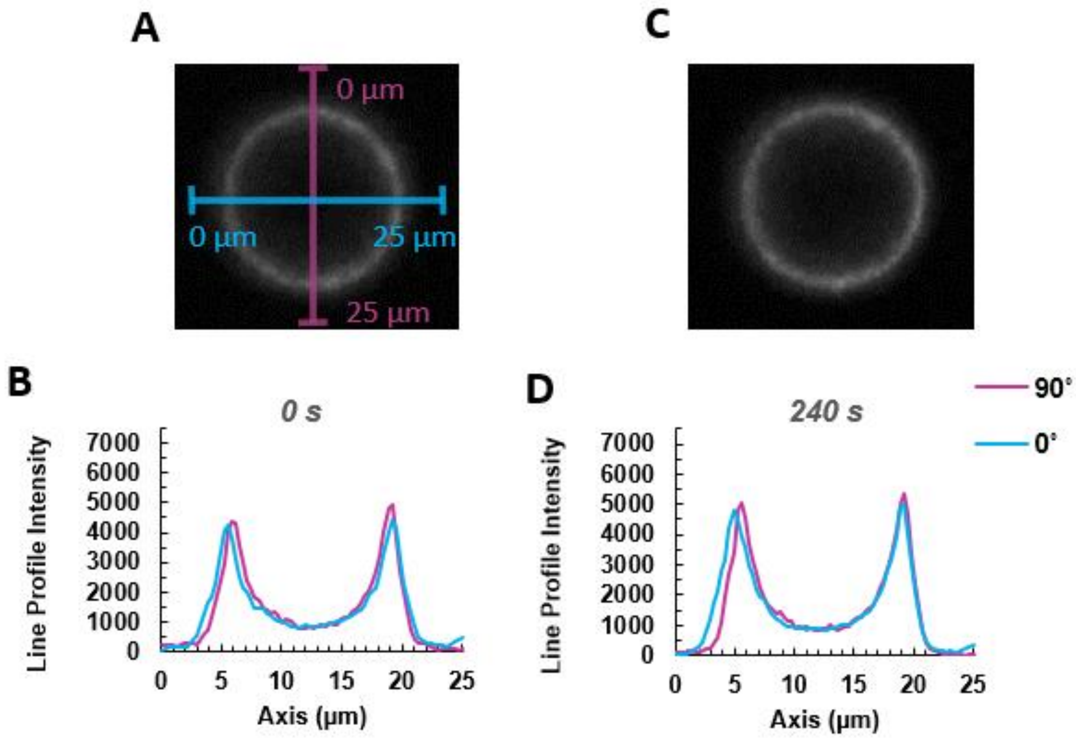

Figure 3.8 Line profile analysis of a cell stimulated with high [K^+] in the absence of external Ca^{2+}. (A) and (C) are wide field fluorescence images showing a chromaffin cell labeled with FM1-43 along with the line profiles at two specific orientations 0˚ and 90 ˚ (blue and magenta, respectively). (B) and (D) are the corresponding line profile analysis captured before stimulation (0 s), and at the end of the stimulation (240 s), respectively.

3.4 Monitoring exocytosis in FM1-43 labeled cells in response to 30 ns, 5 MV/m pulses

3.4.1 A train of ten 30 ns electric pulses evoked an increase in whole cell FM1-43 fluorescence

After establishing the conditions for labeling chromaffin cells with FM1-43 and testing the exocytotic activity of the cells using high [K^+] as a depolarizing stimulus both in the presence and absence of external Ca^{2+}, the next series of experiments investigated the effects of NEPs on the exocytotic activity of chromaffin cells using FM1-43 to monitor this cellular response.

Initial experiments were conducted by exposing chromaffin cells to one or more 30 ns electric pulses using a variable-duration pulse generator (10-100 ns from FID), which was the only one available in the laboratory at the time. The E-field used in the 30 ns experiments was 5 MV/m.

As for the high [K^+] experiments, chromaffin cell membranes were labeled with FM1-43 and the cells stimulated with 30 ns electric pulses under conditions in which FM1-43 was present in the bathing solution. The schematic in Figure 3.9 shows the protocol that was used to deliver the stimulation. Briefly, baseline fluorescence level was monitored for 15 s prior to the application of the NEP stimulus and NEP-evoked changes in fluorescence monitored for 120 s following the stimulus.

When the cells were exposed to a train of five pulses at 1 Hz and 10 Hz, the increase in membrane fluorescence measured 120 s after the pulse train was low (< 17%) and inconsistent from cell to cell (data not shown). Because of the low-level and lack of consistency of FM1-43 fluorescence changes, we increased the number of pulses to ten that resulted in a consistently larger increase in fluorescence in response to a pulse train delivered at both 1 Hz and 10 Hz.

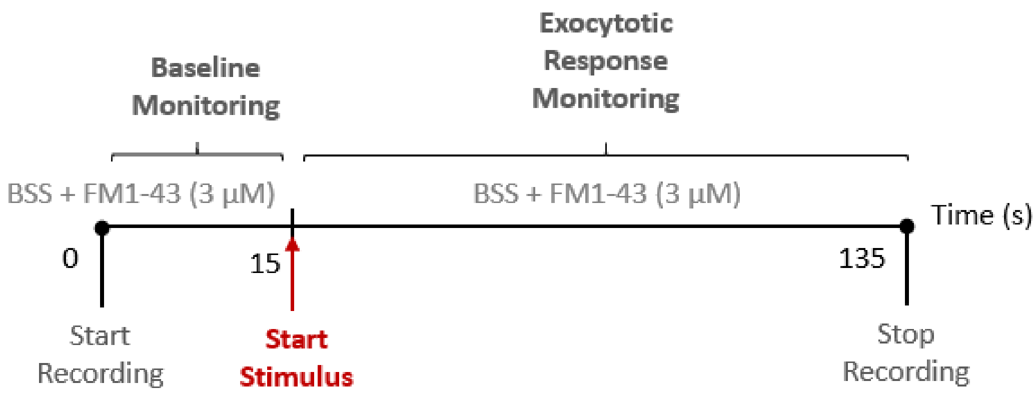

Figure 3.9 Schematic diagram showing the protocol used to monitor the exocytotic activity of cells in response to the application of the electric stimulus. The stimulus consisted of a train of ten 30 ns pulses applied at a repetition rate of either 1 or 10 Hz. Responses were monitored for two minutes.

As shown in Figure 3.10, a train of ten 30 ns pulses at 5 MV/m delivered at 1 Hz or 10 Hz induced a significant increase in whole cell fluorescence. The overall increase in FM1-43 fluorescence reached similar levels 2 minutes after the initiation of the pulses for each type of NEP stimulus. However, the time at which fluorescence began to increase varied according to the frequency. When the pulses were applied at 1 Hz, there was a small decrease in FM1-43 fluorescence (dip) that started at the time of delivery of the pulses (i.e., 15 s) and that gradually started to recover toward baseline during the stimulus train, reaching baseline about 6 s after initiation of the stimulus (Figure 3.10 A and B). From this point onward, fluorescence intensity increased. At 10 Hz, the amplitude and duration of the initial decrease in fluorescence was significantly less than at 1 Hz (Figure 3.10 D) and FM1-43 fluorescence underwent a rapid increase. We compared the rate of increase in fluorescence for 1 Hz and 10 Hz by fitting the data between the start and the end of the pulse train to a linear equation in the form of $y = a*t + b$. These equations are shown in

Figure 3.10 B and D (insets of the plots in A and C) and were applied to the results for the first 25 s of the traces that included the time of application of the E-field. The slopes of the increase in fluorescence (term *a* in the equation) were computed as the first derivatives of the curves. The slope at 10 Hz was twice the magnitude of that estimated at 1 Hz.

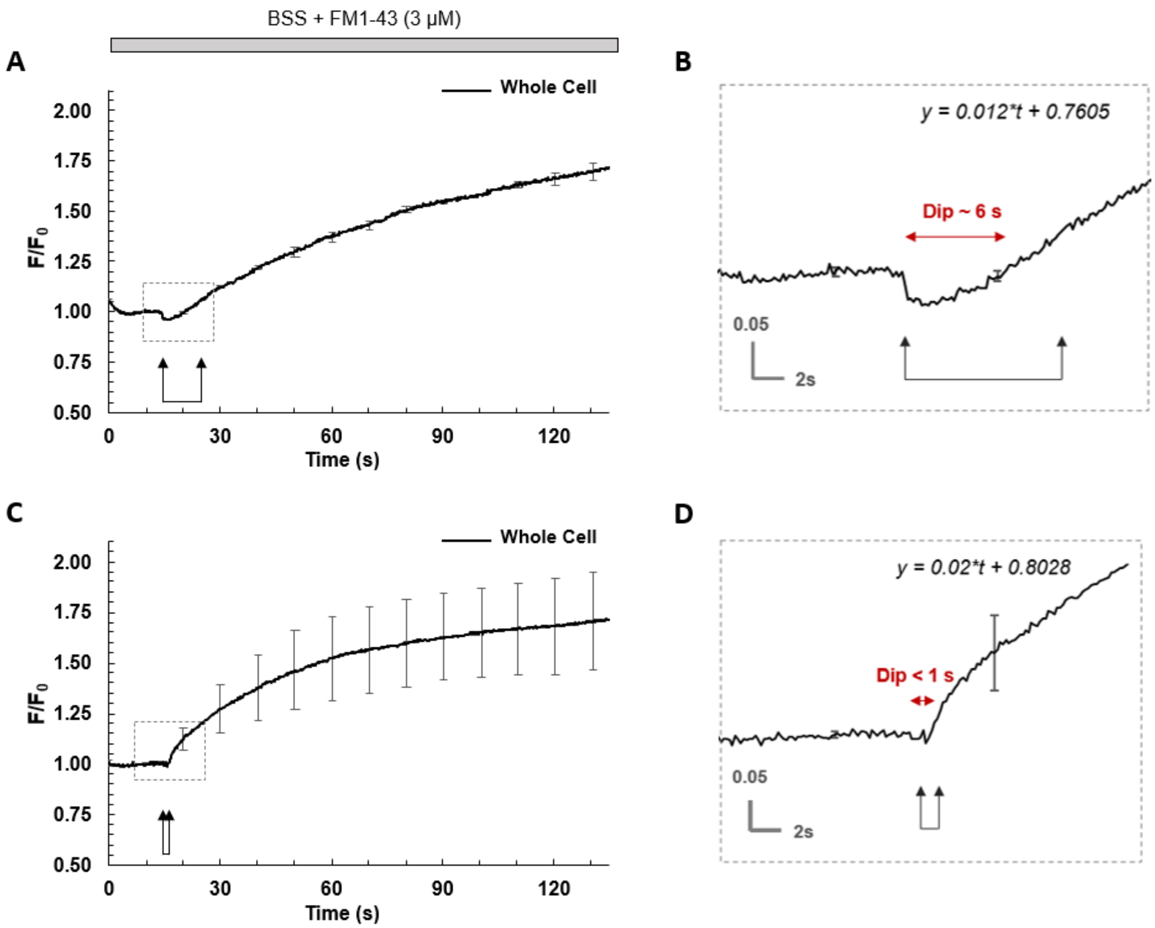

Figure 3.10 Effect of a train of ten 30 ns electric pulses at 1 Hz and 10 Hz on FM1-43 labeled chromaffin cells. (A) and (C) show the averaged whole cell fluorescence ± SE (n = 3). The arrows indicate the start and the end of the pulse trains. (B) and (D) are zoomed-in views of the responses during the application of the E-field (inside the dotted rectangles) for (A) and (C), respectively. The equation $y = a*t + b$ was used to compute the rate of increase in fluorescence between the 15 s and 25 s time points.

These results demonstrate that the time course of the FM1-43 response to a train of NEPs is affected by the frequency at which the pulses are delivered. For faster rates of pulse delivery, the increase in FM1-43 occurred faster, coinciding with a shorter duration and amplitude of an initial decrease in fluorescence which, as found for high [K^+] stimulation of the cells, most likely reflects the sensitivity of the dye to a change in membrane potential. These observations of a dip in fluorescence that varied in magnitude and duration based on the frequency at which the pulse train was applied, followed by an overall increase in fluorescence, will be further confirmed using a train of ten 5 ns pulses to stimulate the cells.

3.4.2 **Line profile analysis of membrane fluorescence revealed a differential effect on the anode and cathode facing sides of the cell**

The previous results were generated by analyzing the fluorescence intensity occurring over the entire surface of the cell. To investigate whether NEPs cause heterogeneous effects on the cell membrane with respect to its location between the electrodes, we performed a line profile analysis as described in the Methods section. We generated line scans, 5 µm in width, across the cell and visualized the changes in fluorescence before and after NEP exposure. At the intersection between the lines and the membrane of each cell, there were two fluorescence peaks on each line profile. Just like the analysis performed using high [K^+] as a stimulus, the same 0˚- and 90˚-line orientations were chosen for the line profile analysis. However, in the experiments using NEPs, 0˚ and the 90˚ lines represent the orientations that are parallel and perpendicular, respectively, to the electrodes. Of note is that for the 0˚ line, the intersection between the drawn line and the membrane of the cell correlated with its equators (Equator Left and Equator Right). In contrast, on the 90˚ line, the intersection between the drawn line and the membrane of the cell correlated with its poles (anode and cathode facing sides).

Figure 3.11 and Figure 3.12 show representative examples of the effect of a train of ten 30 ns pulses delivered to a cell at a frequency of 1 Hz on FM1-43 fluorescence in the presence of extracellular Ca^{2+}. Fluorescence photomicrographs of the cell (left) along with their corresponding line profile analysis (right) are shown at various time points: at the start (A and D), end (B and E) and 2 minutes after (C and F) the stimulus application. Along the 90˚ orientation at the end of the stimulus, the anode facing part of the cell (~ 20 µm) always showed an increase in fluorescence contrasting with the cathode facing side (~ 5 µm) that showed a drop in fluorescence relative to its the baseline before the stimulus. However, the differential effects observed in cells stimulated at 10 Hz were more intense and occurred only within 1 s after the initiation of the pulse train. Thus, increasing the frequency of the stimulus resulted in a faster change in fluorescence. Two minutes after pulse application, all the cells exhibited an overall increase in membrane fluorescence that was mainly explained by the exocytotic activity induced by the NEPs.

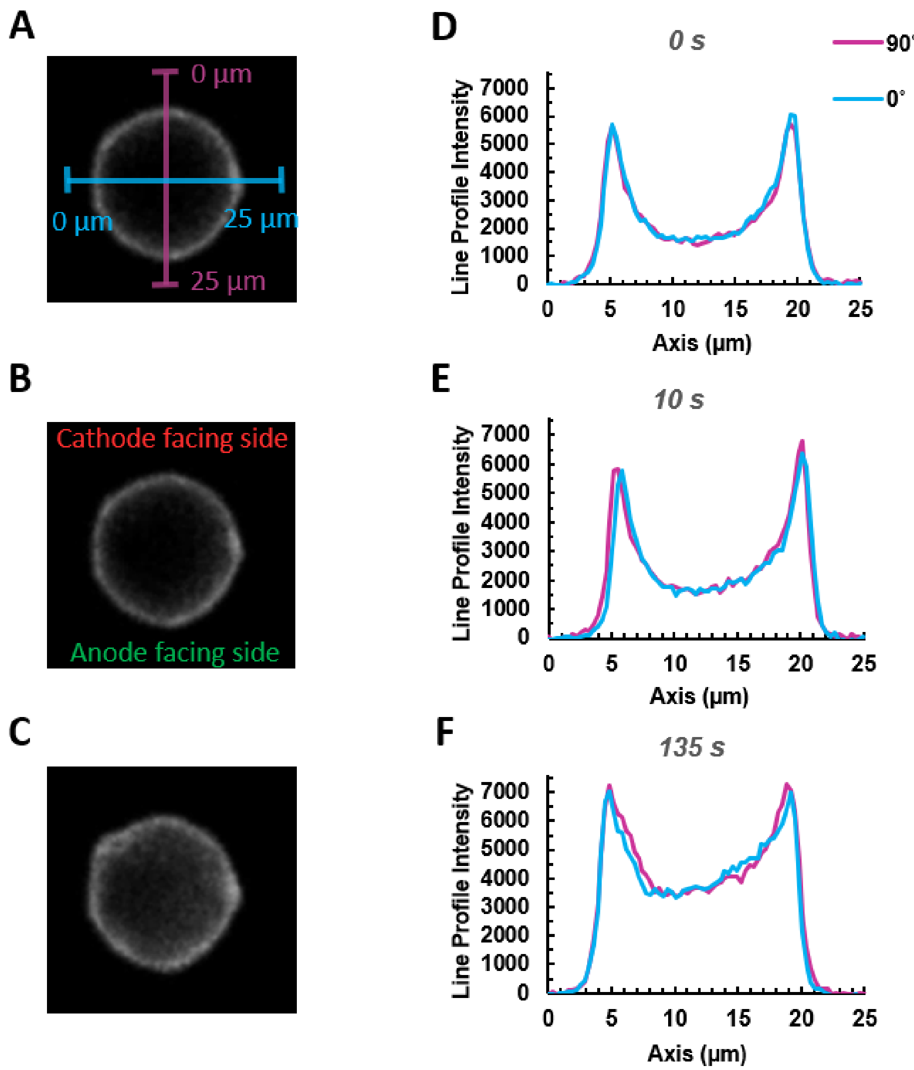

Figure 3.11 Effect of a train of ten 30 ns electric pulses at 1 Hz on FM1-43 labeled chromaffin cells in the presence of Ca^{2+}. The photomicrographs on the left (A, B, and C) show fluorescence images of the stimulated cell along with their corresponding line profiles (D, E, and F) measured respectively at 0 s, at the end of the pulse train (25 s) and 2 minutes after the initiation of the pulses (135 s).

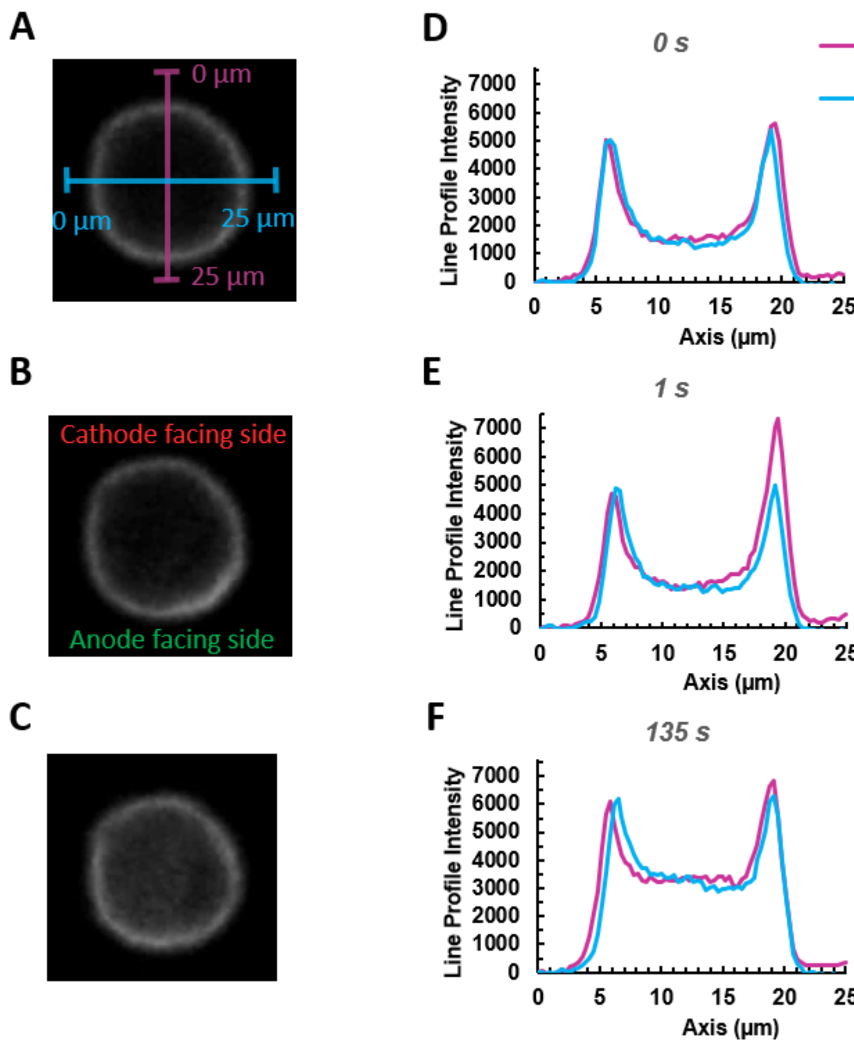

Figure 3.12 Effect of a train of ten 30 ns electric pulses at 10 Hz on FM1-43 labeled chromaffin cells in the presence of Ca^{2+}. The photomicrographs on the left (A, B, and C) show fluorescence images of the stimulated cell along with their corresponding line profiles (D, E, and F) measured respectively at 0 s, at the end of the pulse train (25 s) and 2 minutes after the initiation of the pulses (135 s).

3.5 Monitoring exocytosis in FM1-43 labeled cells in response to 5 ns, 19.8 MV/m pulses

After identifying the effects of stimulating FM1-43 labeled chromaffin cells with 30 ns electric pulses that are much longer in duration than in our previous studies investigating the effects of NEPs on exocytosis, we next investigated the effects of the shorter duration pulses (i.e., 5 ns) on FM1-43 fluorescence using the 2-10 ns FID pulse generator.

3.5.1 Determining the E-field threshold for evoking a fluorescence increase in FM1-43 labeled chromaffin cells in response to a 5 ns electric pulse

As discussed previously, we had established that the E-field amplitude that evoked a Ca^{2+} response in 100% of the cells exposed to a 5 ns pulse was 9 MV/m. Since a goal of this project was to compare the time course of FM1-43 fluorescence changes evoked by a train of ten 5 ns pulses with the time course of exocytotic activity previously monitored by TIRFM in cells similarly exposed to the NEP stimulus, we first determined the E-field amplitude at which 100% of FM1-43 labeled cells exhibited responses to the stimulus. For this analysis, cells showing a response were defined as those with a minimum increase of 5% in F/F_0 measured 2 minutes after the initiation of the pulses.

Figure 3.13 illustrates the average increase in whole cell fluorescence measured 2 minutes after the initiation of the pulses applied at various E-field amplitudes (ranging from 5 to 22 MV/m) either at 1 Hz or at 10 Hz. Note that at 9.9 MV/m, the E-field amplitude sufficient to cause Ca^{2+} responses in 100% of cells exposed to a single 5 ns pulse, fluorescence increases evoked by a train of ten pulses at either 1 or 10 Hz were quite small in magnitude and not observed in all cells. Increasing the amplitude of the applied E-field caused an increase in whole cell fluorescence whether the train of pulses was delivered at 1 Hz or 10 Hz.

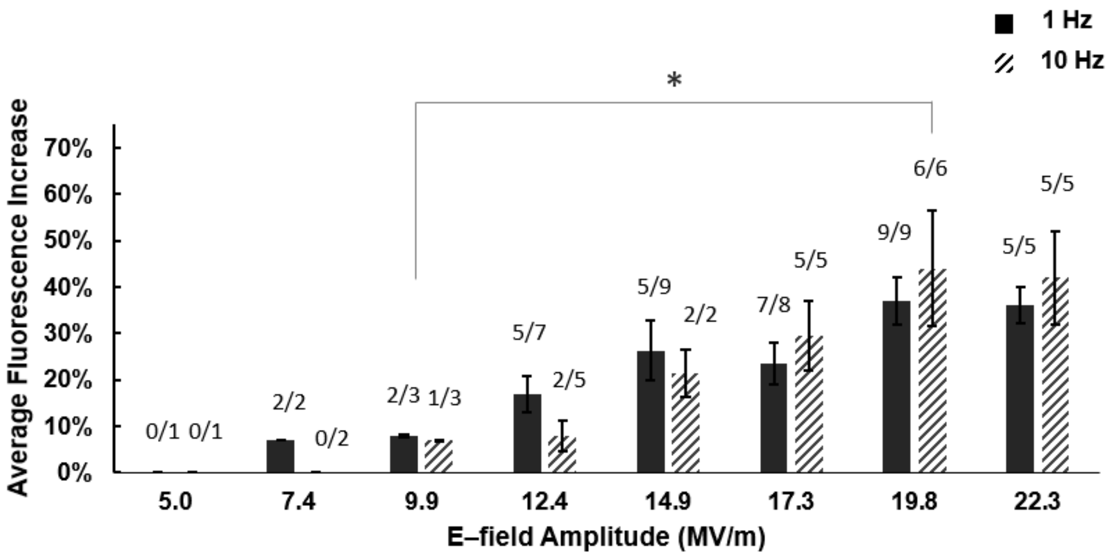

Figure 3.13 Effect of increasing the E-field amplitude on FM1-43 fluorescence. Results represent the average ± SE of the increase in whole cell fluorescence measured two minutes after the initiation of a train of ten 5 ns pulses applied at different electric fields. The E-field increment $\approx$ 2.5 MV/m. * means $p < 0.05$.

Only at E-field amplitudes above 17.3 MV/m did we find that 100% of stimulated cells responded to the train of 10 NEPs at both 1 Hz and 10 Hz. At these higher E-field amplitudes, the cells also exhibited larger increases in FM1-43 fluorescence relative to the increases evoked at low E-field amplitudes. For example, a pulse train delivered at 1 Hz induced an average increase in F/F_0 of 38 ± 3% at 19.8 MV/m that was statistically higher ($p < 0.05$) than that induced at 9.9 MV/m (8 ± 0.4%). Based on these results, all subsequent experiments performed in this project show responses triggered with a train of ten 5 ns pulses applied at 19.8 MV/m.

3.5.2 A train of ten 5 ns pulses evoked long-lived increases in $[Ca^{2+}]_i$ that relied on Ca^{2+} influx

Before assessing FM1-43 fluorescence changes induced by a train of ten 5 ns pulses at 19.8 MV/m, we first investigated the time course, amplitude and Ca^{2+} dependency of the rise in $[Ca^{2+}]_i$ evoked by the pulse train, particularly the latter given the much higher E-field amplitude that could also potentially permeabilize intracellular Ca^{2+} storing organelles such as the endoplasmic reticulum [***50***]. For the analysis, Ca^{2+} responses were monitored in Calcium Green-1-labeled cells stimulated by a train of ten NEPs delivered at 1 or 10 Hz.

As shown in Figure 3.14, cells exhibited an immediate rise in $[Ca^{2+}]_i$ that started with the pulse application. The rise in $[Ca^{2+}]_i$ was faster when the pulse train was delivered at 10 Hz. The average increase in $[Ca^{2+}]_i$ was ~ 142% within 5 s from the initiation of the pulses in the case of 1 Hz and ~ 136% achieved within 0.6 s after the end of the pulses delivered at 10 Hz. The Ca^{2+} responses were long-lived and slowly recovered to lower levels with half-widths of ~ 89 s for 1 Hz and ~ 62 s for 10 Hz.

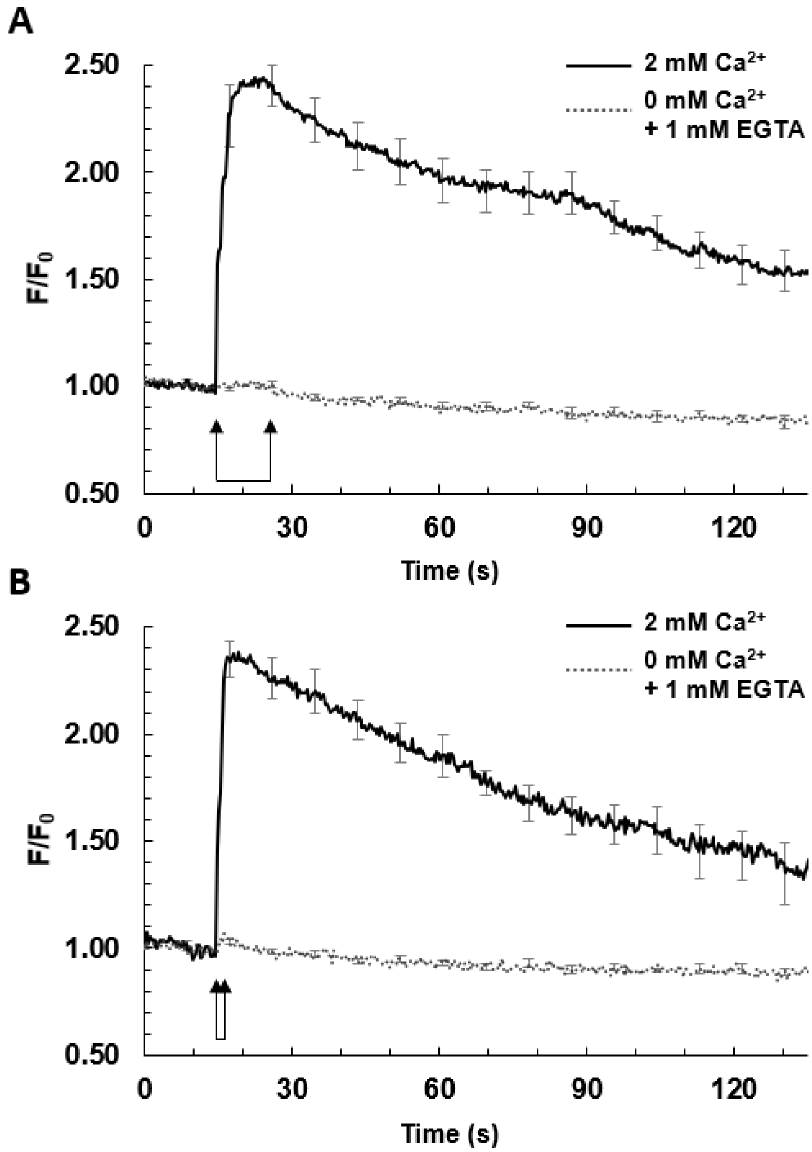

Figure 3.14 Ca^{2+} responses in chromaffin cells exposed to ten 5 ns, 19.8 MV/m electric pulses. (A) shows the averaged Ca^{2+} responses ± SE in the presence (n = 5) or absence (n = 6) of external Ca^{2+} for cells stimulated at 1 Hz. (B) shows the averaged Ca^{2+} responses ± SE in the presence (n = 5) or absence (n = 6) of external Ca^{2+} for cells stimulated at 10 Hz. The arrows indicate the start and the end of the pulse trains.

Figure 3.14 also shows that there was no increase in $[Ca^{2+}]_i$ when Ca^{2+} was absent from the extracellular solution. This result indicates that the source of Ca^{2+} that caused the NEP-induced elevation of $[Ca^{2+}]_i$ in the stimulated cells was extracellular, not Ca^{2+} released from intracellular stores such as the endoplasmic reticulum due to electropermeabilization. Thus, despite the higher E-field amplitude being used for cell stimulation, the internal Ca^{2+} stores' electropermeabilization was not a factor in the Ca^{2+} responses of the cells.

3.5.3 Similar to 30 ns pulses, 5 ns electric pulses evoked a whole cell fluorescence increase in FM1-43 labeled chromaffin cells

After assessing the effect of 5 ns pulse trains on Ca^{2+} responses, we next monitored the effect of ten 5 ns pulses on FM1-43 fluorescence. For these experiments, baseline fluorescence level was monitored for 15 s, then a train of ten 5 ns electrical pulses was applied at either 1 Hz or 10 Hz using the same protocol shown in Figure 3.9. NEP-evoked changes in fluorescence were monitored for 120 s following the stimulus.

When analyzing the whole cell fluorescence of the cells, we found that a train of ten pulses delivered at 1 Hz or 10 Hz in the presence of external Ca^{2+} resulted in an increase in FM1-43 fluorescence (Figure 3.15). The magnitude of the increase was not as pronounced as found for a train of ten 30 ns pulses (Figure 3.10), most likely because 30 ns pulses were a more intense stimulus. On the other hand, as found for a train of 30 ns pulses, at 1 Hz FM1-43 responses showed a small decrease in fluorescence (dip) that started at the time of delivery of the pulses (i.e., 15 s) and lasted about 3 s (Figure 3.15 B). At 10 Hz, a much small and shorter-lived dip was detectable immediately at the start of the train of pulses (Figure 3.15 D). Again, this decrease most likely reflected the sensitivity of the dye to changes in membrane potential.

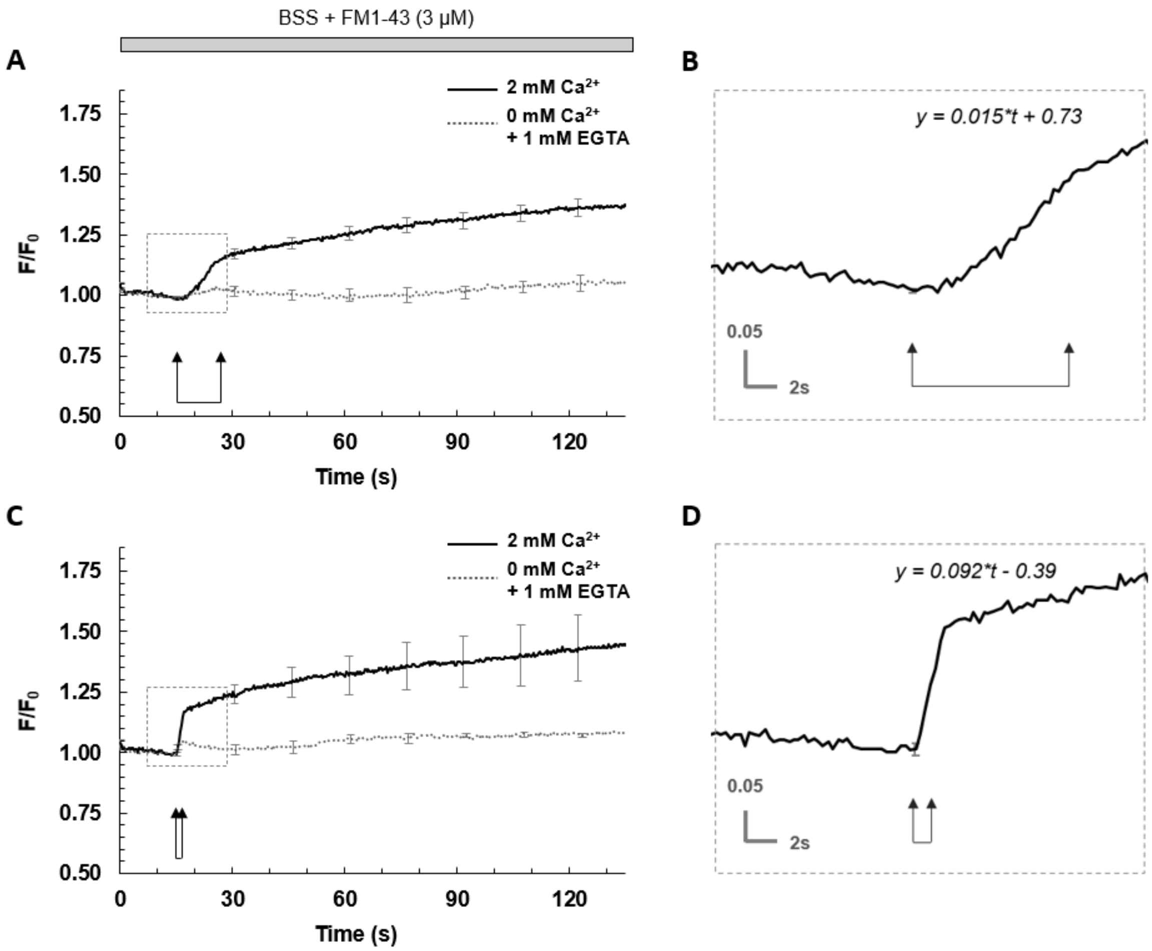

Figure 3.15 Effect of a train of ten 5 ns, 19.8 MV/m pulses at 1 Hz and 10 Hz on FM1-43 labeled chromaffin cells. (A) shows the average response ± SE of cells stimulated at 1 Hz in the presence (n = 9) or absence (n = 3) of Ca^{2+}. (C) shows the average response ± SE of cells stimulated at 10 Hz in the presence (n = 5) or absence (n = 3) of Ca^{2+}. The arrows indicate the start and the end of the pulse trains. (B) and (D) are zoomed-in views of the responses during the application of the E-field (inside the dotted rectangles) for (A) and (C), respectively. The equation $y = a*t + b$ was used to compute the rate of increase in fluorescence between the 15 s and 25 s time points.

For assessing further the changes in FM1-43 fluorescence, three time points were analyzed: 1) at the beginning of the monitoring period, 0 s, 2) at the time when the stimulus ended, which was 25 s for a 1 Hz pulse train and 16 s for a 10 Hz pulse train, and 3) 120 s (2 minutes) after the initiation of the pulses, which was 135 s for all the sequences.

As shown in Figure 3.15, for cells stimulated at 1 Hz, there was an instantaneous dip in FM1-43 fluorescence that was interrupted by the fluorescence increase that started midway in the pulse train, reaching an average of 14 ± 2% at the end of the exposure period (25 s). However, at the faster repetition rate, 10 Hz, the amplitude and duration of the initial decrease in fluorescence was barely noticeable then FM1-43 fluorescence underwent a faster increase than at 1 Hz. The increase in FM1-43 fluorescence in cells stimulated at 10 Hz, was faster and reached an average of 16 ± 3% at the end of the exposure period (16 s). No statistical difference was observed between the average fluorescence increase measured at the 1 Hz and 10 Hz stimuli. Once again, we computed the rate of increase in fluorescence by fitting the data between the start and the end of the pulse train (between the arrows) to a linear equation in the form of $y = a*t + b$. The equations for 1 Hz and 10 Hz are shown in Figure 3.15 B and D (insets of the plots in A and C). The slope of the increase in fluorescence (term a in the equation) estimated at 10 Hz was ~6 times higher than that estimated at 1 Hz. Similar to the results observed with 30 ns pulses, the time course of change in FM1-43 fluorescence during the application of the E-field was dependent on the frequency of application of the pulse train.

We next assessed the amplitude of the increase in FM1-43 fluorescence at 2 minutes post-stimulation (135 s). Cells stimulated with the pulse train delivered at 1 Hz showed an average increase of 38 ± 3% whereas the average increase in FM1-43 fluorescence in cells stimulated with the pulse train delivered at the higher frequency, 10 Hz, reached an average of 44 ± 13% at 135 s. The difference between the average levels of increase at 1 Hz and 10 Hz was not significant ($p > 0.05$). We attributed the increase in fluorescence in each case to exocytosis triggered by the rise in $[Ca^{2+}]_i$ induced by the pulses (Figure 3.14). To confirm this, we conducted experiments in the absence of extracellular Ca^{2+}. We found that the responses triggered by ten 5 ns pulses under Ca^{2+}-free conditions were different than those obtained in the presence of Ca^{2+}. That is, when Ca^{2+} was eliminated from the external solution, whole cell fluorescence at the end of the NEP stimulus train remained near baseline levels. Taken together, these results suggest that the increase in fluorescence that occurred in the presence of Ca^{2+} after stimulus application was mostly due to NEP-induced exocytosis.

3.5.4 **Line profile analysis of membrane fluorescence revealed a differential effect on the anode and cathode facing sides of the cell evoked by a train of 5 ns pulses**

Figure 3.16 shows an example of the effect of a train of ten 5 ns pulses delivered to a cell at a frequency of 1 Hz on FM1-43 fluorescence in the presence of extracellular Ca^{2+}. Representative fluorescence photomicrographs of the cell (left) along with their corresponding line profile analysis (right) are shown at various time points: at the start (A and D), end (B and E) and 2 minutes after (C and F) the stimulus application. Along the 90° orientation at the end of the stimulus, the anode facing part of the cell (~ 20 μm) always showed a significant increase in fluorescence contrasting with the cathode facing side (~ 5 μm) that showed a decrease in fluorescence. Two minutes after pulse application, all the cells exhibited an overall increase in membrane fluorescence that represented the exocytotic activity induced by the NEPs.

In contrast, Figure 3.17 shows an example of the effect of a train of ten 5 ns pulses delivered to a cell at the frequency of 10 Hz in the presence of extracellular Ca^{2+}. Similar to the effects observed at 1 Hz, at the end of application of the 10 Hz stimulus the poles of the cells (along the 90° orientation) exhibited an increase in fluorescence at the anode facing side and a decrease in fluorescence at the cathode facing side of the membrane. However, these differential effects occurred within 1 s after the initiation of the pulse train, which resulted in a faster change in fluorescence than for the 1 Hz stimulus. Two minutes after the stimulation, membrane fluorescence increased in both orientations representing an increase in exocytotic activity induced by the applied NEPs.

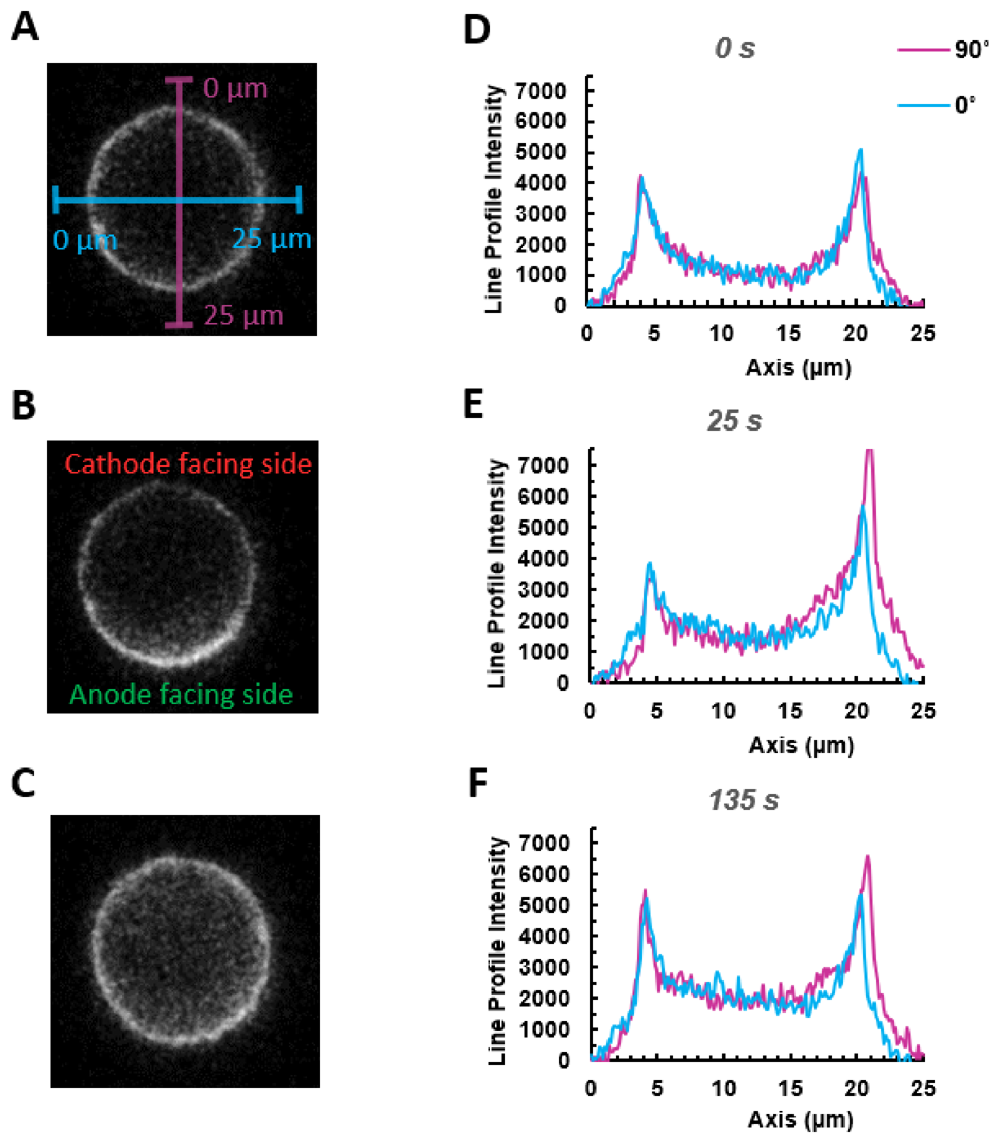

Figure 3.16 Effect of a train of ten 5 ns electric pulses at 1 Hz on FM1-43 labeled chromaffin cells in the presence of Ca^{2+}. The photomicrographs on the left (A, B, and C) show fluorescence images of the stimulated cell along with their corresponding line profiles (D, E, and F) measured respectively at 0 s, at the end of the pulse train (25 s) and 2 minutes after the initiation of the pulses (135 s).

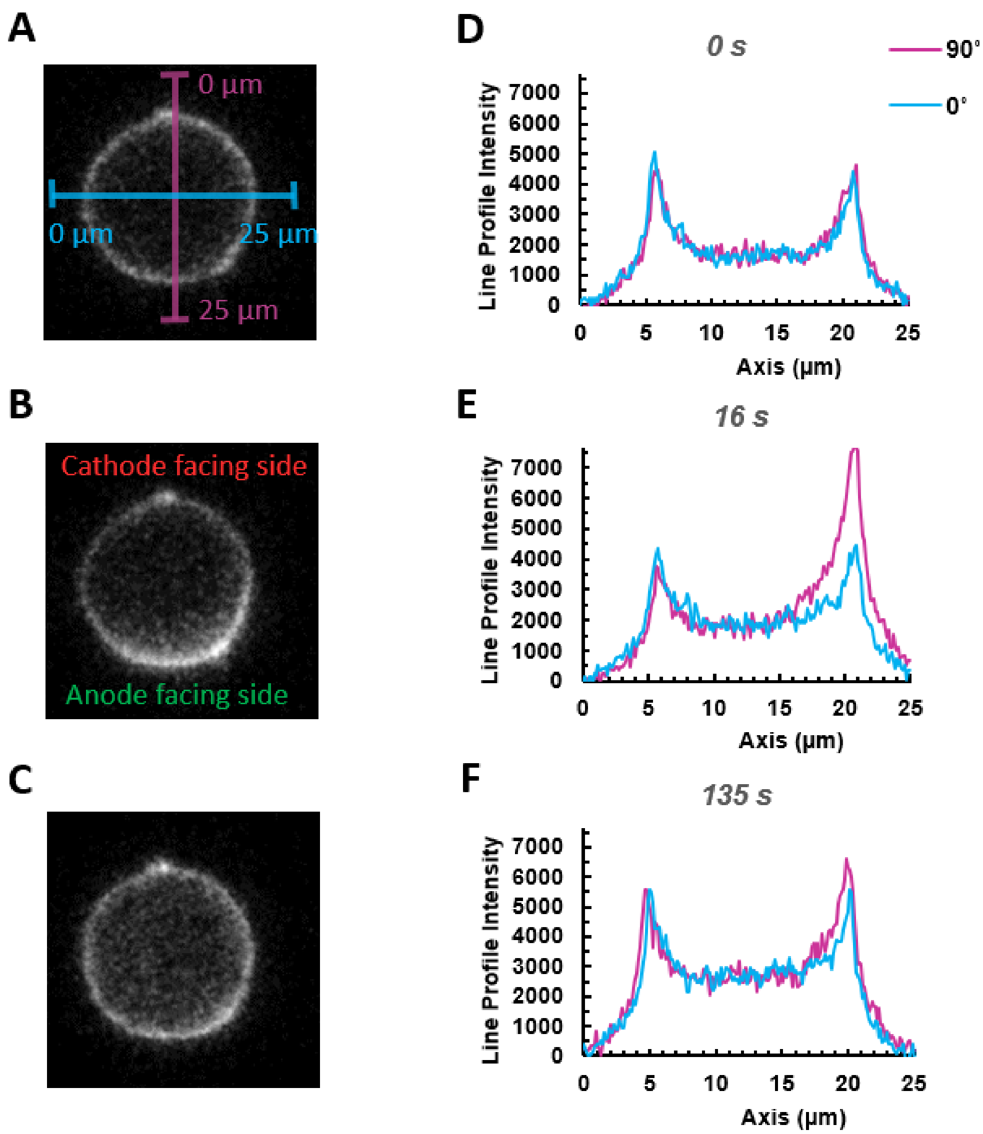

Figure 3.17 Effect of a train of ten 5 ns electric pulses at 10 Hz on FM1-43 labeled chromaffin cells in the presence of Ca^{2+}. The photomicrographs on the left (A, B, and C) show fluorescence images of the stimulated cell along with their corresponding line profiles (D, E, and F) measured respectively at 0 s, at the end of the pulse train (16 s) and two minutes after the initiation of the pulses (135 s).

We also performed a line profile analysis in the absence of external Ca^{2+} to investigate the dependence of the membrane fluorescence changes induced by the application of NEPs to Ca^{2+}. At the end of delivery of the pulses, the differential effects on FM1-43 fluorescence at the poles of the cell (along the 90° orientation) persisted under Ca^{2+}-free conditions. However, after the pulse train ended, we found that eliminating Ca^{2+} from the external solution caused no increase in membrane fluorescence (Figure 3.18 and Figure 3.19) unlike the increase in membrane fluorescence observed in the presence of Ca^{2+}. These results indicate that the increase in fluorescence observed after the end of the 1 and 10 Hz pulse trains in the presence of extracellular Ca^{2+} was Ca^{2+}-dependent and represented NEP-induced exocytosis.

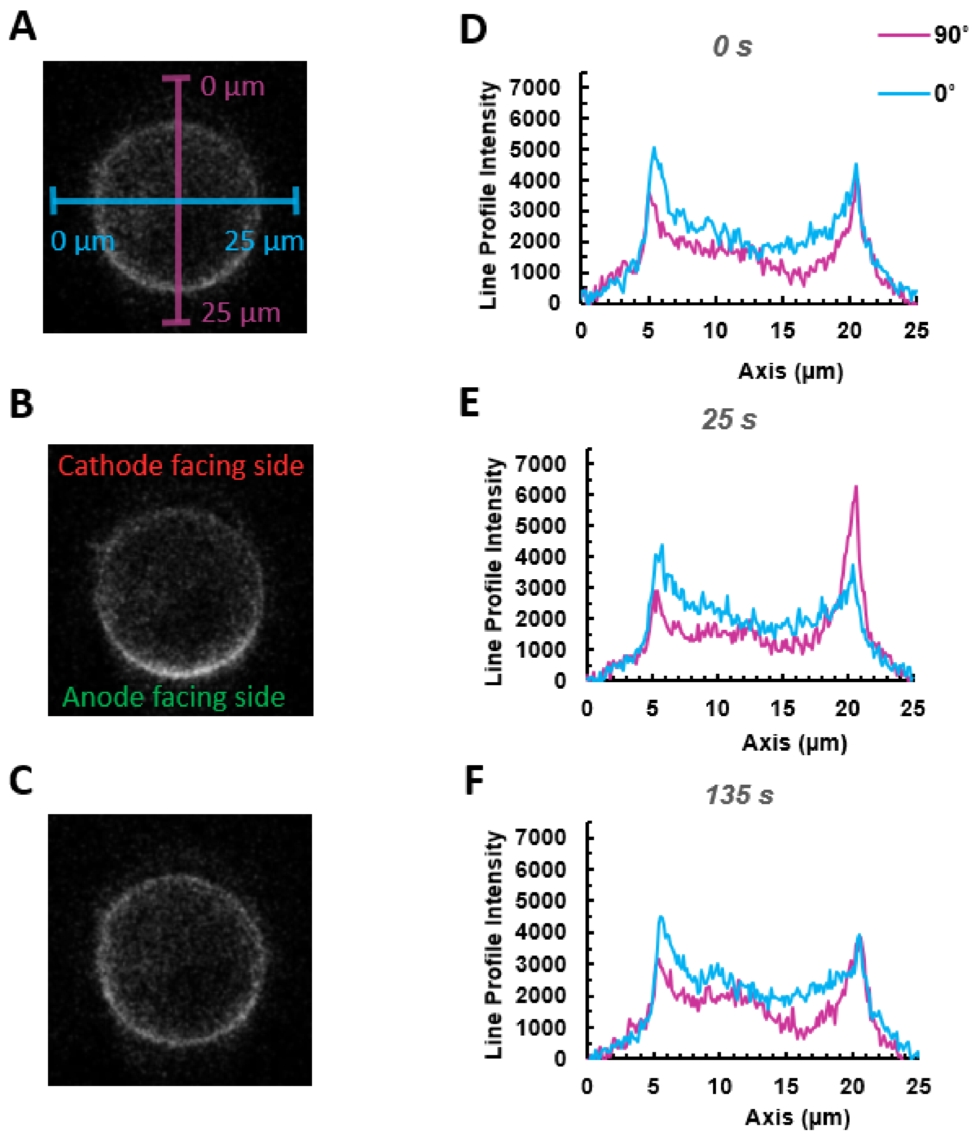

Figure 3.18 Effect of a train of ten 5 ns electric pulses at 1 Hz on FM1-43 labeled chromaffin cells in the absence of Ca^{2+}. The photomicrographs on the left (A, B, and C) show fluorescence images of the stimulated cell along with their corresponding line profiles (D, E, and F) measured respectively at 0 s, at the end of the pulse train (25 s) and two minutes after the initiation of the pulses (135 s).

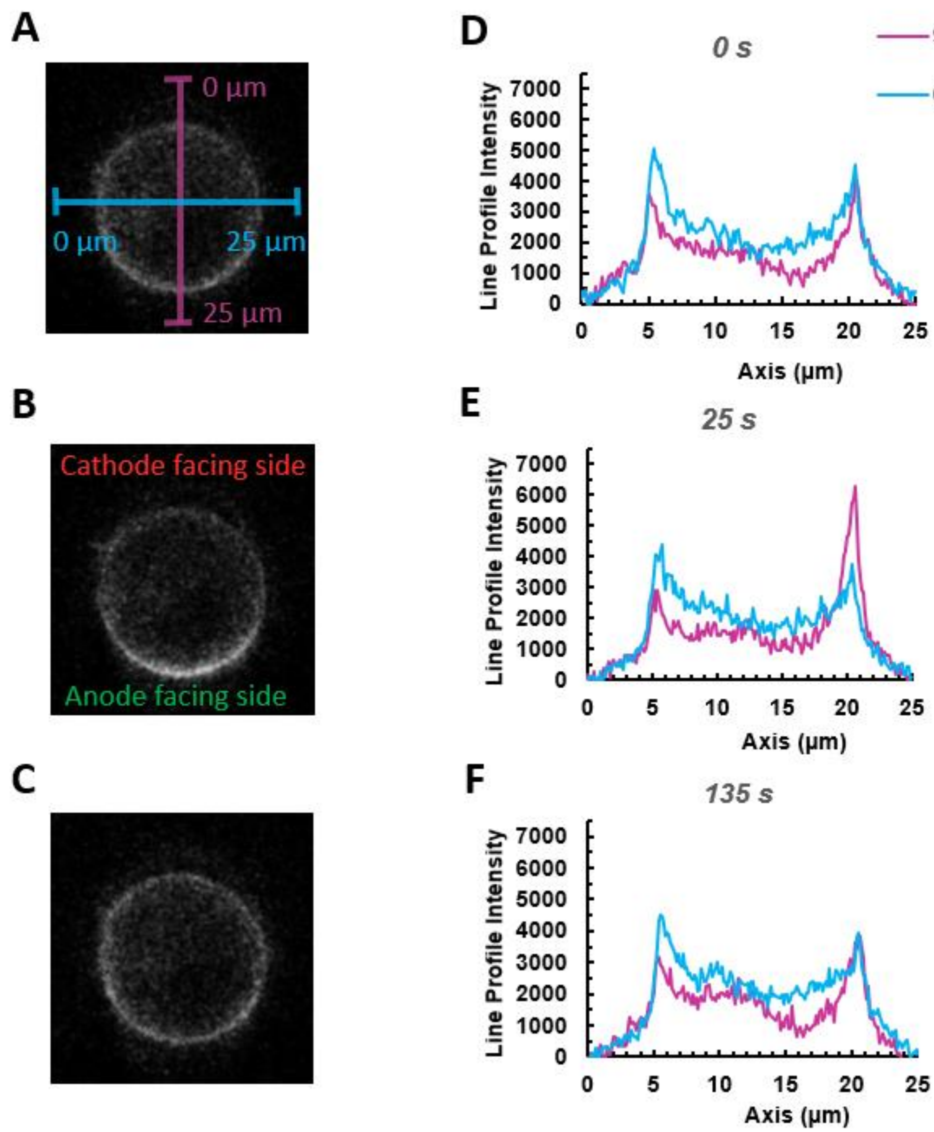

Figure 3.19 Effect of a train of ten 5 ns electric pulses at 10 Hz on FM1-43 labeled chromaffin cells in the absence of Ca^{2+}. The photomicrographs on the left (A, B, and C) show fluorescence images of the stimulated cell along with their corresponding line profiles (D, E, and F) measured respectively at 0 s, at the end of the pulse train (16 s) and two minutes after the initiation of the pulses (135 s).

3.5.5 5 ns electric pulses evoked differential responses in the different parts of the cell membrane dependently to their locations to the electrodes

As revealed in the line profile analysis, a train of ten 5 ns pulses induced differential effects on the different parts of the cell membrane relative to the cell orientation between the electrodes. To assess the characteristics of these differential responses, we next investigated the FM1-43 fluorescence changes over time on each of the four different regions of the cell relative to their position between the electrodes: the anode facing side, the cathode facing side, the equator left and the equator right as shown in Figure 3.20.

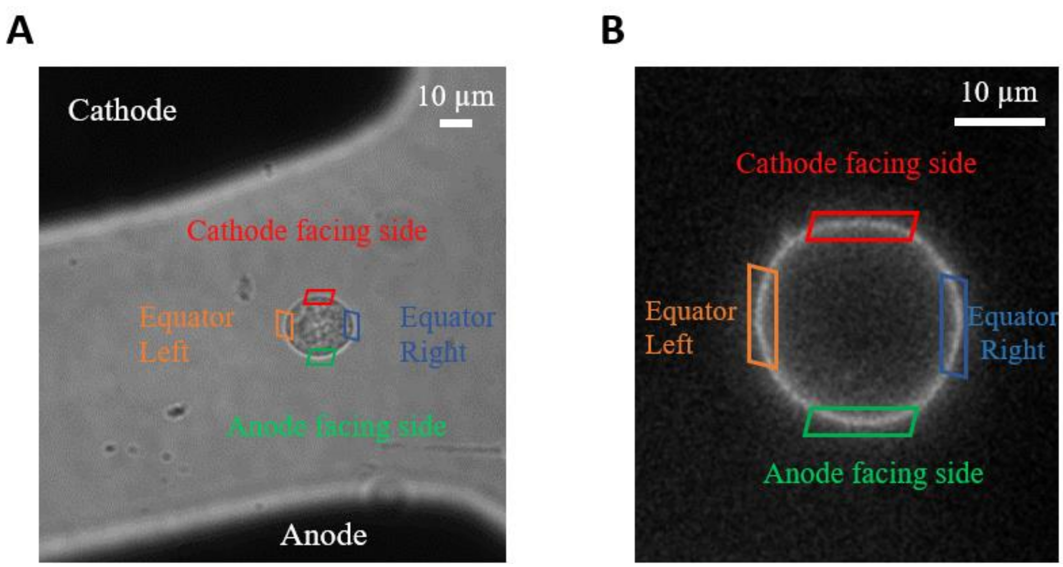

Figure 3.20 Regions of interest analyzed for studying the effect of NEPs on FM1-43 labeled chromaffin cell membranes. (A) and (B) show the four different parts of the cell membrane based on their location relative to the electrodes, respectively, in bright field and in fluorescence mode. As described in the Methods section, the poles of the cells were the anode facing side (in green) and cathode facing side (in red). The equators (in orange and blue) were the left and right areas of the cell membrane away from the electrodes.

Figure 3.21 displays the averaged responses of the four distinct parts of the cell membrane for cells stimulated with 10 NEPs applied at 1 Hz. We found that in the presence of external Ca^{2+}, each part of the cell membrane demonstrated a distinctive change in fluorescence during the application of the pulses. The cathode facing side of the membrane showed a decrease in fluorescence whereas the anode facing side of the membrane showed an increase in fluorescence. The left equator part of the membrane showed an increase in fluorescence that was less intense than that evoked at the anode facing of the membrane. In contrast, the right equator part of the membrane showed a small dip in fluorescence which, unlike that at cathode facing side of the membrane, did not last as long as the duration of the entire stimulus. After the pulse train ended, all four parts of the cell membrane showed an increase in fluorescence that can be explained by exocytotic activity induced by the applied NEP stimulus.

When experiments were conducted in the absence of extracellular Ca^{2+}, either an increase (anode facing side) or a decrease (cathode facing and equatorial sides) in fluorescence was observed only during pulse application. The effect at the anode facing side of the cell membrane was significantly attenuated relative to the one observed in the presence of external Ca^{2+}, and the small decrease in fluorescence on the cathode facing side of the membrane was sustained, remaining slightly below baseline during the entire monitoring period. As a whole, the fluorescence of all four parts of the membrane tended to return to baseline after the pulse train ended, supporting the conclusion that the increase in fluorescence occurring after the pulse train in the presence of external Ca^{2+} represented Ca^{2+}-dependent exocytosis.

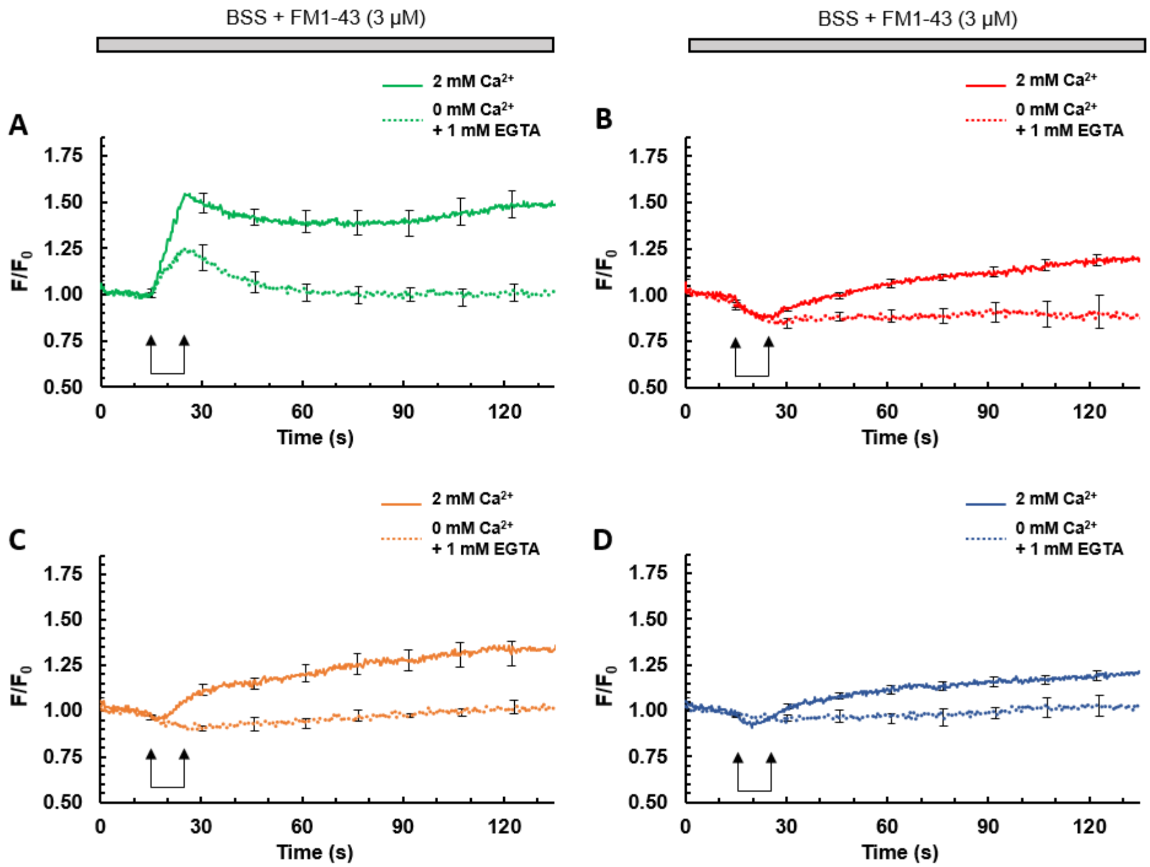

Figure 3.21 Effect of ten 5 ns pulses delivered at 1 Hz on the different parts of the cell membrane. The four panels show, respectively, the responses at the anode facing side (green) in (A), cathode facing side (red) in (B), equator left (orange) in (C) and equator right (blue) in (D). The arrows indicate the start and the end of the pulse train. The graphs represent the averaged responses ± SE from cells in the presence of Ca^{2+} (n = 9) or the absence (n = 3) of Ca^{2+}.

We next changed the frequency of delivery of the pulse train from 1 Hz to 10 Hz. As seen in Figure 3.22, we found that both in the presence or absence of Ca^{2+}, the differential effects on FM1-43 fluorescence seen at 1 Hz were also observed at 10 Hz. However, at 10 Hz the effects occurred faster than in the case of 1 Hz. Specifically, the differential changes in fluorescence detected largely on the poles of the cells occurred only

1 s post-stimulation, instead of 10 s as seen at the slower stimulation rate. This suggests that the time course of the differential effects detected using FM1-43 during the application of the pulse train was dependent on the frequency of the stimulus.

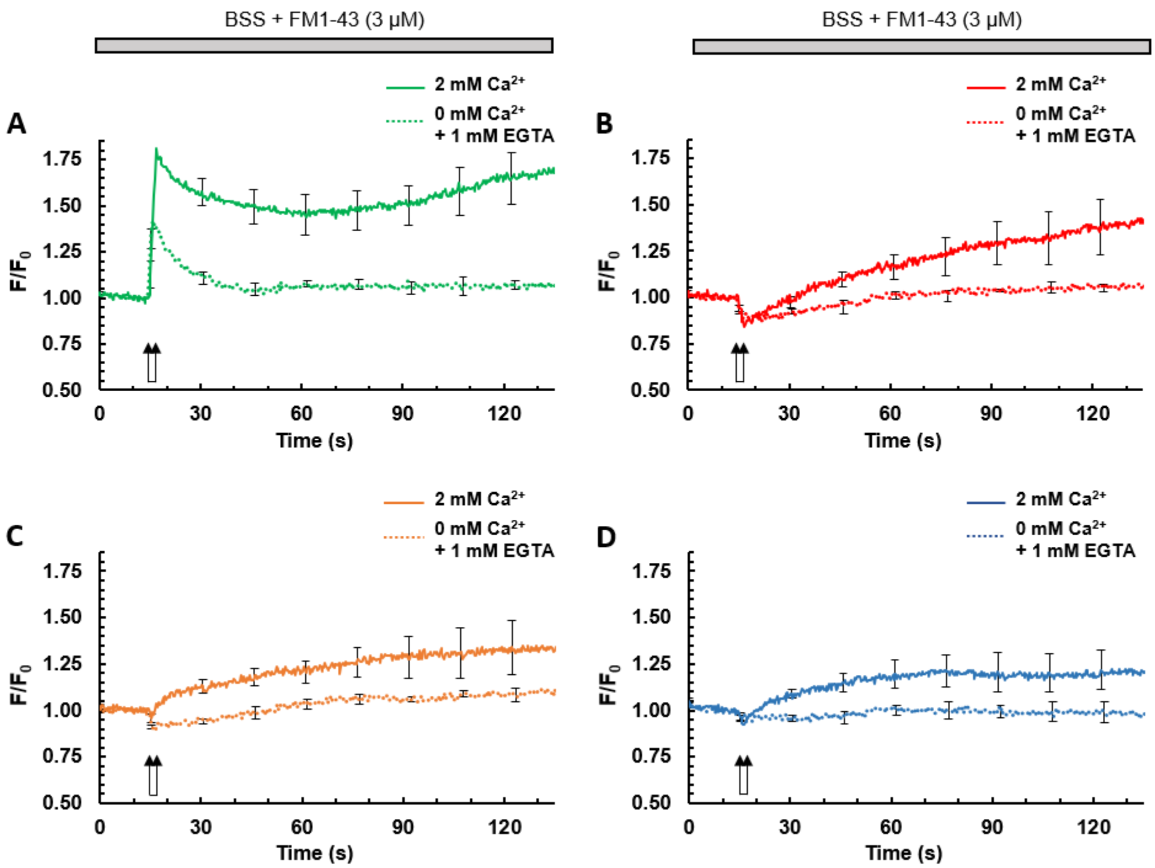

Figure 3.22 Effect of ten 5 ns pulses delivered at 10 Hz on the different parts of the cell membrane. The four panels show, respectively, the responses at the anode facing side (green) in (A), cathode facing side (red) in (B), equator left (orange) in (C) and equator right (blue) in (D). The arrows indicate the start and the end of the pulse train. The graphs represent the averaged responses ± SE from cells in the presence of Ca^{2+} (n = 5) or the absence (n = 3) of Ca^{2+}.

Figure 3.23 summarizes the differential FM14-3 fluorescence changes measured at the end of the 1 Hz and 10 Hz pulse trains delivered in the presence of Ca^{2+}. Our results indicate that the differential effect was more pronounced on the poles of the stimulated cells. The anode facing part (in green) showed an increase in fluorescence and the cathode facing part (in red) showed a decrease in fluorescence. These differential changes in FM1-43 fluorescence occurring only during E-field exposure were obviously dependent on the polarity of the electrodes and were attributed to the ability of the dye to detect changes in membrane potential, similar to the differential changes in fluorescence observed during the application of 30 ns pulses and analogous to the decrease in fluorescence in response to membrane depolarization elicited by high [K^+] stimulation. We explain the differential effects induced by the 5 ns pulse trains as changes in TMP at the poles of the cells induced by the propagation of the electric current from the anode to the cathode. The decrease in fluorescence captured at the cathode facing part and the increase in fluorescence at the anode facing part were interpreted as the depolarization and the hyperpolarization, respectively, of these parts of the membrane.

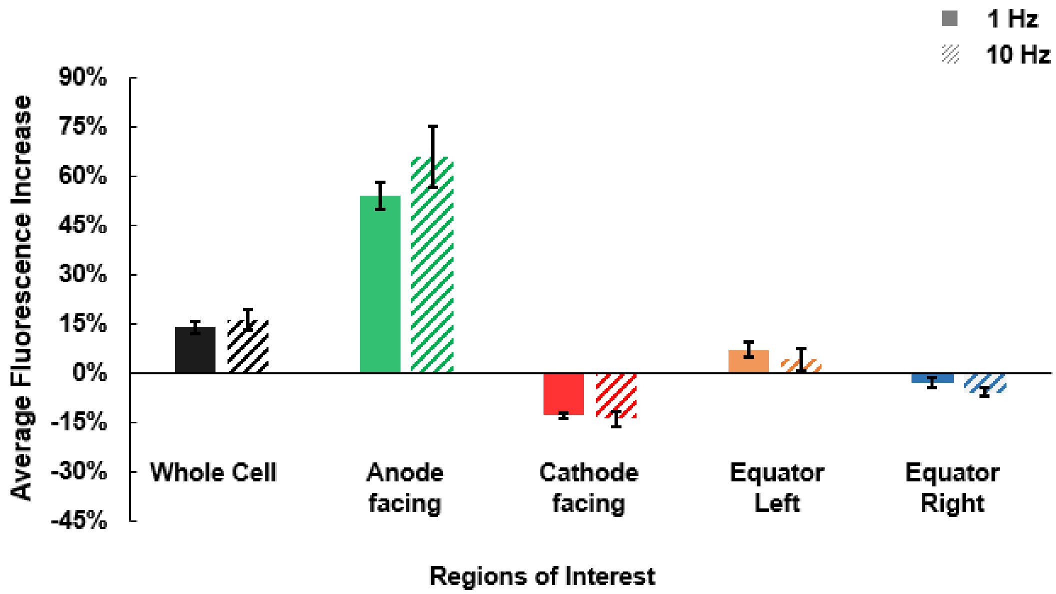

Figure 3.23 Summary of the differential effects of a train of ten 5 ns pulses at 19.8 MV/m on the different parts of the cell membrane. The bars represent the average change in FM1-43 fluorescence ± SE measured at the end of the pulse train at the different regions of interest of cells stimulated at 1 Hz (n = 9) or 10 Hz (n = 5). Extracellular Ca^{2+} was present in the solution. No statistically significant difference was observed between 1 Hz and 10 Hz data ($p > 0.05$).

Figure 3.24 summarizes the differential FM14-3 fluorescence changes measured two minutes after the end of the 1 Hz and 10 Hz pulse trains for the same cells in Figure 3.23. FM1-43 fluorescence increased in intensity on all parts of the cell membrane. As stated previously, there was no significant increase in membrane fluorescence observed in the absence of Ca^{2+} after the pulse train ended, indicating that the fluorescence increase occurring in the cell membrane after the application of the E-field was likely representative of Ca^{2+}-dependent exocytotic activity.

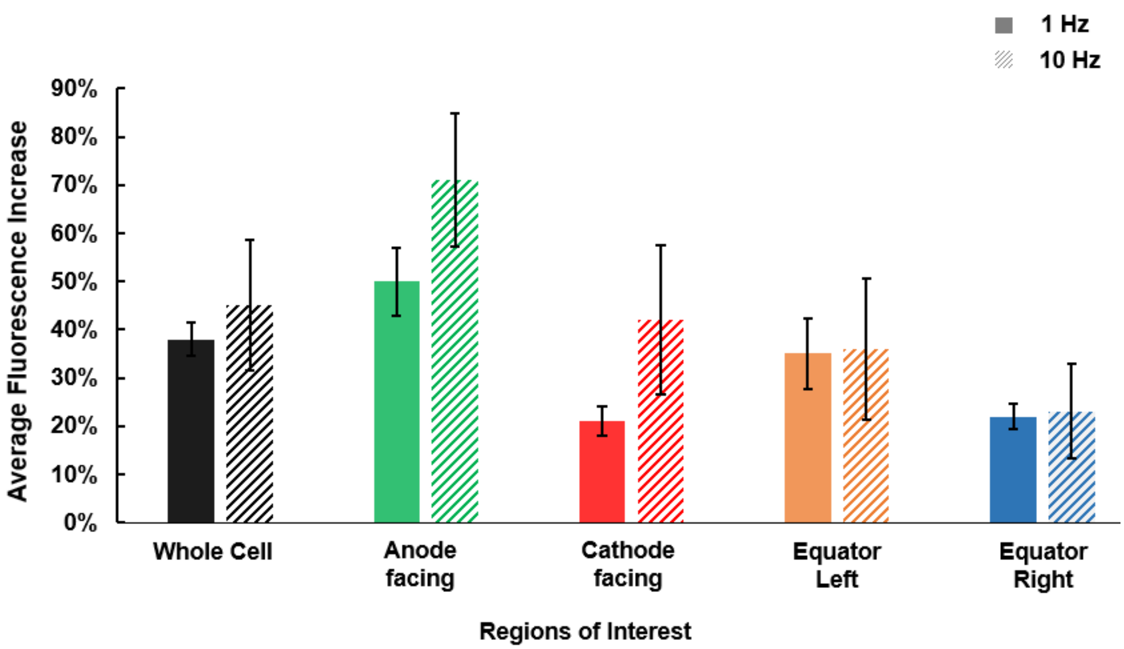

Figure 3.24 Summary of the exocytotic effects of a train of ten 5 ns pulses at 19.8 MV/m on the different parts of the cell membrane in the presence of extracellular Ca^{2+}. The bars represent the average change in FM1-43 fluorescence ± SE measured two minutes after the initiation of the pulse train at the different regions of interest of cells stimulated at 1 Hz (n = 9) or 10 Hz (n = 5). No statistically significant difference was observed between 1 Hz and 10 Hz data ($p > 0.05$).

3.5.6 Assessing the Ca^{2+}-dependent exocytotic response evoked by the pulse train and monitored by FM1-43

The increase in fluorescence measured two minutes after the delivery of the 5 ns pulse trains (ten pulses at 1 Hz and 10 Hz) reflected mainly the increase in exocytotic activity that was dependent on the presence of extracellular Ca^{2+} in the solution. To assess the amount of increase in membrane fluorescence attributed only to the NEP-induced exocytosis, we subtracted the averaged response obtained in the absence of Ca^{2+} from the averaged response obtained in the presence of Ca^{2+}.

The traces shown in Figure 3.25 and Figure 3.26 display the fluorescence differences computed at the anode facing (green), cathode facing (red), equator Left (orange) and equator Right (blue) parts of the membrane for cells stimulated at 1 Hz and 10 Hz, respectively. We found that similar trends were observed at both 1 and 10 Hz stimulations. The subtracted fluorescence traces on the various parts of the membrane had positive increasing trends. These results confirm once again that the fluorescence increase captured with FM1-43 is caused by the NEP-induced exocytotic activity dependent on the presence of extracellular Ca^{2+}. Consistently with the previous observations, the rate of the increase in fluorescence measured during the application of the E-field at 10 Hz was faster compared to the one at 1 Hz.

Noteworthy is even after the subtraction of the Ca^{2+}-independent signals captured with FM1-43, such as TMP changes observed during the application of the pulse train, the increasing trends were still differential among the distinct parts of the cell membrane. We attribute this difference to several potential explanations, like a possible lack of sensitivity of FM1-43 to the exocytotic activity occurring simultaneously with the differential TMP changes during the delivery of the pulses. Another possible explanation is that the application of NEPs produces a differential exocytotic effect on the poles and equators of the cell, however no clear-cut justification is available now as this is still under investigation.

Normally, subtraction of the fluorescence traces in the absence of Ca^{2+} from the traces obtained in the presence of Ca^{2+}, would allow us to scrutinize the Ca^{2+}-dependent

NEP-induced exocytosis. However, due to the sensitivity of FM1-43 to TMP changes that were particularly detected during the pulse train, we could not assess the onset of the exocytotic events due to NEPs. Thus, no clear evidence of a delay between the initiation of the pulses and the beginning of exocytosis was observed when the latter was monitored using the styryl dye FM1-43.

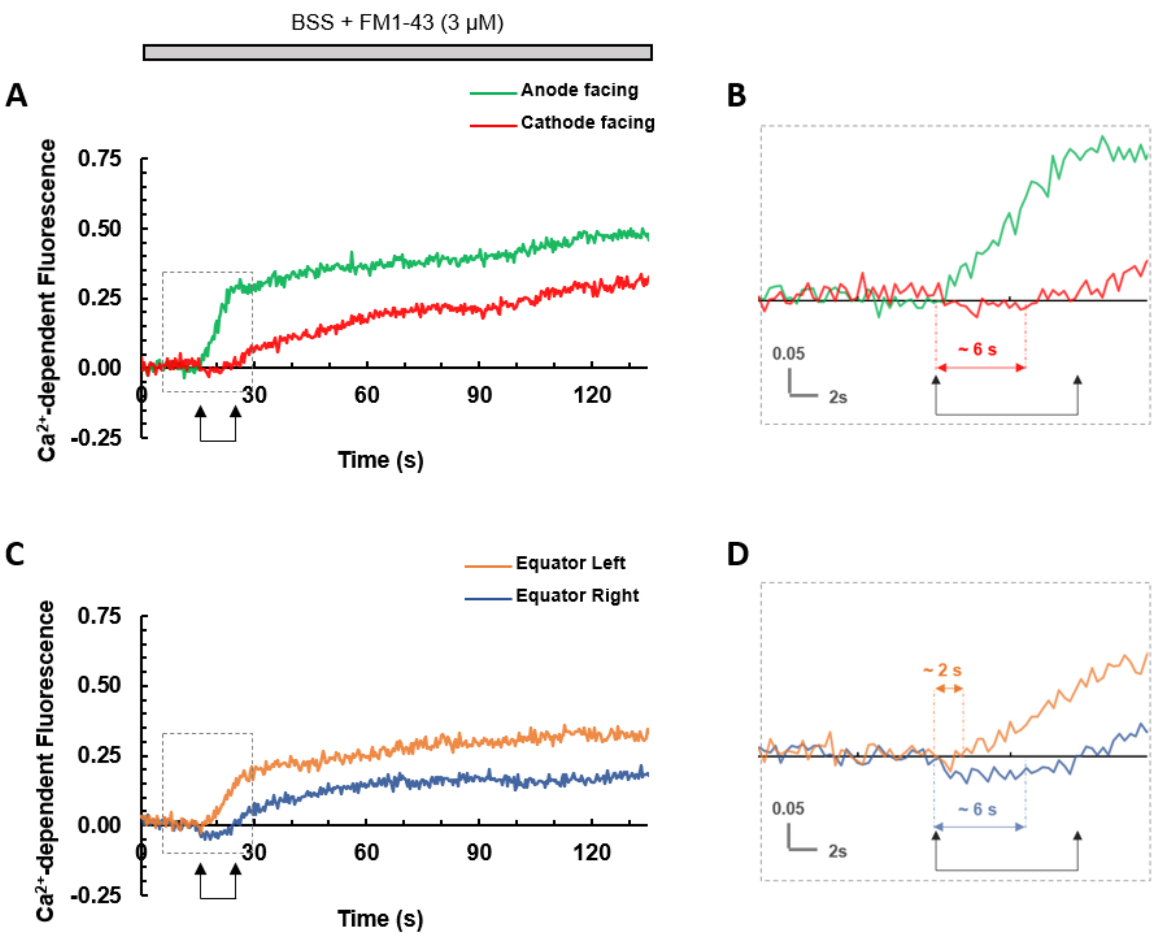

Figure 3.25 Ca^{2+}-dependent FM1-43 fluorescence changes at the poles (A and B) and the equators (C and D) in cells stimulated with ten 5 ns pulses applied at 1 Hz. The "Fluorescence difference" in each plot represent the result of the subtraction of averaged response in the absence of Ca^{2+} (n = 3) from the averaged response in the presence of Ca^{2+} (n = 9). The arrows indicate the duration of the pulse train.

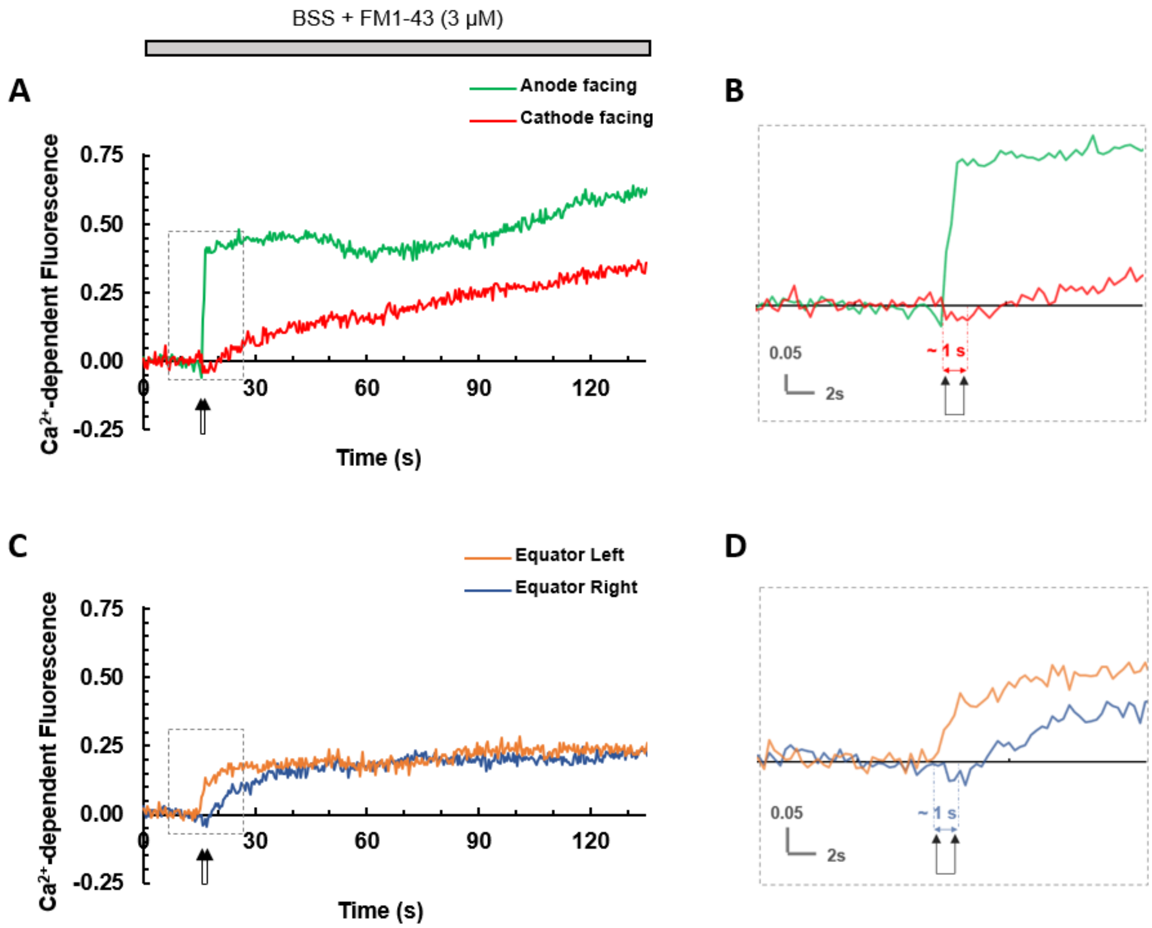

Figure 3.26 Ca^{2+}-dependent FM1-43 fluorescence changes at the poles (A and B) and the equators (C and D) in cells stimulated with ten 5 ns pulses applied at 10 Hz. The "Fluorescence difference" in each plot represent the result of the subtraction of averaged response in the absence of Ca^{2+} (n = 3) from the averaged response in the presence of Ca^{2+} (n = 5). The arrows indicate the duration of the pulse train.

3.6 The differential effects on FM1-43 fluorescence evoked by a 5 ns pulse train are strictly dependent to the E-field orientation

As shown in previous sections, NEPs induced a differential change in FM1-43 fluorescence on the anode facing side (increase in fluorescence) and the cathode facing side (decrease in fluorescence) of a cell membrane during the application of the E-field. The ability of FM1-43 to sense TMP changes allowed us to detect this differential effect, especially on the poles of the cell that were the closest to the electrodes. That is, the decrease in fluorescence at the cathode facing side of the cells and the increase in fluorescence at the anode facing side of the cell were attributed to depolarization and hyperpolarization, respectively. Experiments to validate this conclusion were carried out next.

3.6.1 Reversing the E-field polarity caused the reversing of the differential changes in FM1-43 fluorescence at the poles of the cells

The diagram shown in Figure 3.27 illustrates the strategy that was used to assess the effect of changing the polarity of the stimulation electrodes. Essentially, the cells were stimulated twice. The first stimulation consisted of a train of ten, 5 ns pulses of a polarity. The second stimulation consisted of a train of ten, 5 ns pulses having the same voltage amplitude, pulse width and rate of repetition (1 Hz or 10 Hz) but the opposite polarity Bright field images of the cells were always captured before and after the recorded sequence ended.

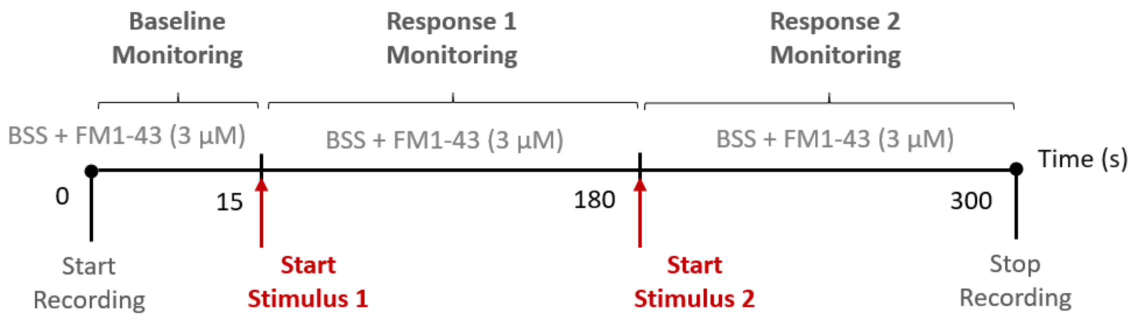

Figure 3.27 Schematic diagram showing the protocol used to monitor the differential changes in FM1-43 fluorescence in response to the application of NEP stimulations having different polarities. A train of ten NEPs were applied at a repetition rate of 1 Hz or 10 Hz at 15 s, then a second train of the opposite polarity applied at 180 s.

We first established that the same cell was able to be stimulated twice and still preserve its morphology and membrane integrity. The results are shown in Figure 3.28 and Figure 3.29 that provide representative photomicrographs of cells stimulated with a positive pulse train and a negative pulse train at 1 Hz and 10 Hz, respectively.

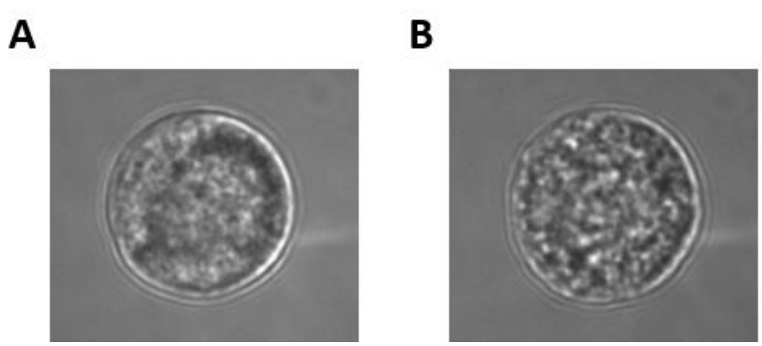

Figure 3.28 Representative images of a chromaffin cell stimulated with a train of ten positive pulses at 15 s and a train of ten negative pulses at 180 s delivered at 1 Hz. (A) and (B) are bright field images captured before (at 0 s) and at the end of monitoring (at 300 s).

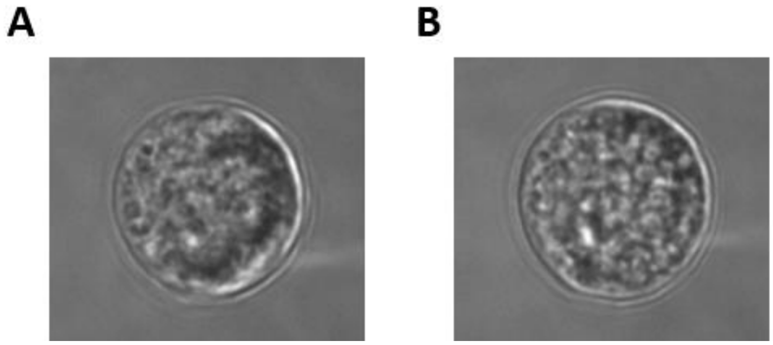

Figure 3.29 Representative images of a chromaffin cell stimulated with a train of ten positive pulses at 15 s and a train of ten negative pulses at 180 s delivered at 10 Hz. (A) and (B) are bright field images captured before (at 0 s) and at the end of monitoring (at 300 s).

Figure 3.30 and Figure 3.31 show the results for each of two cells exposed to a train of 5 ns pulses followed by exposure to a second train of 5 ns pulses applied at the opposite polarity. The frequency of each pulse train was 1 Hz. The whole cell traces show that there was an increase in fluorescence that occurred in response to each pulse train. As expected, we found that the effect on the poles of the cell reversed in accordance with the polarity of the pulses. The pole that was facing the anode and showed an increase in fluorescence during the first stimulation displayed a decrease in fluorescence during the second stimulation and vice versa. Figure 3.32 and Figure 3.33 show the results for each of two cells exposed first to a train of 5 ns pulses followed by exposure to a second train of 5 ns pulses applied at the opposite polarity. Here, the frequency of each pulse train was 10 Hz. The results were the same as those found for the series of NEP stimulations applied at the lower frequency.

In summary, modifying the polarity of the delivered pulses demonstrated that the differential effects of the applied E-field on FM1-43 fluorescence at the poles of an exposed cell (i.e., depolarization and hyperpolarization) were strictly associated with the orientation of the applied pulses.

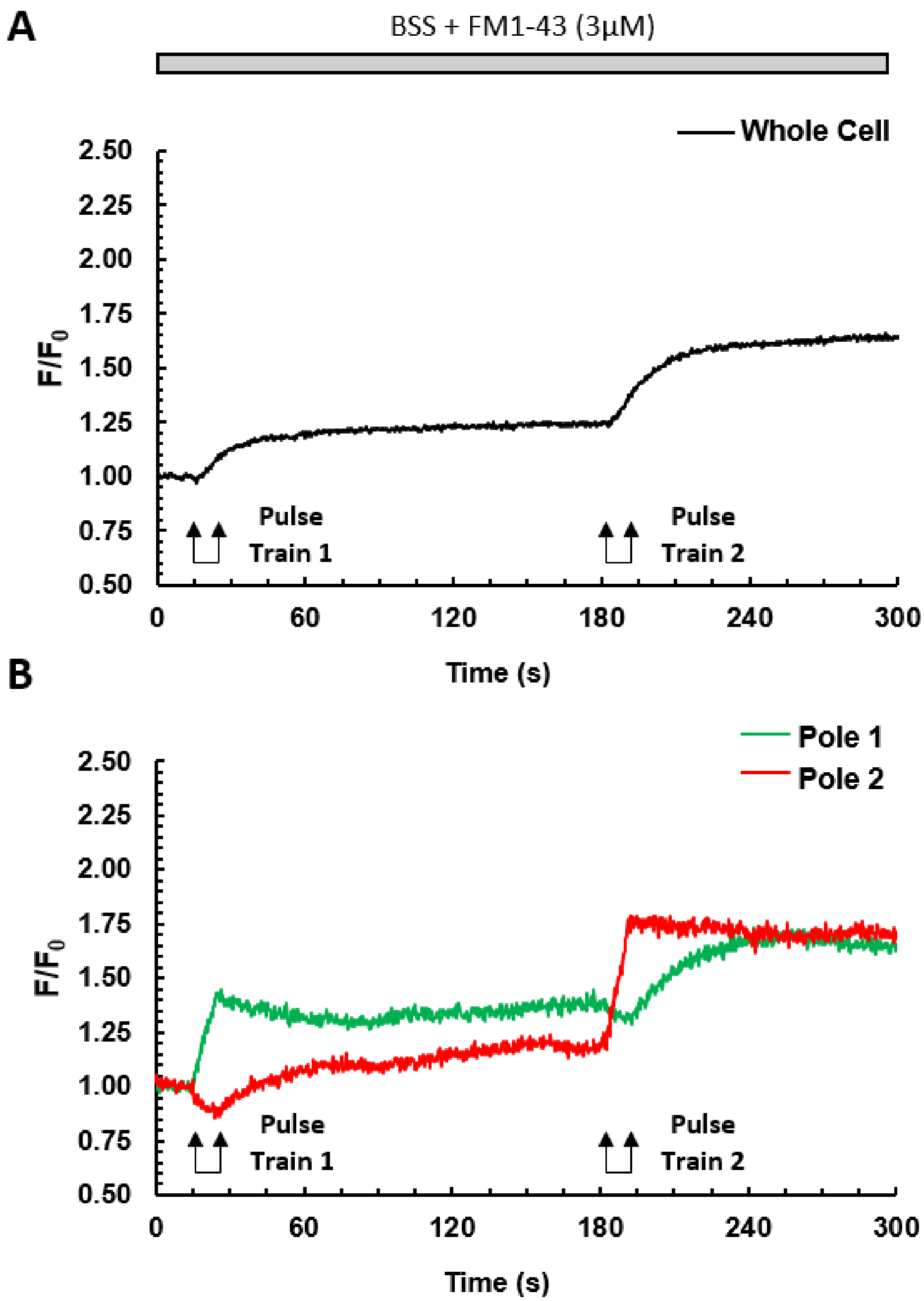

Figure 3.30 An example of the effect of reversing the NEP stimulus polarity on FM1-43 fluorescence at the anode and cathode facing sides of the cell. (A) shows the whole cell fluorescence response and (B) shows the responses at the poles designated by Pole 1 and Pole 2 instead of Anode facing and Cathode facing Poles. The arrows indicate the duration of the pulse trains, which were applied at 1 Hz.

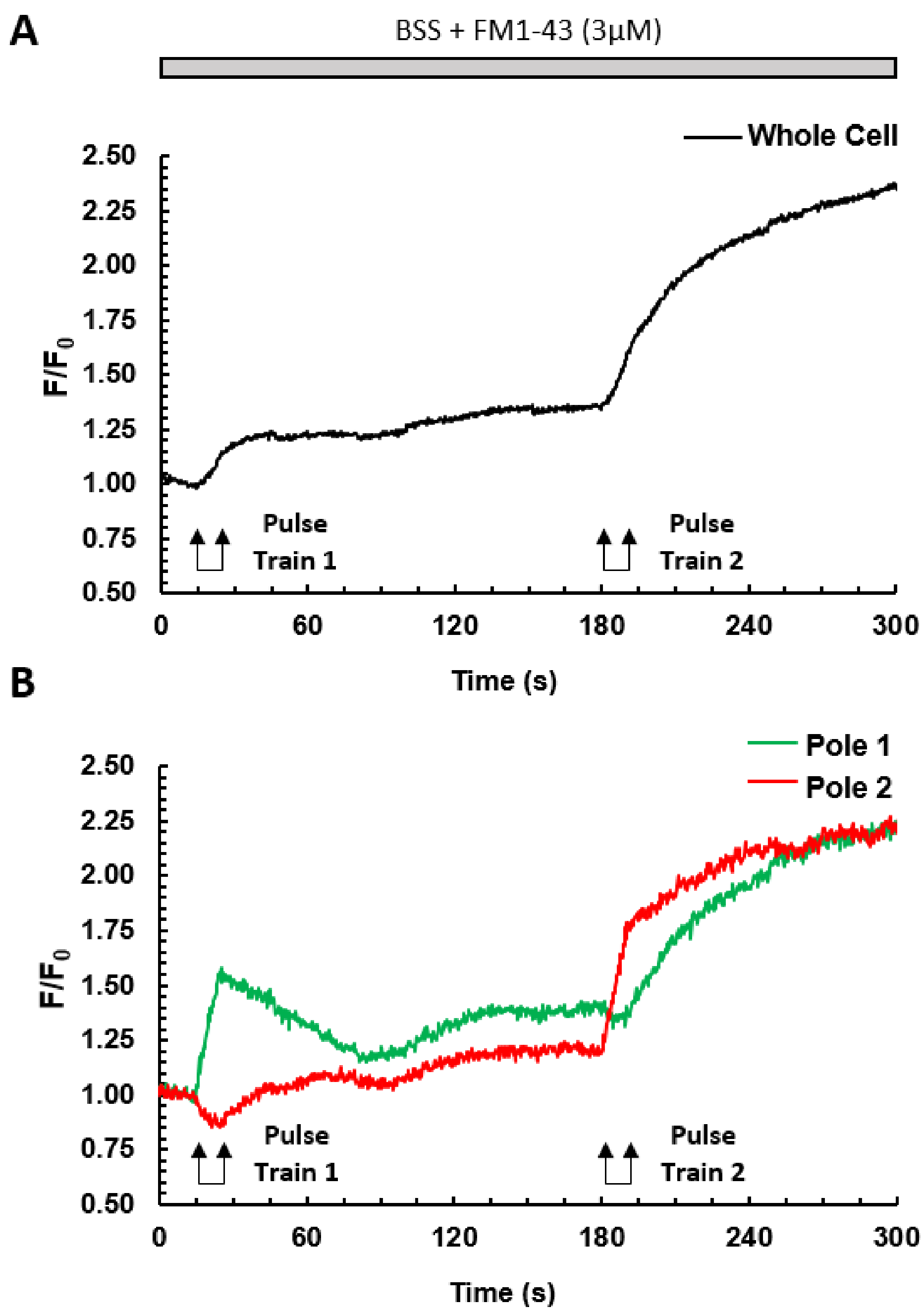

Figure 3.31 Another example of the effect of reversing the NEP stimulus polarity on FM1-43 fluorescence at the anode and cathode facing sides of the cell. (A) shows the whole cell fluorescence response and (B) shows the responses at the poles designated by Pole 1 and Pole 2 instead of Anode facing and Cathode facing Poles. The arrows indicate the duration of the pulse trains, which were applied at 1 Hz.

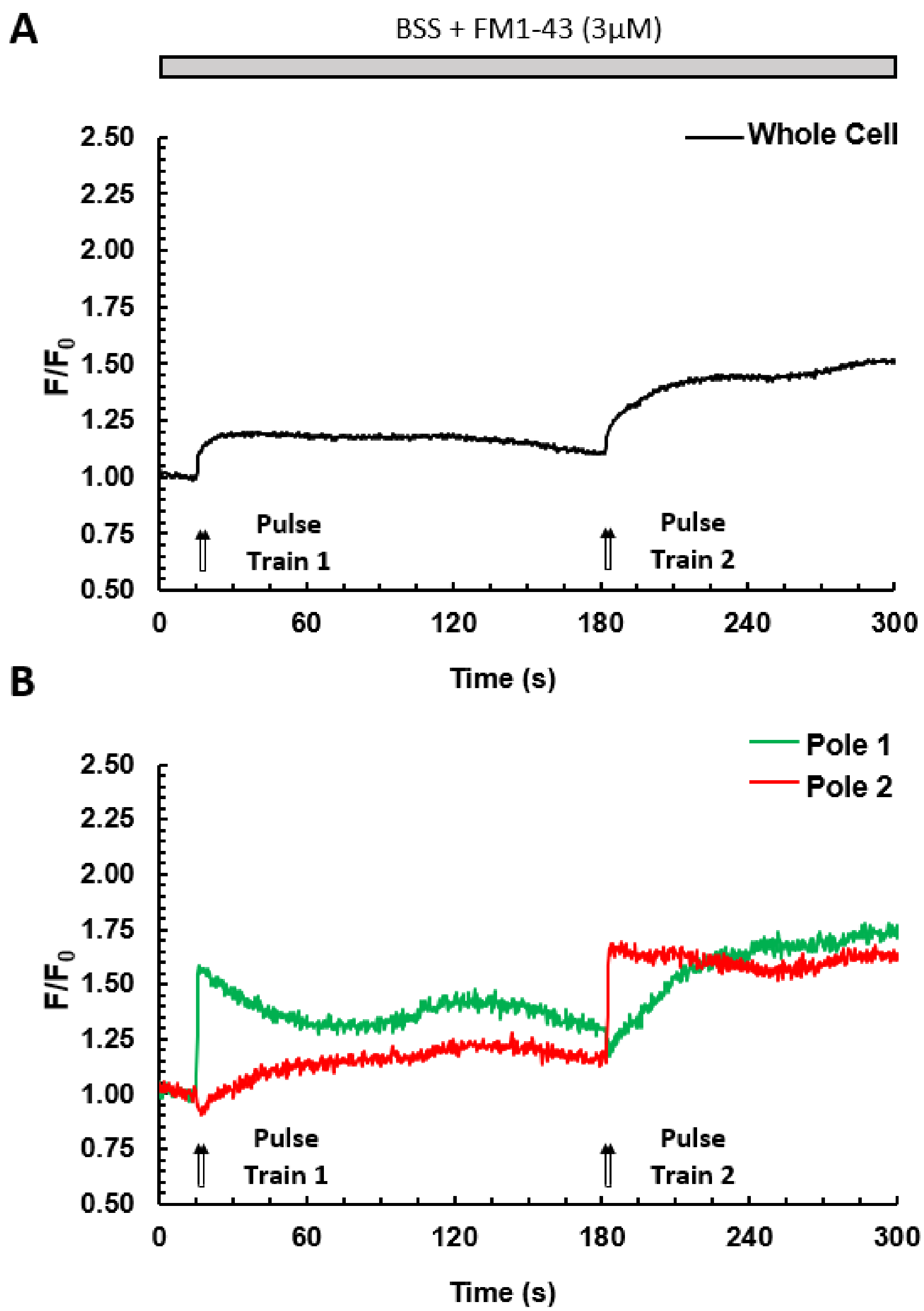

Figure 3.32 An example of the effect of reversing the NEP stimulus polarity on FM1-43 fluorescence at the anode and cathode facing sides of the cell. (A) shows the whole cell fluorescence response and (B) shows the responses at the poles designated by Pole 1 and Pole 2 instead of Anode facing and Cathode facing Poles. The arrows indicate the duration of the pulse trains, which were applied at 10 Hz.

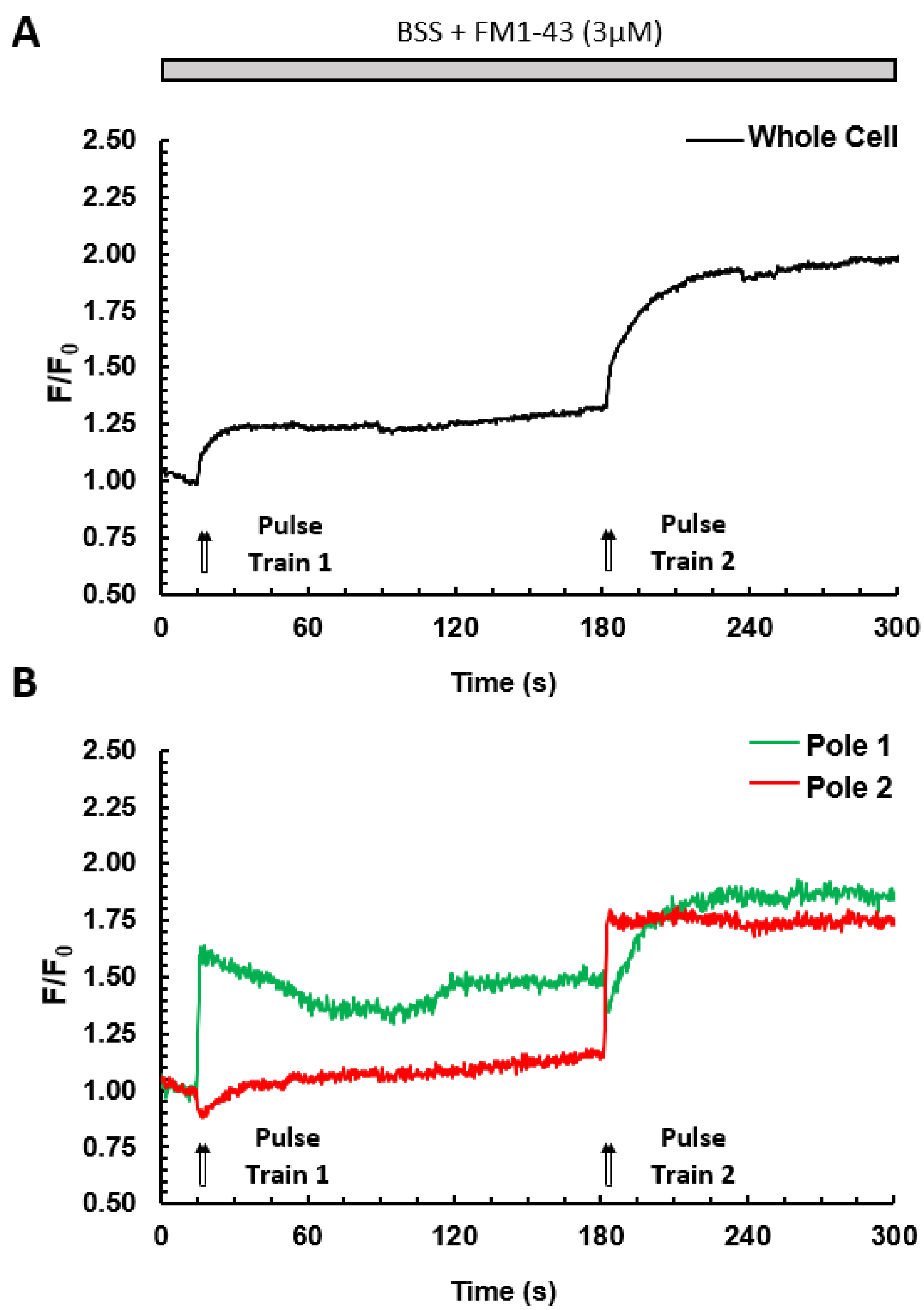

Figure 3.33 Another example of the effect of reversing the NEP stimulus polarity on FM1-43 fluorescence at the anode and cathode facing sides of the cell. (A) shows the whole cell fluorescence response and (B) shows the responses at the poles designated by Pole 1 and Pole 2 instead of Anode facing and Cathode facing Poles. The arrows indicate the duration of the pulse trains, which were applied at 10 Hz.

3.7 The increase in FM1-43 fluorescence on the anode facing side of NEP stimulated cells did not involve PS externalization

As mentioned in the Introduction, the application of NEPs to different types of cells has been reported to cause PS to translocate to the outer leaflet of the membranes, resulting in the disruption of the membrane asymmetry [***41, 51***]. Moreover, FM1-43 dye has the ability to detect PS externalization [***39***], which occurs preferentially on the anode facing side of the membrane [***41, 52***]. Thus, the sensitivity of FM1-43 to externalized PS might contribute to the pronounced increase in FM1-43 fluorescence observed at the anode facing side of chromaffin cells exposed to a train of ten, 5 ns pulses. To begin investigating this possibility, we assessed the presence of PS externalization in NEP exposed cells using the specific PS fluorescent marker lactadherin-FITC. For the analysis, three different concentrations of lactadherin-FITC (0.3, 0.87, and 2.61 μM) were used.

As shown in Figure 3.34, Figure 3.35, and Figure 3.36, the application of a train of ten 5 ns pulses (10 Hz at 19.8 MV/m) did not cause detectable lactadherin-FITC fluorescence staining on the anode facing side of the cell regardless of the concentration used for the staining. Furthermore, there was no detectable staining 2 minutes after the application of the pulse train.

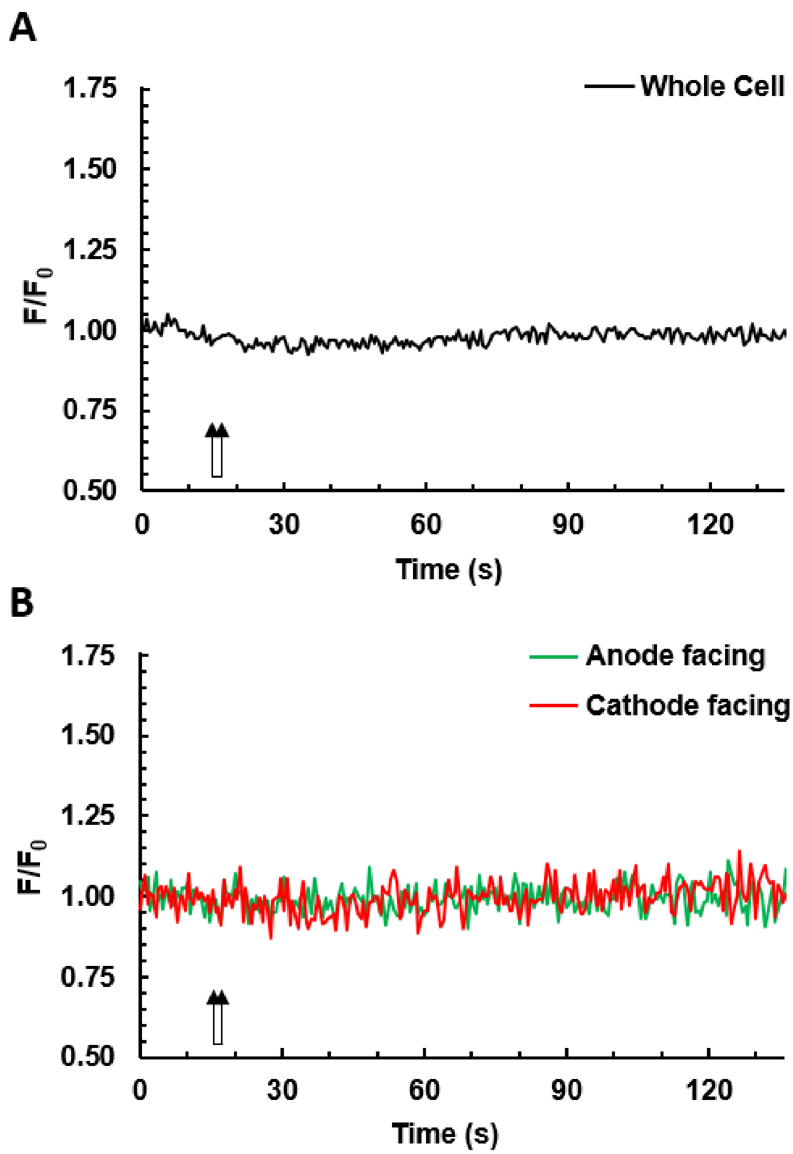

Figure 3.34 PS externalization assessed during and after the application of a train of ten, 5 ns pulses at 10 Hz using 0.3 μM lactadherin-FITC. (A) shows the whole cell fluorescence and (B) shows the fluorescence at the poles of a stimulated chromaffin cell. The arrows indicate the time and duration of the pulse train.

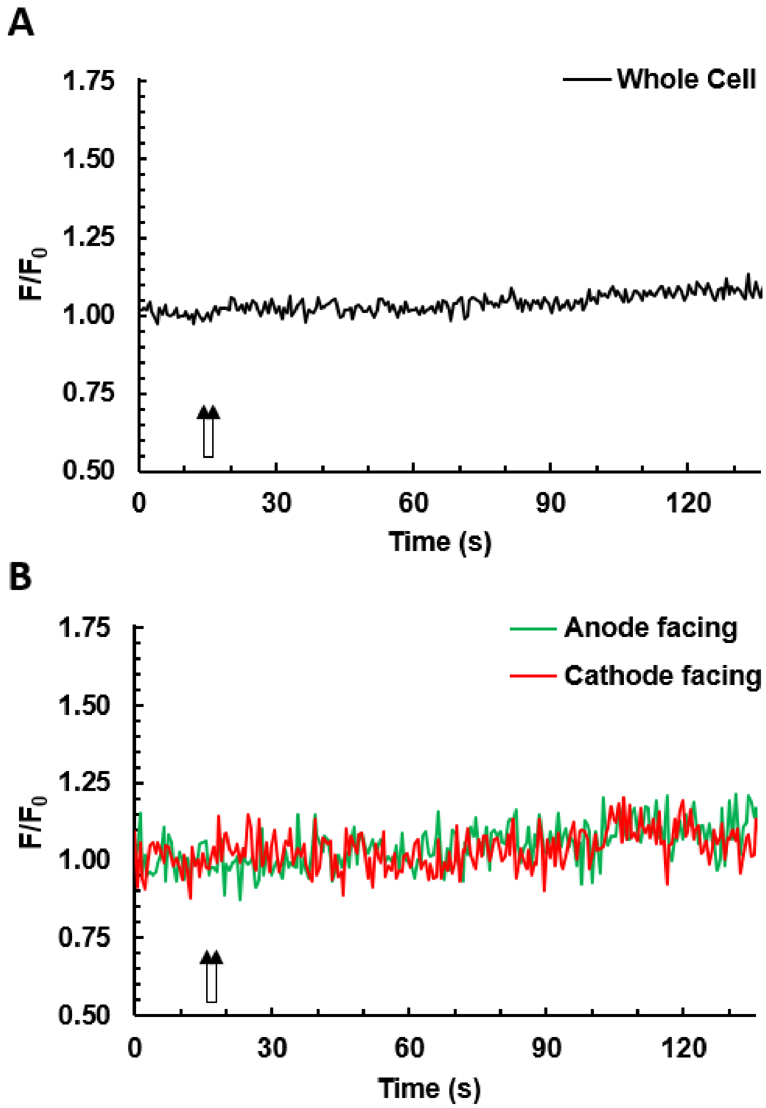

Figure 3.35 PS externalization assessed during and after the application of a train of ten, 5 ns pulses at 10 Hz using 0.87 µM lactadherin-FITC. (A) shows the whole cell fluorescence and (B) shows the fluorescence at the poles of a stimulated chromaffin cell. The arrows indicate the time and duration of the pulse train.

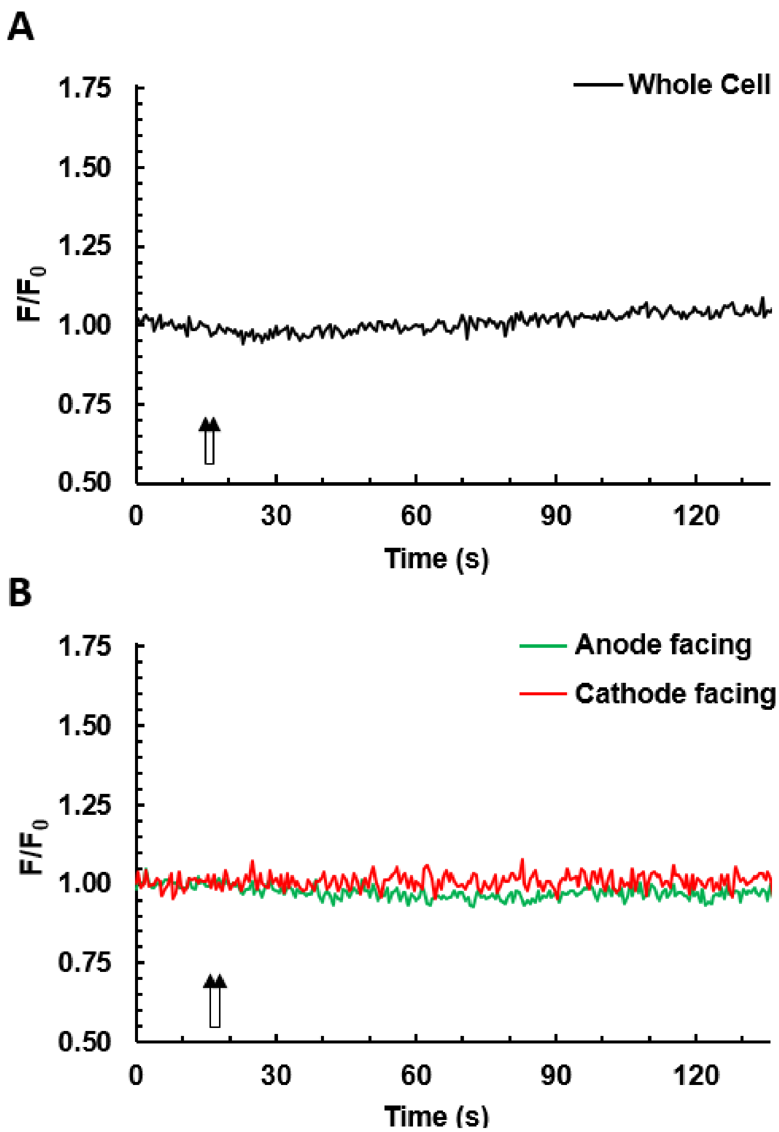

Figure 3.36 PS externalization assessed during and after the application of a train of ten, 5 ns pulses at 10 Hz using 2.61 µM lactadherin-FITC fluorescence. (A) shows the whole cell fluorescence and (B) shows the fluorescence at the poles of a stimulated chromaffin cell. The arrows indicate the time and duration of the pulse train.

We next investigated whether PS externalization could be detected in response to multiple trains of NEPs. Figure 3.37 shows a series of fluorescence images of a cell that was exposed to three trains of ten 5 ns electric pulses delivered at 10 Hz. Similar to the results shown in Figure 3.36 that were obtained using 2.61 µM lactadherin-FITC, we found no evidence of PS externalization either during or 2 minutes after the first pulse train. However, 60 s after the second pulse train, lactadherin-FITC fluorescence was evident on the anode facing side of the cell. A third pulse train caused an increased level of fluorescence 60 s after the stimulus ended. Taken as a whole, these preliminary results suggest that a single train of ten 5 ns pulses delivered at an E-field of 19.8 MV/m did not cause PS externalization in cells during or at least 2 minutes after the NEP stimulus. Thus, the immediate increase in FM1-fluorescence observed at the anode facing part of the cell membrane did not appear to involve PS externalization. Our preliminary results suggest instead that PS externalization may start to appear after a second train of 5 ns, 19.8 MV/m pulses.

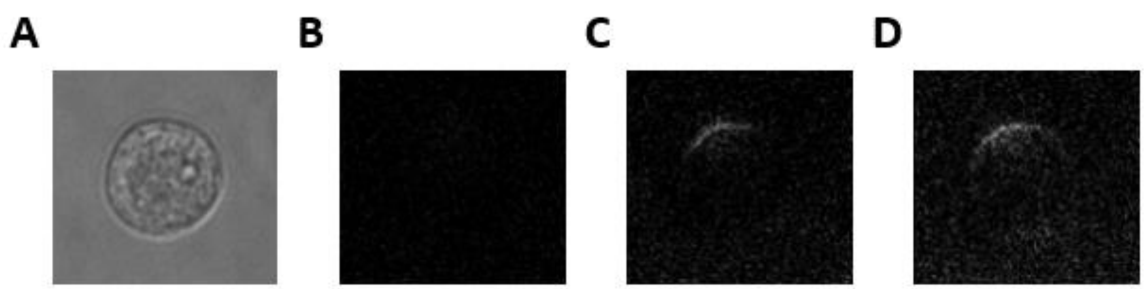

Figure 3.37 Effect of multiple trains of 5 ns pulses delivered at 10 Hz on lactadherin-FITC fluorescence. (A) shows a bright field image of the cell before stimulation. (B), (C), and (D) show fluorescence images of the cell 120 s after the first pulse train, 60 s after the second pulse train and 60 s after the third pulse train, respectively. Lactadherin-FITC was used at a concentration of 2.61 µM.

Chapter 4. DISCUSSION

This study investigated the use of NEPs as a trigger for neurosecretion in neuroendocrine adrenal chromaffin cells. The objective was to monitor in real-time NEP-evoked exocytotic activity using the membrane fluorescent dye, FM1-43, which undergoes an increase in fluorescence that reflects secretory granule fusion with the plasma membrane [***19, 26, 30, 31***]. The first aim was to investigate whether there is a delay between the initiation of a train of pulses delivered at 1 Hz and the beginning of secretory events, which was found using TIRFM where secretory granules were labeled with AO. Because FM1-43 is sensitive to changes in TMP [***19, 33***] and also can serve as a marker of PS externalization [***39-40***], a second aim was to use FM1-43 to assess these effects of NEP exposure on chromaffin cells. Thus, these latter two potential changes on the cell membrane were also considered when studying NEP-induced exocytosis in FM1-43 labeled chromaffin cells.

In summary we found that a train of ten NEPs induced two main effects on the FM1-43 labeled cell membrane. The initial response was a heterogeneous change in TMP on different parts of the cell membrane that depended on their orientation relative to the electrodes. This initial response was followed by an increase in membrane fluorescence on all parts of the cell membrane, which we attributed to exocytotic activity. There was no evidence that PS externalization contributed to NEP-evoked increases in FM1-43 fluorescence. The results obtained from this study together with their significance are discussed in the following sections.

4.1 Initial changes in FM1-43 fluorescence evoked by a train of NEPs represent differential effects on TMP on different parts of the cell membrane

Results obtained in experiments where high [K^+] stimulation was applied to the cells showed that the entire cell membrane was depolarized causing an initial decrease (dip) in FM1-43 fluorescence due to the TMP change [***19, 26, 30, 31***]. The dip gradually disappeared as cell fluorescence underwent an increase due to the exocytotic activity induced by the high [K^+] stimulus. This finding agrees with those of other researchers who similarly reported the sensitivity of FM1-43 to voltage changes [***19, 33***]. For instance, Smith and Betz, 1996 described an initial decrease in whole cell fluorescence in FM1-43 labeled chromaffin cells in response to a depolarizing stimulus [***19***], followed by an increase in fluorescence.

Of note is that the change in FM1-43 fluorescence observed in response to high [K^+] stimulation was homogenous across the entire cell membrane, unlike what we found using a train of NEPs as the stimulus. Application of a pulse train applied at either 1 Hz or 10 Hz resulted in differential changes in FM1-43 fluorescence on different parts of the cell membrane that were dependent on their orientation relative to the electrodes. Specifically, we consistently observed a decrease in fluorescence on the cathode facing side and an increase in fluorescence on the anode facing side of the cell. The changes lasted for the entire duration of the stimulus and were observed both in the presence and absence of extracellular Ca^{2+} (**Error! Reference source not found.** and **Error! Reference source no t found.**). However, they were smaller in amplitude in the absence of external Ca^{2+}.

Table 4.1 Summary of the averaged differential changes in fluorescence ± SE at the poles of the stimulated cells at the end of the application of ten NEPs in the presence of extracellular Ca^{2+} at 1 Hz (n = 9) or 10 Hz (n = 5).

	***F/F₀* change at the end of the pulse train**	
	1 Hz	**10 Hz**
Anode	54 ± 4%	66 ± 9%
Cathode	- 13 ± 1%	- 14 ± 3%

Table 4.2 Summary of the averaged differential changes in fluorescence ± SE at the poles of the stimulated cells at the end of the application of ten NEPs in the absence of extracellular Ca^{2+} at 1 Hz (n = 3) or 10 Hz (n = 3).

	***F/F₀* change at the end of the pulse train**	
	1 Hz	**10 Hz**
Anode	24 ± 4%	34 ± 7%
Cathode	- 13 ± 2%	- 11 ± 3%

Hence, during the application of the E-field, the differential FM1-43 fluorescence changes were the result of variations in the TMP [***19, 33***] mainly at the poles of the stimulated cell where the E-field is maximal. The changes in TMP are attributed to the redistribution of ions in the solution due to the polarity of the electrodes as shown in **Error! Reference source not found.**. Once the E-field is applied, anions are repelled from the cathode (the negative electrode) and accelerate towards the anode (the positive electrode). Merrill et al., 2000 explain that this flow results in the accumulation of the negatively charged ions near the cathode facing side of the cell. Consequently, positively charged ions accumulate on the inner side of the cell membrane, which leads to the depolarization of the membrane at that location [***53, 54***]. Similarly, when the E-field is applied, cations accelerate towards the cathode (the negative electrode). The current of cations causes the accumulation of positively charged ions near the anode facing pole of the cell. This results in the hyperpolarization of that part of the membrane.

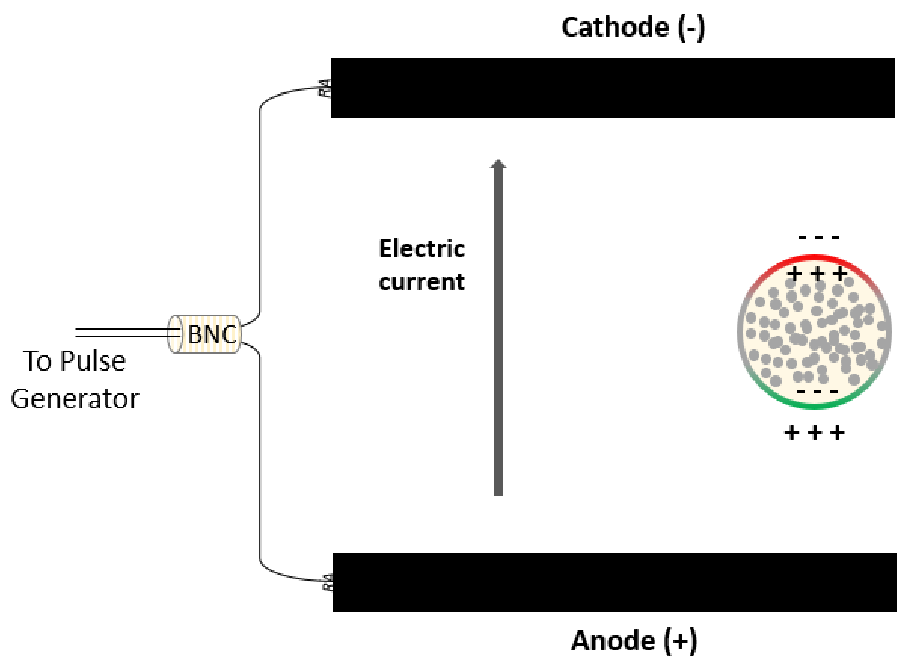

Figure 4.1 Schematic showing the differential effects on the anode and cathode facing poles of a stimulated cell placed in between the electrodes. The green color represents hyperpolarization near the anode and the red color represents depolarization near the cathode. The gray arrow indicates the direction of the electric current between the electrodes which is similar to the direction of cations in the solution during E-field application.

The variations in TMP at the poles of the cells captured with FM1-43 agree with the results of Hassan et al. 2002 that were obtained using the voltage sensitive dye di-8-

ANEPPS in electrically stimulated adrenal chromaffin cells. Their study also showed membrane depolarization near the cathode facing side of the cell and membrane hyperpolarization near the anode facing side of the cell due to an applied E-field of 2 KV/m [***44***]. Moreover, our results confirmed that the observed differential changes are indeed dependent on the polarity of the electrodes. By changing the polarity of the applied E-field, FM1-43 fluorescence changes at the cathode and the anode facing poles of the cell reversed in accordance with reversing the polarity.

Although differential FM1-43 fluorescence changes at the poles of the exposed cell were due to TMP changes, the absolute change in fluorescence at the anode facing pole was consistently greater than the change at the cathode facing pole. A plausible explanation can be that although FM1-43 is sensitive to voltage changes [***19, 32, 33***], it is not effective in ratiometric TMP measurements [***32***]. This suggests that the dye might have a different sensitivity to a depolarizing versus a hyperpolarizing stimulus. Another possibility is that since FM1-43 is a non-specific probe for detecting PS externalization on the membrane of cells, the disparity in fluorescence intensity changes between the anode and cathode facing sides of the cell is that NEP exposure leads to PS externalization primarily on the anode facing side of the cell, as has been described in other reports [***41, 52***]. To address this possibility, we used the selective PS marker lactadherin-FITC in cells exposed to a train of NEPs. No PS was detected on the cell membrane during the time a pulse train was applied and differential effects on FM1-43 on the poles of the cell are most prominent. Instead, only after a second pulse train was applied was PS detected on the anode facing pole of the cell. This finding suggested that PS externalization was likely not contributing to the FM1-

43 fluorescence increase at the anode facing pole of the cell when cells were exposed to a single pulse train. Nevertheless, further experiments using a confocal microscope, which has a better resolution and sensitivity than the current imaging system we used, will be carried out to rule out the possibility of PS externalization during pulse application.

Our results also show that FM1-43 detected changes in TMP at the equators of NEP-exposed cells, which were characterized by a dip in fluorescence that started with the initiation of the pulse train. In either the presence or absence of extracellular Ca^{2+}, both equators demonstrated minima in F/F_0 during the delivery of the pulse train, as shown in Table 4.3 and

Table **4.4**. The fluorescence decreases suggested that both equators underwent a depolarization, the reason for which is not currently known. However, the absolute F/F_0 changes were smaller than the decrease observed on the depolarized side of the cell membrane (cathode facing pole). This could be attributed to the fact that the E-field propagates from the anode to the cathode (parallel to the equators) during NEPs exposure. As a consequence, TMP changes are more intense on the poles of the cell, which are the most affected by the E-field propagation. This point is strongly supported by the computations for the electric potential distribution during the application of NEPs that was reported in Smith and Weaver, 2008 [***55***].

Table 4.3 Summary of the average differential changes in fluorescence ± SE at the equators of the stimulated cells during the application of ten NEPs in the presence of extracellular Ca^{2+} at 1 Hz (n = 9 cells) or 10 Hz (n = 5 cells).

	***F/F₀* minima during the pulse train**	
	1 Hz	**10 Hz**
Equator Left	- 5 ± 1%	- 4 ± 3%
Equator Right	- 9 ± 1%	- 8 ± 1%

Table 4.4 Summary of the averaged differential changes in fluorescence ± SE at the poles of the stimulated cells at the end of the application of ten NEPs in the absence of extracellular Ca^{2+} at 1 Hz (n = 3) or 10 Hz (n = 3).

	***F/F₀* change at the end of the pulse train**	
	1 Hz	**10 Hz**
Equator Left	- 9 ± 1%	- 9 ± 2%
Equator Right	- 4 ± 2%	- 4 ± 3%

Taken as a whole, our results indicate that the ability of the FM1-43 dye to detect TMP changes during the time of application of the NEP stimulus impeded our ability to detect whether exocytosis occurred with a delay, as observed in TIRFM. Alternative approaches that can be used to address this issue are presented in the Future Directions section.

4.2 Ca^{2+}-dependent increases in FM1-43 membrane fluorescence that occur following a train of NEPs are indicative of exocytotic activity

A high $[K^+]$ depolarizing stimulus was used as a control to assess the use of FM1-43 for monitoring exocytosis. Following an initial decrease in fluorescence due to depolarization, continued perfusion of the cells with high $[K^+]$ resulted in a slow increase in whole cell fluorescence that was observed in the presence of external Ca^{2+} (Figure 3.6). This increase in fluorescence agrees with the findings in Smith and Betz, 1996 and Kilic, 2002, where C_m was measured simultaneously with FM1-43 fluorescence [***19, 56***]. These researchers showed that whole cell fluorescence increased continuously whereas C_m levelled off. The researchers explained that these results suggest the onset of endocytosis with an equal rate as exocytosis, which explains the leveling of C_m. On the other hand, the continuous increase in the overall fluorescence of FM1-43 labeled cells is the result of the unabated exocytotic response due to the strong stimulus likely with the occurrence of endocytosis which causes dye internalization.

Whereas perfusion of FM1-43 labeled cells with high $[K^+]$ caused a continuous increase in FM1-43 fluorescence, Ca^{2+} responses monitored under the same high $[K^+]$ perfusion conditions did not similarly show a sustained increase in $[Ca^{2+}]_i$. Instead, after an initial rise, $[Ca^{2+}]_i$ gradually returned to baseline, which we attributed to a possible inactivation of VGCCs due to the long stimulation period. These results are summarized in Figure 4.2.

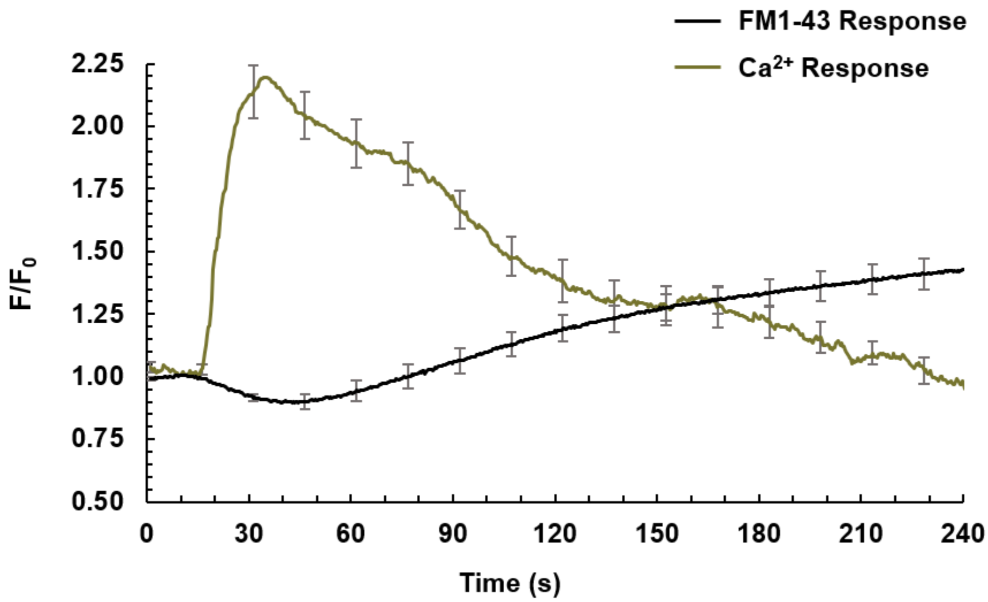

Figure 4.2 Ca^{2+} and exocytotic responses induced in chromaffin cells by high $[K^+]$. The graphs represent the average of whole cell fluorescence ± SE triggered by the depolarizing stimulus in the presence of extracellular Ca^{2+} in Calcium Green-1 loaded cells (n = 17) versus FM1-43 labeled cells (n = 12).

Rosa et al., 2011 simultaneously studied exocytotic responses in conjunction with changes in $[Ca^{2+}]_i$ using FM1-43 and Fura-2, respectively, in chromaffin cells stimulated with continuous 59 mM $[K^+]$ perfusion. The researchers reported that FM1-43 fluorescence increased and reached a plateau that was higher than the initial labeling level (F_0). At the same time, the $[Ca^{2+}]_i$ response was transient but did not reach baseline by the end of the 3-minute high $[K^+]$ perfusion [***31***]. These results agree with our transient Ca^{2+} responses versus the sustained increase in FM1-43 fluorescence in the presence of extracellular Ca^{2+}, which reflects the persistent increase in secretory responses due to a prolonged stimulation. Furthermore, similar results were observed in a different secretory cell model system in

Shorte et al, 1995. The researchers also used Fura-2 and FM1-43 in anterior pituitary secretory cells to report changes due to the continuous perfusion of the cells with thyrotropin releasing hormone, which was used as a stimulus for prolactin secretion [***57***].

As for NEP stimulation, we have shown in previous studies that a single 5 ns pulse at 5-7 MV/m induces Ca^{2+} entry into chromaffin cells that in turn triggers exocytosis and release of catecholamines [***20, 22***]. However, in this project, a train of ten 5 ns pulses had to be applied at a higher E-field (19.8 MV/m) to visualize a consistent increase in fluorescence when monitoring exocytosis using FM1-43 labeled cells. During the application of the pulse train, the increase in FM1-43 fluorescence coincided with $[Ca^{2+}]_i$ rises. Responses were dependent on the frequency of the applied stimulus as the rate of increase was always faster at 10 Hz than at 1 Hz. After the end of the pulse train applied at 1 Hz or 10 Hz, FM1-43 labeled cells exhibited an increase in fluorescence that reached a plateau that was higher than the initial baseline, whereas $[Ca^{2+}]_i$ slowly returned towards baseline (Figure 4.3). Like high $[K^+]$ perfusion, the increase in fluorescence occurred only in the presence of extracellular Ca^{2+}. Thus, the increase in fluorescence induced in the presence of Ca^{2+} in the external solution was attributed to the NEP-induced exocytosis triggered by Ca^{2+} entry into the cell.

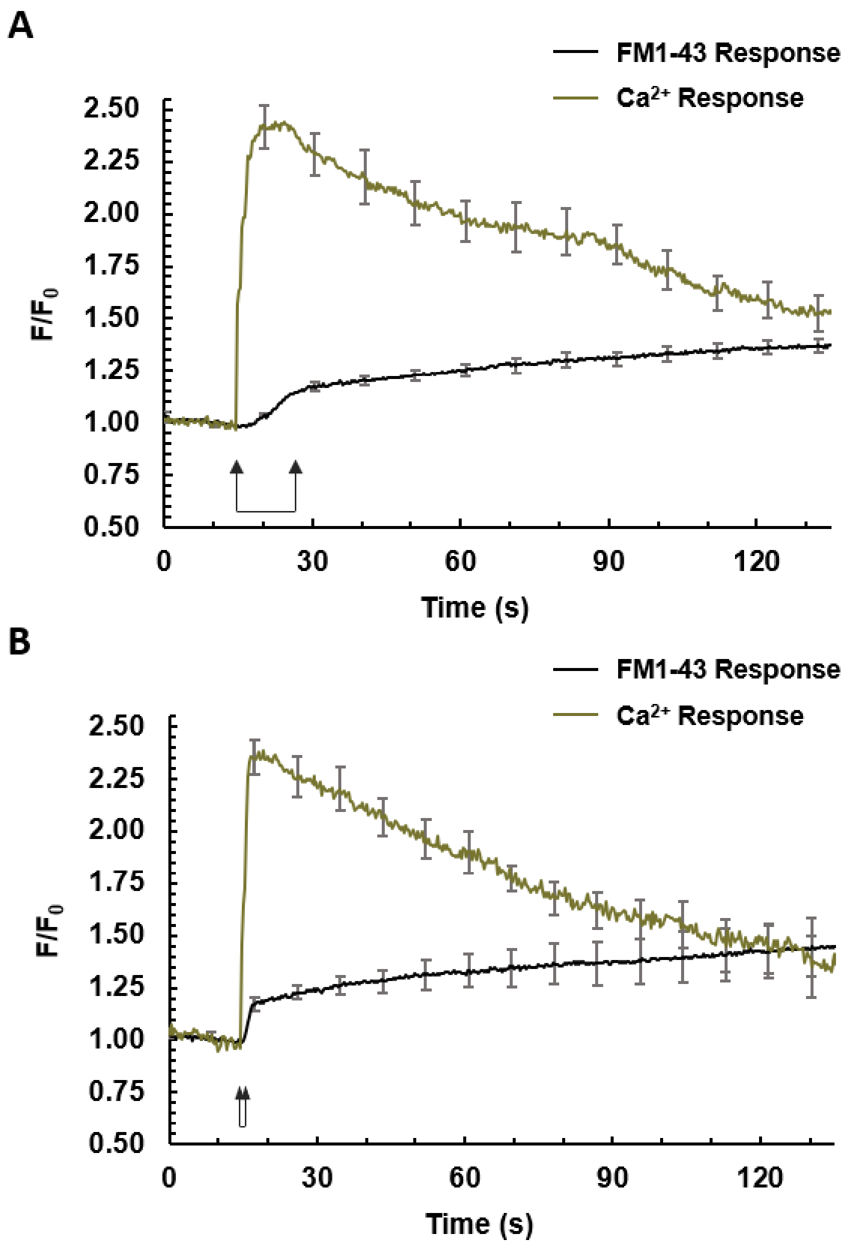

Figure 4.3 Ca^{2+} and exocytotic responses induced in chromaffin cells by a train of ten NEPs. The graphs represent the average of whole cell fluorescence ± SE triggered by the NEP stimulus at 1 Hz (A) or 10 Hz (B) in the presence of extracellular Ca^{2+} in Calcium Green-1 loaded cells (n = 5 for both 1 Hz and 10 Hz) versus FM1-43 labeled cells at 1 Hz (n = 9) and 10 Hz (n = 5), respectively.

As described in the Introduction, in a recent unpublished study by our group, exocytosis was monitored using TIRFM where secretory granules were labeled with AO that is fluorescent. Exocytotic events were observed as a loss of granule fluorescence that appeared as a sudden flash when granules fused with the plasma membrane. The study compared Ca^{2+} and exocytotic responses induced by a train of ten 5 ns pulses to the responses induced by a train of ten 5 ms applications of the nicotinic receptor agonist, DMPP. Both stimuli were applied at 1 Hz. Whereas each stimulus induced an immediate rise in $[Ca^{2+}]_i$, only DMPP evoked an immediate exocytotic response. NEP stimulation resulted in a delay of several seconds in the onset of exocytosis. In this project, monitoring NEP-induced exocytosis using FM1-43 was achieved. However, due to the initial changes in FM1-43 fluorescence attributed to the changes in TMP, the time of onset of the response could not be investigated. To discriminate the Ca^{2+}-dependent fluorescence signals induced by the pulse train (exocytosis) from the TMP changes, curves obtained in the absence of Ca^{2+} were subtracted from the ones in its presence. We hoped that this subtraction would result in the ability to assess the time course of Ca^{2+}-dependent exocytosis during the time that the pulses were applied to cells, as done for the TIRFM experiments. However no clear conclusion could be drawn about the kinetics of the exocytotic response because despite the subtraction, it was evident that FM1-43 fluorescence was still influenced by the TMP changes, especially on the poles of the cell. Thus, during the application of the pulse train, the sensitivity of FM1-43 to TMP changes interfered with the ability to monitor NEP-induced exocytosis in real-time.

As discussed before, the rate of increase in FM1-43 fluorescence during the application of NEPs can be a result of exocytosis and TMP changes. Therefore, the delay in exocytotic events captured in the TIRFM experiments could not be detected here due to the sensitivity of FM1-43 to TMP changes during the application of the pulses. However, our results showed that FM1-43 responses during the pulse trains were highly dependent on the frequency of the pulses, being faster at 10 Hz. Of note is that the delay in the release of AO in TIRFM was observed in response to a train of pulses applied at 1 Hz. Thus, if this delay was also dependent on the frequency of the pulses applied, then it may either be reduced or eliminated by increasing the frequency of the pulses.

On a final note, it is worth mentioning that PS externalization occurs during exocytosis in neuroendocrine cells [***36, 37***]. For instance, Ory et al. 2013 have shown that secretagogue-evoked exocytosis is accompanied by cell surface PS exposure at the close vicinity of the granule membrane transiently inserted into the plasma membrane [***37***]. This secretagogue induced PS externalization requires scramblase activation, which is a Ca^{2+}-dependent process. These results suggest that PS externalization could be a potential part of the Ca^{2+}-dependent response observed, which requires further investigation.

Chapter 5. CONCLUSION AND FUTURE WORK

In this project, real-time monitoring of exocytosis in adrenal chromaffin cells was performed using the fluorescent styryl dye FM1-43. The cells were exposed to two different stimuli, high $[K^+]$ perfusion and a train of ten NEPs at 19.8 MV/m. The high $[K^+]$ stimulus depolarized the entire cell membrane causing an initial overall decrease in fluorescence. In contrast, a train of NEPs caused heterogeneous changes in FM1-43 fluorescence on the cell membrane due to hyperpolarization occurring at the anode facing pole versus depolarization occurring at the cathode facing pole and the equators. Thus, during the time at which the pulse train was delivered to the cells, there was a decrease in FM1-43 fluorescence where the membrane was depolarized, and an increase in FM1-43 fluorescence where the membrane was hyperpolarized.

Following the initial decrease in fluorescence evoked by high $[K^+]$, there was a slow continuous increase in fluorescence that reflected the unabated exocytotic response caused by the rise of $[Ca^{2+}]_i$. Similarly, following the initial changes in FM1-43 fluorescence occurring during the application of a train of ten NEPs, there was an increase in FM1-43 fluorescence that too reflected exocytosis caused by the rise in $[Ca^{2+}]_i$. The rises both increased in a manner that was dependent on the frequency of the applied pulses during the application of the stimulus (i.e. faster for the higher frequency). After the end of the pulse train, the long-lived Ca^{2+} responses slowly returned to baseline whereas FM1-43 fluorescence increase did not, instead it tended to reach a higher plateau relative to baseline. In conclusion, real-time fluorescence microscopy using FM1-43 helped us to monitor the exocytotic response in chromaffin cells exposed to a train of NEPs, which was similar to the one induced by the physiological stimulus.

One of the main findings of this research was that FM1-43 was quite sensitive to changes in membrane potential evoked by both high [K^+] and a train of NEPs. With respect to the latter, we detected differential effects on the poles and the equators of the cell that were directly related to the E-field polarity and the frequency of the applied train of NEPs. The differential F/F_0 changes were more intensely observed on the poles of the cells. Since a cell is located between the electrodes during the application of the E-field, these TMP changes are caused by the local charge redistribution around the membrane. Unlike the poles, the equators of an exposed cells showed a smaller decrease in fluorescence that started with the initiation of the E-field but ended before the end of the pulse train. These differential effects persisted in the absence of Ca^{2+}. Because differential TMP changes due to the polarity of stimulating electrodes might potentially affect the ability to monitor responses in NEP-exposed chromaffin cells, which is alluded to below, future experiments would be to use potentiometric probes (voltage sensitive dyes) like di-8-ANEPPS and FluoVolt™ to study further the spatial and temporal TMP changes that occur during a NEP pulse train.

Based on our use of the specific PS marker, lactadherin-FITC, increases in FM1-43 fluorescence evoked by a single train of NEPs were likely not related to PS externalization, a known effect of NEPs on biological membranes. However, in cells exposed to a second pulse train, there was evidence of PS externalization. In light of these results, more experiments using Lactadherin-FITC as well as Annexin V, another PS marker, are necessary to assess the risk of PS externalization to the outer layer of the membrane that could be deleterious to the cell and hence affect its function, exocytosis that relies on the integrity of the plasma membrane. Only in this way can we establish the future use of NEPs as an exogenous neuromodulation stimulus since PS externalization can also be an indicator of cell apoptosis, as has been shown for longer durations NEPs in other cell types.

Due to the differential effects on FM1-43 fluorescence caused by TMP changes during the application of a train of NEPs at 1 Hz, we could not establish whether there is a delay in the onset of exocytosis, as captured in the previous study using TIRFM. In this project, a faster response was obtained when applying a 10 Hz pulse train compared to the slower response in case of 1 Hz. Thus, future work would be to investigate in TIRFM experiments whether the exocytotic events induced by a train of NEPs delivered at 10 Hz also occur faster and possibly without a delay. Knowing the effects of changing the frequency of NEP delivery is crucial for establishing the optimal parameters for applying NEPs for neuromodulation purposes in future therapeutic applications.

Another experimental approach to assess the onset of NEP-induced exocytosis is single cell amperometry using a carbon fiber electrode for direct measurement of catecholamine release. This real-time approach would also serve to address the frequency-dependent effects of NEPs on the stimulated cells, thereby providing an answer to the delay seen in TIRFM experiments. Furthermore, changing the location of the carbon fiber electrode relative to the cathode and anode may help with the investigation of the differential effects induced by NEPs at the poles and equators of the cell membrane.

REFERENCES

1. Perlmutter JS, Mink JW. Deep brain stimulation. *Annual Review of Neuroscience.* 2006;29:229-257.
2. Rodriguez-Oroz M, Zamarbide I, Guridi J, Palmero M, Obeso J. Efficacy of deep brain stimulation of the subthalamic nucleus in Parkinson's disease 4 years after surgery: double blind and open label evaluation. *Journal of Neurology, Neurosurgery & Psychiatry.* 2004;75(10):1382-1385.
3. Nitsche MA, Boggio PS, Fregni F, Pascual-Leone A. Treatment of depression with transcranial direct current stimulation (tDCS): a review. *Experimental neurology.* 2009;219(1):14-19.
4. Nitsche MA, Cohen LG, Wassermann EM, et al. Transcranial direct current stimulation: state of the art 2008. *Brain stimulation.* 2008;1(3):206-223.
5. John Hopkins Medicine. Adrenal Glands. https://www.hopkinsmedicine.org/health/conditions-and-diseases/adrenal-glands. Published 2020. Accessed.
6. Carmichael S, Winkler H. The Adrenal Chromaffin Cell. In. Vol 253. Scientific American: Scientific American, a division of Nature America, Inc.; 1985:40-49.
7. Bornstein S, Ehrhart-Bornstein M, Androutsellis-Theotokis A, et al. Chromaffin cells: the peripheral brain. *Molecular psychiatry.* 2012;17(4):354-358.
8. Plattner H, Artalejo AR, Neher E. Ultrastructural organization of bovine chromaffin cell cortex—analysis by cryofixation and morphometry of aspects pertinent to exocytosis. *The Journal of cell biology.* 1997;139(7):1709-1717.
9. Burgoyne RD. Mechanisms of secretion from adrenal chromaffin cells. *Biochimica et Biophysica Acta (BBA)-Reviews on Biomembranes.* 1984;779(2):201-216.
10. Winkler H. The adrenal chromaffin granule: a model for large dense core vesicles of endocrine and nervous tissue. *Journal of anatomy.* 1993;183(Pt 2):237.
11. Garcia AG, Garcia-De-Diego AM, Gandia L, Borges R, Garcia-Sancho J. Calcium signaling and exocytosis in adrenal chromaffin cells. *Physiological Reviews.* 2006;86(4):1093-1131.
12. Augustine GJ, Neher E. Calcium requirements for secretion in bovine chromaffin cells. *The Journal of physiology.* 1992;450(1):247-271.
13. Engisch KL, Nowycky MC. Calcium dependence of large dense-cored vesicle exocytosis evoked by calcium influx in bovine adrenal chromaffin cells. *Journal of Neuroscience.* 1996;16(4):1359-1369.
14. Albillos A, Dernick G, Horstmann H, Almers W, De Toledo GA, Lindau M. The exocytotic event in chromaffin cells revealed by patch amperometry. *Nature.* 1997;389(6650):509-512.
15. Schroeder TJ, Jankowski JA, Kawagoe KT, Wightman RM, Lefrou C, Amatore C. Analysis of diffusional broadening of vesicular packets of catecholamines released from biological cells during exocytosis. *Analytical Chemistry.* 1992;64(24):3077-3083.
16. Steyer JA, Horstmann H, Almers W. Transport, docking and exocytosis of single secretory granules in live chromaffin cells. *Nature.* 1997;388(6641):474-478.

17. Neher E, Marty A. Discrete changes of cell membrane capacitance observed under conditions of enhanced secretion in bovine adrenal chromaffin cells. *Proceedings of the National Academy of Sciences.* 1982;79(21):6712-6716.
18. Betz WJ, Mao F, Bewick GS. Activity-dependent fluorescent staining and destaining of living vertebrate motor nerve terminals. *Journal of Neuroscience.* 1992;12(2):363-375.
19. Smith CB, Betz WJ. Simultaneous independent measurement of endocytosis and exocytosis. *Nature.* 1996;380(6574):531-534.
20. Craviso GL, Chatterjee P, Maalouf, G, Cerjanic, A, Yoon, J, Chatterjee, I, & Vernier, PT. Nanosecond electric pulse-induced increase in intracellular calcium in adrenal chromaffin cells triggers calcium-dependent catecholamine release. *IEEE Transactions on Dielectrics and Electrical Insulation.* 2009;16(5):1294-1301.
21. Craviso GL, Chatterjee I, Publicover NG. Catecholamine release from cultured bovine adrenal medullary chromaffin cells in the presence of 60-Hz magnetic fields. *Bioelectrochemistry.* 2003;59(1-2):57-64.
22. Craviso GL, Choe S, Chatterjee P, Chatterjee I, Vernier PT. Nanosecond electric pulses: a novel stimulus for triggering Ca^{2+} influx into chromaffin cells via voltage-gated Ca^{2+} channels. *Cellular and molecular neurobiology.* 2010;30(8):1259-1265.
23. Yoon J, Leblanc N, Zaklit J, Vernier PT, Chatterjee I, Craviso GL. Enhanced monitoring of nanosecond electric pulse-evoked membrane conductance changes in whole-cell patch clamp experiments. *The Journal of membrane biology.* 2016;249(5):633-644.
24. Henkel AW, Mouihate A, Welzel O. Differential release of exocytosis marker dyes indicates stimulation-dependent regulation of synaptic activity. *Frontiers in Neuroscience.* 2019;13:1047.
25. Sikdar S, Kreft M, Pangrsic T, Grilc S, Zorec R. FM1–43 measurements of local exocytotic events in rat melanotrophs. *FEBS letters.* 2005;579(29):6575-6580.
26. Takahashi M. FM1-43. In: Binder MD, Hirokawa N, Windhorst U, eds. *Encyclopedia of Neuroscience.* Berlin, Heidelberg: Springer Berlin Heidelberg; 2009:1589-1591.
27. Brumback AC, Lieber JL, Angleson JK, Betz WJ. Using FM1-43 to study neuropeptide granule dynamics and exocytosis. *Methods.* 2004;33(4):287-294.
28. Kay AR, Alfonso A, Alford S, Cline HT, Holgado AM, Sakmann B, Snitsarev VA, Stricker TP, Takahashi M, Wu LG. Imaging synaptic activity in intact brain and slices with FM1-43 in C. elegans, lamprey, and rat. *Neuron.* 1999;24(4):809-817.
29. Wu Y, Yeh FL, Mao F, Chapman ER. Biophysical characterization of styryl dye-membrane interactions. *Biophysical journal.* 2009;97(1):101-109.
30. Perez Bay AE, Ibañez LI, Marengo FD. Rapid recovery of releasable vesicles and formation of nonreleasable endosomes follow intense exocytosis in chromaffin cells. *American Journal of Physiology-Cell Physiology.* 2007;293(5):C1509-1522.
31. Rosa JM, Torregrosa-Hetland CJ, Colmena I, Gutiérrez LM, García AG, Gandía L. Calcium entry through slow-inactivating L-type calcium channels preferentially triggers endocytosis rather than exocytosis in bovine chromaffin cells. *American Journal of Physiology-Cell Physiology.* 2011;301(1):C86-C98.

32. Foley J, Muschol M. Action spectra of electrochromic voltage-sensitive dyes in an intact excitable tissue. *Journal of biomedical optics.* 2008;13(6):064015.
33. Neves G, Lagnado L. The kinetics of exocytosis and endocytosis in the synaptic terminal of goldfish retinal bipolar cells. *The Journal of physiology.* 1999;515(1):181-202.
34. Martin SJ, Reutelingsperger CP, McGahon AJ, et al. Early redistribution of plasma membrane phosphatidylserine is a general feature of apoptosis regardless of the initiating stimulus: inhibition by overexpression of Bcl-2 and Abl. *Journal of Experimental Medicine.* 1995;182(5):1545-1556.
35. Chang CP, Zhao J, Wiedmer T, Sims PJ. Contribution of platelet microparticle formation and granule secretion to the transmembrane migration of phosphatidylserine. *Journal of Biological Chemistry.* 1993;268(10):7171-7178.
36. Malacombe M, Ceridono M, Calco V, Chasserot ‐ Golaz S, McPherson PS, Bader MF, Gasman S. Intersectin ‐ 1L nucleotide exchange factor regulates secretory granule exocytosis by activating Cdc42. *The EMBO journal.* 2006;25(15):3494-3503.
37. Ory S, Ceridono M, Momboisse F, Houy S, Chasserot-Golaz S, Heintz D, Calco V, Haeberlé AM, Espinoza FA, Sims PJ, Bailly Y. Phospholipid scramblase-1-induced lipid reorganization regulates compensatory endocytosis in neuroendocrine cells. *Journal of Neuroscience.* 2013;33(8):3545-3556.
38. Vermes I, Haanen C, Steffens-Nakken H, Reutellingsperger C. A novel assay for apoptosis flow cytometric detection of phosphatidylserine expression on early apoptotic cells using fluorescein labelled annexin V. *Journal of immunological methods.* 1995;184(1):39-51.
39. ZWEIFACH A. FM1-43 reports plasma membrane phospholipid scrambling in T-lymphocytes. *Biochemical Journal.* 2000;349(1):255-260.
40. Vernier PT, Ziegler MJ, Sun Y, Chang WV, Gundersen MA, Tieleman DP. Nanopore formation and phosphatidylserine externalization in a phospholipid bilayer at high transmembrane potential. *Journal of the American Chemical Society.* 2006;128(19):6288-6289.
41. Vernier PT, Sun Y, Gundersen MA. Nanoelectropulse-driven membrane perturbation and small molecule permeabilization. *BMC cell biology.* 2006;7(1):37.
42. Ibey BL, Pakhomov AG, Gregory BW, Khorokhorina VA, Roth CC, Rassokhin MA, Bernhard JA, Wilmink GJ, Pakhomova ON. Selective cytotoxicity of intense nanosecond-duration electric pulses in mammalian cells. *Biochimica et Biophysica Acta (BBA)-General Subjects.* 2010;1800(11):1210-1219.
43. Waymire JC, Bennett WF, Boehme R, Hankins L, Gilmer-Waymire K, Haycock JW. Bovine adrenal chromaffin cells: high-yield purification and viability in suspension culture. *Journal of neuroscience methods.* 1983;7(4):329-351.
44. Hassan N, Chatterjee I, Publicover NG, Craviso GL. Mapping membrane-potential perturbations of chromaffin cells exposed to electric fields. *IEEE transactions on plasma science.* 2002;30(4):1516-1524.

45. Craviso GL. Generation of functionally competent single bovine adrenal chromaffin cells from cell aggregates using the neutral protease dispase. *Journal of Neuroscience Methods.* 2004;137(2):275-281.
46. Fulop T, Radabaugh S, Smith C. Activity-dependent differential transmitter release in mouse adrenal chromaffin cells. *Journal of Neuroscience.* 2005;25(32):7324-7332.
47. Fluorescence Spectra Viewer. https://www.thermofisher.com/us/en/home/life-science/cell-analysis/labeling-chemistry/fluorescence-spectraviewer.html?gclid=CjwKCAjwlZf3BRABEiwA8Q0qqxoa6CAqSH-EcSVsIRl--KC28_-8U0ORoQoT4kSSqwdQEBM2sLJQyBoCAkIQAvD_BwE&ef_id=CjwKCAjwlZf3BRABEiwA8Q0qqxoa6CAqSH-EcSVsIRl--KC28_-8U0ORoQoT4kSSqwdQEBM2sLJQyBoCAkIQAvD_BwE:G:s&s_kwcid=AL!3652!3!231922595944!e!!g!!spectra%20viewer&cid=bid_pca_aup_r01_co_cp1359_pjt0000_bid00000_0se_gaw_nt_pur_con#!/. Accessed.
48. Muratori C, Pakhomov AG, Gianulis E, Meads J, Casciola M, Mollica PA, Pakhomova ON. Activation of the phospholipid scramblase TMEM16F by nanosecond pulsed electric fields (nsPEF) facilitates its diverse cytophysiological effects. *Journal of Biological Chemistry.* 2017;292(47):19381-19391.
49. Yang L, Craviso GL, Vernier PT, Chatterjee I, Leblanc N. Nanosecond electric pulses differentially affect inward and outward currents in patch clamped adrenal chromaffin cells. *PLoS One.* 2017;12(7):e0181002.
50. Zaklit J, Craviso GL, Leblanc N, Yang L, Vernier PT, Chatterjee I. Adrenal Chromaffin Cells Exposed to 5-ns Pulses Require Higher Electric Fields to Porate Intracellular Membranes than the Plasma Membrane: An Experimental and Modeling Study. *The Journal of Membrane Biology.* 2017;250(5):535-552.
51. Vernier PT, Sun Y, Marcu L, Craft CM, Gundersen MA. Nanoelectropulse-induced phosphatidylserine translocation. *Biophysical journal.* 2004;86(6):4040-4048.
52. Vincelette RL, Roth CC, McConnell MP, Payne JA, Beier HT, Ibey BL. Thresholds for phosphatidylserine externalization in Chinese hamster ovarian cells following exposure to nanosecond pulsed electrical fields (nsPEF). *PloS one.* 2013;8(4).
53. Merrill DR, Bikson M, Jefferys JG. Electrical stimulation of excitable tissue: design of efficacious and safe protocols. *Journal of neuroscience methods.* 2005;141(2):171-198.
54. Vogel RW. Understanding Anodal and Cathodal Stimulation. https://www.asnm.org/blogpost/1635804/290597/Understanding-Anodal-and-Cathodal-Stimulation. Published 2017. Accessed.
55. Smith KC, Weaver JC. Active mechanisms are needed to describe cell responses to submicrosecond, megavolt-per-meter pulses: cell models for ultrashort pulses. *Biophysical journal.* 2008;95(4):1547-1563.
56. Kilic G. Exocytosis in bovine chromaffin cells: studies with patch-clamp capacitance and FM1-43 fluorescence. *Biophysical journal.* 2002;83(2):849-857.

57. Shorte S, Stafford S, Collett V, Schofield J. Simultaneous measurement of $[Ca^{2+}]$ i and secretion-coupled membrane turnover, by single cell fluorescence microscopy. *Cell Calcium.* 1995;18(5):440-454.